Cross-Relaxation and Energy Transfer Processes in Praseodymium-Doped Gadolinium Gallium Garnet ($Gd_3Ga_5O_{12}:Pr^{3+}$) Bulk and Nanocrystalline Systems

Rafik Naccache

A Thesis

in

The Department

of

Chemistry and Biochemistry

Presented in Partial Fulfillment of the Requirements
for the Degree of Master of Science at
Concordia University
Montreal, Quebec, Canada

December 2006

Your file Votre référence
ISBN: 978-0-494-28881-8
Our file Notre référence
ISBN: 978-0-494-28881-8

ABSTRACT

Cross-Relaxation and Energy Transfer Processes in Praseodymium-Doped Gadolinium Gallium Garnet ($Gd_3Ga_5O_{12}:Pr^{3+}$) Bulk and Nanocrystalline Systems

Rafik Naccache

The luminescence properties of singly-doped Pr^{3+} and Pr^{3+}/Yb^{3+} co-doped nanocrystalline gadolinium gallium garnet (GGG, $Gd_3Ga_5O_{12}$) are investigated. Dominant blue/green emission emanating from the $^3P_0 \rightarrow {}^3H_4$ and $^3P_0 \rightarrow {}^3H_6$ transitions was observed after excitation using a wavelength of 457.9 nm. The luminescence properties of the nanocrystals were compared to the bulk material (single crystal) with identical Pr^{3+} concentrations (1 mol%) and no noticeable shift in peak position was observed. Increasing the Pr^{3+} concentration in the nanocrystals resulted in a decrease in $^3P_0$ and $^3P_1$ emission to lower lying states via the $[^3P_0, {}^3H_4] \rightarrow [{}^3H_6, {}^1D_2]$ cross relaxation (CR) mechanism. Furthermore, a decrease in the $^1D_2$ emission was observed and was attributed to the $[^1D_2, {}^3H_4] \rightarrow [{}^1G_4, {}^3F_{3,4}]$ CR mechanism. The increase in CR efficiency was attributed to the smaller interionic distances between the dopant ions.

Continuous wave excitation into the $^1D_2$ level of the Pr^{3+} ion at 606.9 nm transition produced blue upconversion luminescence. Based on the increase in transition lifetimes, an energy transfer (ET) upconversion mechanism was proposed. Furthermore, weak blue, green and red upconversion emission was observed from the $^3P_0$, $^3P_1$ and $^1D_2$ states following excitation into the $^1G_4$ energy level with 980 nm. Upconversion was determined to primarily occur through excited state absorption.

Co-doping the nanocrystalline GGG:Pr^{3+} (1 mol%) samples with Yb^{3+} (1–10 mol%) results in a 3-fold increase in upconversion emission intensity relative to the

singly doped samples excited under the same conditions (λ_{exc} = 980 nm). The observed lifetimes obtained using 457.9 nm excitation suggest back transfer from the Pr^{3+} ion to neighboring Yb^{3+} ions which results in decrease in room temperature visible emission and upconversion luminescence.

ACKNOWLEDGEMENTS

While my name stands alone on the cover of this thesis, this work would not have come about without the invaluable contribution of many people whom I am indebted to and wish to acknowledge.

First, I would like to thank my supervisor Dr. John A. Capobianco who has taught me a great deal about science and spectroscopy. No matter how busy and involved he has been in his research and work with the university, he has always been available to answer my questions be it about science or sports. I am thankful for his hands-off approach which has allowed me the chance to explore and learn on my own, that taught me that even when I stumble and fall, I can simply get up, brush myself off and move onwards. My relationship with Dr. Capobianco started as an undergraduate student looking for a Chemistry 450 research supervisor and thankfully has blossomed into a Master's research degree. I retain fond memories especially during world cup matches, which seemed to provide an endless source of entertainment and exciting discussion, especially in 1998 when Dr. Capobianco experienced a life-changing event.

I am grateful to my graduate committee members Dr. H. M. Muchall and Dr. G. Dénès. Their guidance and support has been critical towards the completion of the work and this manuscript. Their constructive views and insightful comments have helped me in my work and for that I am very grateful.

I am also indebted to our colleagues Professors Marco Bettinelli and Adolfo Speghini. Our collaborations first started during my undergraduate degree as I worked on silicate glasses and continued with the nanocrystals. Their synthesis of the nanoparticles was instrumental towards this work and that of others in our laboratory; however, beyond

our collaborative efforts, I have learned a tremendous amount of science through many valuable discussions and communications. Professors Bettinelli and Speghini's approach to spectroscopy was certainly stimulating.

I would like to thank all my lab colleagues with whom I have accumulated numerous fond memories and some of whom I have known for over 12 years. Sean, our relationship goes back all the way back to a Vanier locker in building N during the first week of classes in 1996. We became friends and never looked back. I thank you for drawing me to spectroscopy and introducing me to Dr. John A. Capobianco. Your enthusiasm for the science has had a profound effect on me and thankfully I followed my instinct and went on to study in this field.

Chris, I will certainly remember the many outings we had as we explored our gastronomic limits. I have many fond memories, as well as some darker ones. I am sure I will always cherish those times.

To my friend Dr. Fiorenzo Vetrone, I cannot begin to describe the extent of my appreciation towards everything you have done to help me throughout my degree. You eased my transition in going from large bulky glasses and crystals to the nano aspect of science. I have learned a tremendous amount from you. You are a truly great scientist and individual and as I write these acknowledgements, I recognize that we are certainly going to maintain scientific collaboration and more importantly a friendship for many years to come. I have many fond memories of working many hours spent on weeknights and weekends.

I would like to thank the graduate program director; Dr. Cameron Skinner. His advice and support especially during my last year in the program are greatly appreciated. I thank him for putting up with my numerous email and incessant phone calls.

I would also like to thank Dr. L. Cuccia and my colleague and Nabil Al-Yassir. I have enjoyed many great discussions with them and they have certainly been there when I needed their help.

I would like to express my gratitude to the entire administrative staff of the Department of Chemistry and Biochemistry; Carole Coutts, Donna Gordon, Lisa Montesano, Lisa Kalaschnick, Kathy Usas, and Maria Ciaramella for all their help all through the many long years of graduate school. They were always there and ready to keep me on track and sending me numerous gentle reminders. I thank them for all their hard work.

To my beloved parents Nagwa and Georges, I don't know if my words can or ever will be able to express my gratitude for everything you have ever done for me. You left behind your well established life and came to Canada with one thought in your mind; the future of your son and daughter and for that I thank you. You have taught me everything I know in life today and made me the person I am proud to be and for that I thank you. You have always believed in me and you continuously encouraged me to achieve and push my limits, to go beyond what I thought I was capable of, and for that I thank you. Your unconditional love and support has meant the world to me and I know this degree would never have come about without you in my life. Thank you for always being there and being great parents, great teachers and great friends.

To my incredible sister Rania, thank you for being my rock for all these years. Thank you for always having faith in me and for putting me ahead of yourself every chance you had. All my life, you have been my closest friend and confidante and have always been there for me, ready to listen to me when no one else would. Your kindness, support and love have always guided me in my life, my career and my education. While you never voiced it, I always sensed your silent encouragement as it helped me through the course of this degree and gently pushed me onwards. Thank you for being a great influence in my life and for always being there.

Finally, to my wonderful girlfriend Caroline, whose love and devotion, and continuous and persistent encouragement, have given me the strength to finish this degree. Thank you for your unwavering support, your patience, you understanding and your love. You never lost your faith in me and always gave me hope when things looked bleak and this has undoubtedly helped me in writing this manuscript and these words. Thank you for coming into my life and always believing in me.

"The most exciting phrase to hear in science, the one that heralds new discoveries, is not Eureka! (I found it!) but rather, "hmm.... that's funny...."

- Isaac Asimov

Table of Contents

List of Figures

Chapter 1

Chapter 2

Chapter 3

Chapter 4

Chapter 5

Chapter 6

List of Tables

Chapter 1

Chapter 4

Table 5

Chapter 6

List of Abbreviations

CR	Cross relaxation
D-D	Dipole-dipole
D-Q	Dipole-quadrupole
ESA	Excited state absorption
ET	Energy transfer
ETU	Energy transfer upconversion
FRET	Fluorescence resonance energy transfer
GGG	Gadolinium gallium garnet
IUPAC	International Union of Pure and Applied Chemistry
IH	Inokuti Hirayama
Ln	Lanthanide
IR	Infrared
MIR	Mid infrared
NIR	Near infrared
PA	Photon avalanche
Q-Q	Quadrupole-quadrupole
SAMMS	Self assembled molecules on mesoporous supports
TEM	Transmission electron microscopy
UV	Ultraviolet
VIS	Visible
YAG	Yttrium aluminium garnet

Chapter I

1.1 Luminescence

The International Union of Pure and Applied Chemistry (IUPAC) defines luminescence as:

> *" Spontaneous emission of radiation from an electronically or vibrationally excited species not in thermal equilibrium with its environment."* [1]

Luminescence encompasses bioluminescence, chemiluminescence, phosphorescence, photoluminescence and radioluminescence to simply name a few. Photoluminescence is of particular interest to our research and is defined as luminescence generated by photoexcitation. From a spectroscopic point of view, photoluminescence is said to occur when an ion relaxes to the ground state having been previously excited. The energy associated with the de-excitation process may be released in the form of a packet of energy, otherwise a photon (ultraviolet, visible, near IR or IR).

A hypothetical energy level diagram of an imaginary lanthanide ion is shown in Figure 1.1. Using a suitable wavelength of light, the ion is excited to the corresponding energy level, S_4 (step ①). This may be followed by blue emission (step ②) or non-radiative decay (step ③) to the lower lying S_3 energy level resulting in green emission (step ④). The process of non-radiative decay may reoccur (steps ⑤ and ⑥) followed by emission from lower lying levels until the ion eventually relaxes to the ground state, S_0. It is noteworthy to mention that emission does not necessarily involve the return of the ion to the ground state. Emission may occur when an ion relaxes to any lower lying states releasing a photon of light.

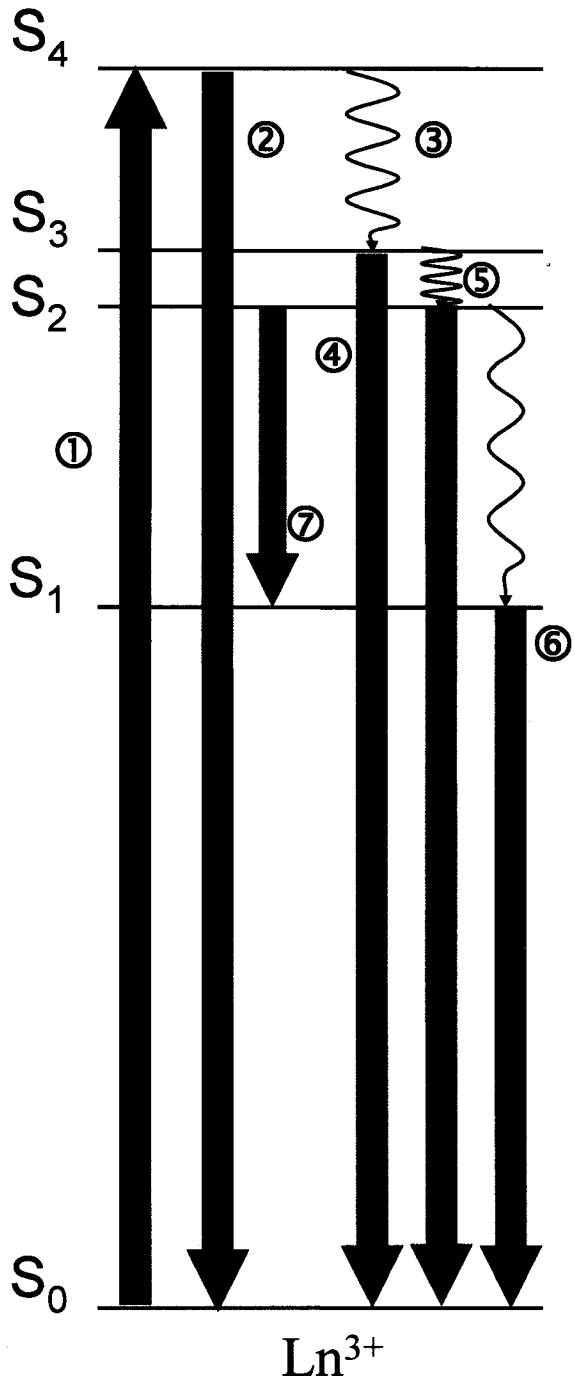

Figure 1. 1. A hypothetical energy level diagram of an imaginary lanthanide ion.

For example in step ⑦, the ion in the intermediate excited state S_2, relaxes to the lower lying state S_1 giving off emission. It follows that the wavelength (and thus colour) of the emission is related to the energy gap separating the states. The luminescence and the various energy states of the ions are very strongly affected by their surroundings namely, the host, the crystals field, symmetry and by the associated selection rules. This will be further discussed in Chapter 2.

1.2 The Lanthanides

G.C. Pimentel & R.D. Sprately published a book in 1971 entitled *Understanding Chemistry* in which they stated that:

> *"Lanthanum has only one important oxidation state in aqueous solution, the +3 state. With few exceptions, this tells the whole boring story about the other 14 Lanthanides"* [2]

Ironically enough, little did they understand or foresee that many years later, the lanthanides would become an essential part of everyday life and seamlessly integrate into current technology, as well as become a key player in the forefront of novel scientific developments.

The lanthanides comprise the sixth row of the periodic table which begins with cesium (Z=55) and barium (Z=56) with electronic configurations of [Xe]$6s^1$ and [Xe]$6s^2$, respectively. The lanthanide series is named after lanthanum and all lanthanides are f-block elements, corresponding to the filling of the 4*f* electron shell. The lanthanides excluding promethium, together with scandium, yttrium, and lutetium, are commonly referred to as the "rare earths"; however, this is in fact a misnomer as the lanthanides are not as rare as was once thought. Even the scarce rare earths, most notably europium and

lutetium, are more common than the platinum-group metals which include nickel and palladium [3]. Table 1.1 summarizes the electronic properties of the lanthanide series [4].

Table 1. 1. Electronic properties of the lanthanide series.

Lanthanide Ln	Ln^{3+} Configuration	Ground State	Number of Unpaired Electrons	Colour
La	$4f^0$	$^1S_0$	0	colourless
Ce	$4f^1$	$^2F_{5/2}$	1	colourless
Pr	$4f^2$	$^3H_4$	2	green
Nd	$4f^3$	$^4I_{9/2}$	3	lilac
Pm	$4f^4$	$^5I_4$	4	pink
Sm	$4f^5$	$^6H_{5/2}$	5	yellow
Eu	$4f^6$	$^7F_0$	6	pale pink
Gd	$4f^7$	$^8S_{7/2}$	7	colourless
Tb	$4f^8$	$^7F_6$	6	pale pink
Dy	$4f^9$	$^6H_{15/2}$	5	yellow
Ho	$4f^{10}$	$^5I_8$	4	yellow
Er	$4f^{11}$	$^4I_{15/2}$	3	rose-pink
Tm	$4f^{12}$	$^3H_6$	2	pale green
Yb	$4f^{13}$	$^2F_{7/2}$	1	colourless
Lu	$4f^{14}$	$^1S_0$	0	colourless

Figure 1.2 summarizes the different energy levels for the lanthanide ions [5]. The $4f$ electrons are well shielded from external charge by $5s^2$ & $5p^6$ shells which results in strong *f-f* absorption bands and consequently, the lanthanides are known for their well resolved and sharp emission profiles. To a certain extent, this may minimize crystal field effect (discussed later); however, with the introduction of the lanthanide in glass, crystals and nanocrystals, this, in fact, no longer holds particularly true. Nonetheless, due to their intense and characteristic sharp emission, the lanthanides have found uses in a myriad of applications including coloured glass, photography and cinematic applications, phosphors in television screens (Eu^{3+} and Ce^{3+}), and lasing hosts, the most common being Nd^{3+}:YAG (yttrium aluminium garnet) to simply name a few.

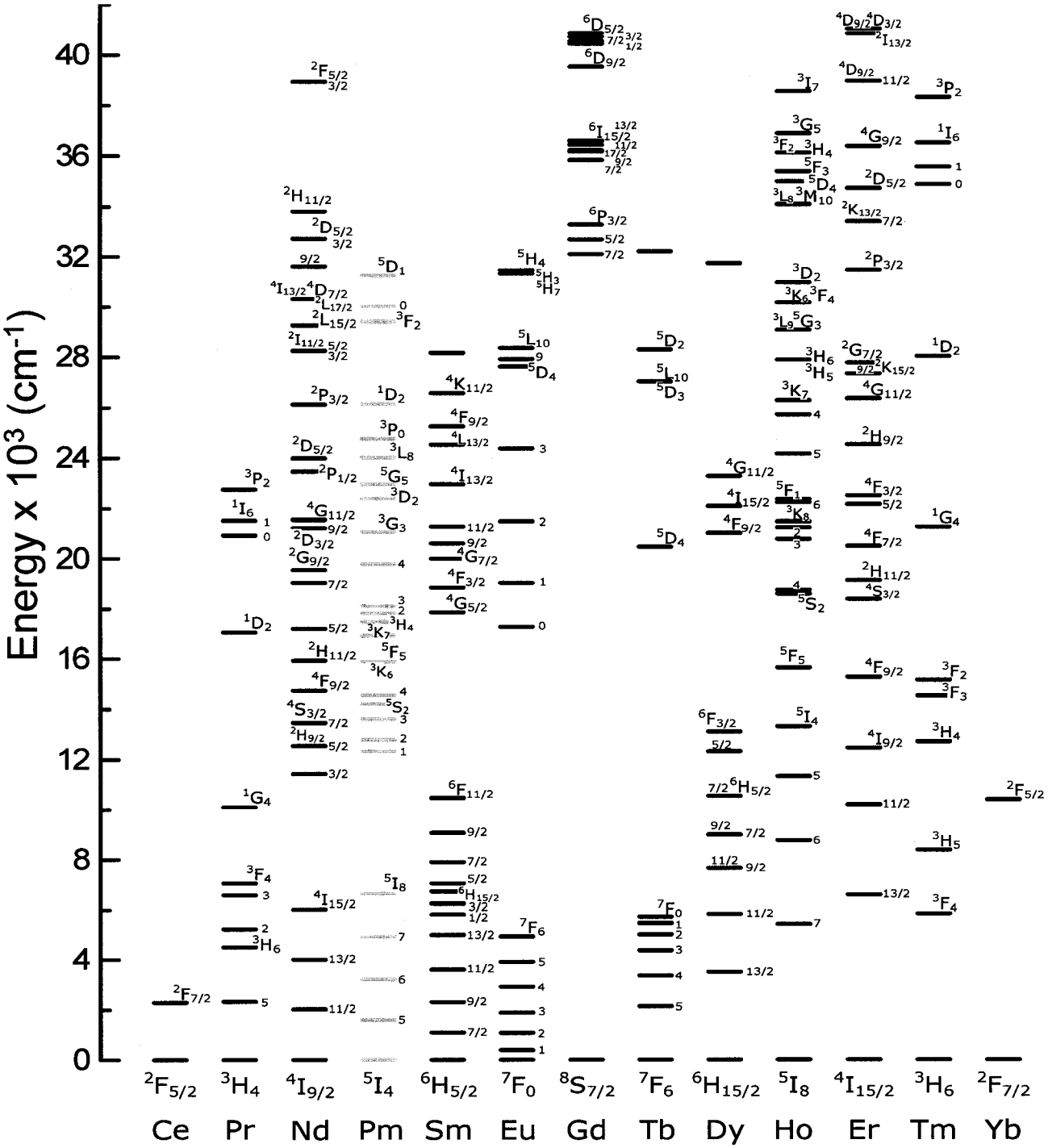

Figure 1. 2. Dieke Diagram of the energy levels of the Lanthanide in $LaCl_3$ [6] (used with permission: F. Vetrone, Ph. D. Thesis, Concordia University (2005)).

The potential for biological applications has only recently been investigated and the future of the lanthanides in the bio-medical field certainly promises to be colourful.

1.3 Praseodymium

The name, Praseodymium, is derived from the Greek *"prasios"* and *"didymos"* which means *'green twin'*. The lanthanide element was isolated and identified by von Welsbach in 1885 from what was known at the time as *didymium*. Based on his work, it was revealed that the material isolated actually consisted of two new elements, one of which was praseodymium and the other being neodymium [7].

Pure praseodymium is silvery-white and fairly soft. One of the most common uses for praseodymium is in alloying steel which is especially useful for aircraft engine constructions. Praseodymium however also finds simpler uses such as for sparks in lighters. The element occurs along with other rare-earth elements in a variety of minerals. Monazite and bastnasite are the two principal commercial sources of the rare-earth metals. Like the other rare-earth oxides, praseodymium oxides (Pr_2O_3) are among the most refractory substances known and find uses as carbon arcs used for studio lighting and projection. Salts of praseodymium are used to color glasses and enamels; when mixed with certain other materials, praseodymium produces an intense and unusually clean yellow color in glass [7, 8]. From a spectroscopic point of view, the interest in the praseodymium tripositive ion (Pr^{3+}) stems from it being an attractive optical activator, which offers the possibility of blue, green and red emission for laser action, as well as IR emission for optical amplification at 1.3 μm (Figure 1.3).

Furthermore, there are a multitude of transitions which allow for detailed studies of non-radiative mechanisms such as multiphonon relaxation and energy transfer

processes between the lanthanide ions (*e.g.* excited state upconversion or cross-relaxation). The latter are quite prominent in Pr^{3+} due to resonant energy gaps separating the various levels. Cross-relaxation phenomena are of interest as they are responsible for emission quenching phenomena especially as a function of increasing dopant concentration [9-12]. Previously published manuscripts have shown that emission quenching and cross relaxation in praseodymium doped hosts can occur with dopant concentrations as low as 0.01 mol% [9, 13]. Consequently, concentration studies are essential in trying to elucidate the various radiationless pathways which may be probable within a given host. The multitude of allowable pathways by which cross-relaxation can occur renders praseodymium a challenging ion to investigate.

1.4 Nanocrystals

It has been over twenty years that scientists first pondered the idea of nano-sized material, that is material which is 1/80,000th the diameter of a human hair. Initial work in the literature dating from the mid-eighties to mid nineties has focused on the development of the physics and applications of quantum dots [14-26]; the latter being typically a few nanometers in size. In the last ten years however, scientists from all domains have sought out to build on that knowledge and have very diligently worked on the development of nanoscience and nanotechnology.

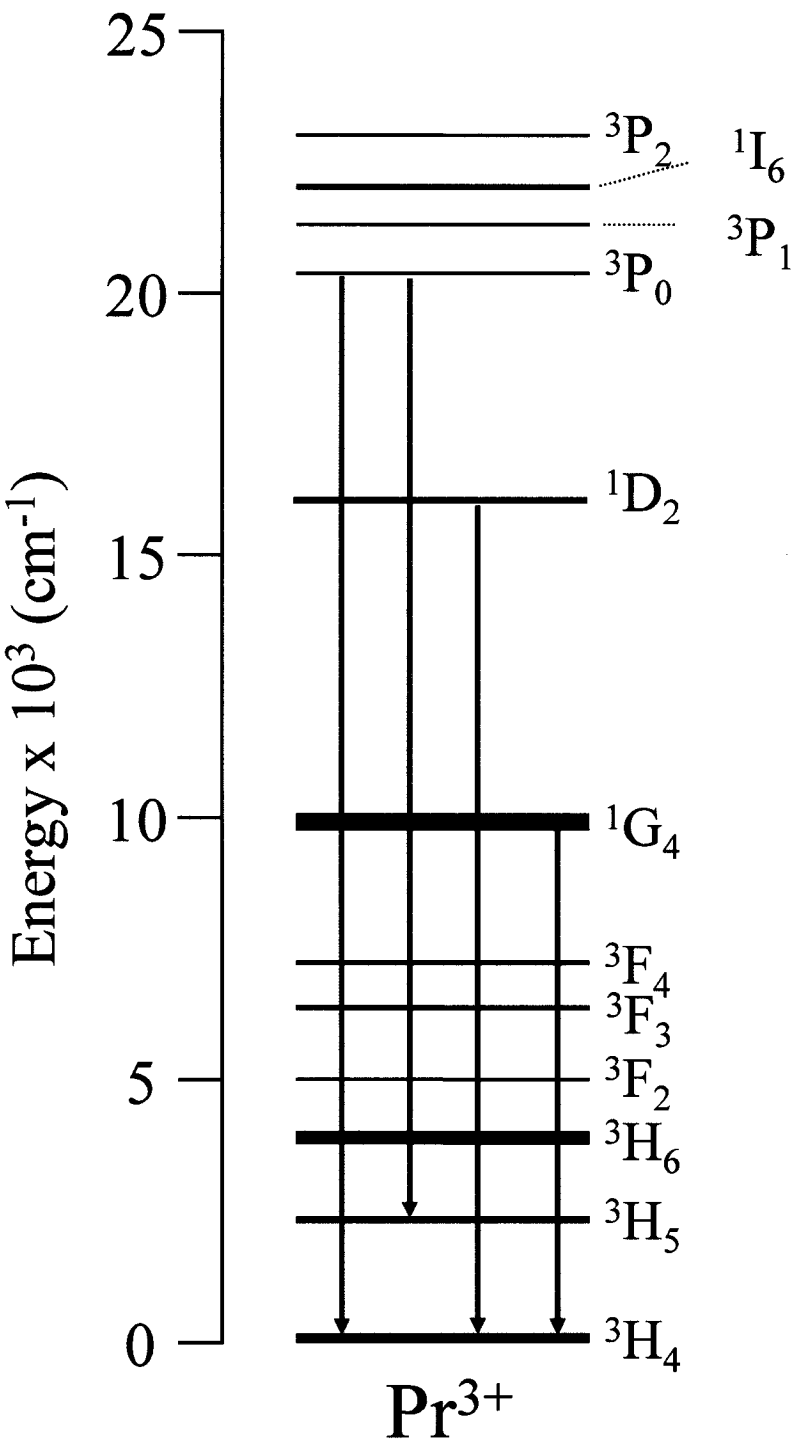

Figure 1. 3. Blue, green, red and IR emission of the tripositive praseodymium ion.

Some of the early research suggested that moderate quantum efficiencies can be obtained in the nanosystems and almost acting as a catalyst, it propelled other scientists on their search and soon after, the field flourished with novel luminescent materials which have found and continue to find uses in many applications in industry.

The field of nanoscience does not only concern itself with novel materials and technology but it seeks bringing forth improvements and enhancements to what already exists. Many industries have already realized the necessity of becoming "small-minded" and have understood that the integration of nanoscale products will not only energize, but drive them forward beyond their competition. The textile industry is starting to incorporate nanomaterials in their products. For example, Eddie Bauer has developed clothes with embedded nanoparticles in an effort to render them stain-resistant [27]. While this may seem to be a relatively small application in a huge industry, it represents a solid start and huge stepping stone for other potential nano-applications [27].

Nanotechnology has also found its way in environmental friendly applications as is the case with researchers at Pacific Northwest National Laboratory (PNNL) who have used nanoparticles as well as self-assembled monolayers on mesoporous supports (SAMMS) to easily capture heavy metals such as lead and mercury [28-33]. The surface area of one teaspoon of this substance is equivalent to that of a football field. Mattigod and his group have projected that the SAMMS technology can be easily adapted to target other toxins such as lead, chromium and radionuclides. As a result, the environmental aspects associated with these novel materials are vast. Further developments can result in other nanomaterials which can be used to capture a variety of other metals and chemicals, which are currently polluting our lakes and rivers.

The automobile industry is not sitting idle and has taken several steps towards the incorporation of nanosolids in their product lineups. From side-steps to bumpers, nanoparticles are finding their way in the manufacturing lineups of key automakers. Many components are now manufactured from plastic nanocomposites not only for cost cutting measures but due to the fact that these materials are scratch-resistant, light-weight, and rust-proof. Advancements are not only reserved to personal automobiles but will likely be extended to public transportation where carbon-based fibers which are 100 times stronger than steel, at only one-sixth the weight, can be used to build safer and more durable means of transportation. It is even projected that nanoparticles can be used to improve public safety. Currently scientists are evaluating the possibility of using nanomaterials as smart sensors for collision avoidance in automobiles; nano-reinforced, glare-resistant car windows and windshields; chemical and biological weapon detectors at airports; and sensors that monitor rail track structural integrity. The possibilities seem to be endless in a field on the brink of explosion with unlimited potential [27].

1.5 Statement of the Problem

Behind the marvelous and vast potential of nanocrystals, lies very interesting scientific concepts and theories which have allowed for the field to experience what can be qualified as a giant leap in such a limited period of time. It is based on that the research described in this thesis has been undertaken. The optical versatility of praseodymium renders it an ideal candidate in the development of novel luminescent materials which may be used for applications in a variety of technologies. Building on previous work in the literature which had predominantly focused on yttrium oxide, Y_2O_3 [34-62], the field of nanoscience has targeted novel host materials in its continual quest

for improved performance and efficiency. Many hosts including fluorides and oxides are currently being evaluated. More recently, much work reported in the literature has suggested that the garnets may be of interest. The garnets make up one of the most important groups of hosts for laser centers namely the rare earths. They are optically transparent from the UV to the mid IR range. They possess low phonon energies and may have more favorable physico-chemical properties relative to other host materials [63, 64]. Most importantly, garnets are a relatively novel material to study in the nanocrystalline phase. Aside from yttrium aluminium garnet (YAG) [65-68], there has been little work published in the literature on nanocrystalline garnet host systems [69-71]. In fact work carried out on garnets excluding YAG only appeared in the literature in 2004.

In the work described herein, the luminescent properties of singly-doped GGG:Pr^{3+} bulk (1 mol%) and nanocrystals (0.1–10 mol%) are reported. The optical properties as a function of dopant concentration and the effect of cross-relaxation on upconversion are evaluated in great detail. The luminescent properties are also evaluated in co-doped nanocrystalline systems where Yb^{3+} is added. Energy transfer and cross-relaxation mechanisms are proposed in an effort to explain the observed phenomena within the bulk and nanosystems.

Chapter II

2.1 Free Energy Hamiltonian

The Hamiltonian which describes the energies of the free ion states can be written as follows (Equation 2.1)

$$H = -\frac{\hbar^2}{2m}\sum_{i=1}^{N}\nabla_i^2 - \sum_{i=1}^{N}\frac{Z^* e^2}{r_i} + \sum_{i<j}^{N}\frac{e^2}{r_{ij}} + \sum_{i=1}^{N}\zeta(r_i)\mathbf{s}_i.\mathbf{l}_i \qquad (2.1)$$

where N = 1...14 is the number of the 4*f* electrons, m is the mass of the electron, $\hbar^2\nabla_i^2$ is the square of the momentum operator for the i^{th} electron, r_i is the distance from the nucleus to the i^{th} electron, r_{ij} is the distance between the i^{th} and j^{th} electrons, e is the charge of the electron, s_i and l_i are the spin and orbital angular momentum respectively of the i^{th} electron. The term Z*e, is the effective nuclear charge, and finally $\zeta(r_i)$ is the spin-orbit coupling function. Since all the electronic shells, except for the 4*f* shells, are spherically symmetric and therefore do not contribute significantly to the relative positions of the 4*f* energy levels [72], the Hamiltonian, in Equation 2.2, may be re-expressed into three distinct parts,

$$\hat{H}_{FI} = \hat{H}_O + \hat{H}_C + \hat{H}_{SO} \qquad (2.2)$$

where $\hat{H}_{FI}$ represents the sum of all the contributors to the free ion energy Hamiltonian. The term $\hat{H}_O$ describes the orbital component of the Hamiltonian and contributes the following to Equation 2.1.

$$\hat{H}_O = -\frac{\hbar^2}{2m}\sum_{i=1}^{N}\nabla_i^2 - \sum_{i=1}^{N}\frac{Z^* e^2}{r_i} \qquad (2.3)$$

The first term in Equation 2.3 describes the kinetic energy of the 4*f* electrons, while the second term represents their Coulombic interaction with the nucleus. This interaction occurs within a closed shell thereby only modifying the magnitude and not the symmetry allowing for the replacement of the real charge by a screened charge. The spherical symmetry of the first two terms in the Hamiltonian does not remove any of the degeneracy within the 4*f* electron configuration and can therefore be ignored [72].

The remaining two terms represent Coulombic interaction of the 4*f* electrons ($\hat{H}_C$) and their spin-orbit coupling ($\hat{H}_{SO}$). Equations 2.4 and 2.5 show the components of $\hat{H}_C$ and $\hat{H}_{SO}$ respectively. Note that the $\hat{H}_C$ component of Equation 2.4 is responsible for partially lifting the degeneracy of the energy levels.

$$\hat{H}_C = \sum_{i<j}^{N}\frac{e^2}{r_{ij}} \qquad (2.4)$$

$$\hat{H}_{SO} = \sum_{i=1}^{N}\zeta(r_i)\mathbf{s}_i.\mathbf{l}_i \qquad (2.5)$$

There are two limiting cases for the relative size of those two interactions in atomic theory. In the first case, $\hat{H}_C >> \hat{H}_{SO}$ which is known as the Russell-Saunders coupling scheme. The Russell-Saunders coupling scheme is based on the concept that if spin-orbit coupling is weak, then it is only effective when all orbital momenta are operating cooperatively. Thus, all orbital angular momenta of the electrons couple to give

a total, L, and all the spins similarly couple to give a total, S, and the two kinds of momenta coupling through the spin orbit interaction to give a total, J [73]. Permitted values of J can be obtained by the Clebsch-Gordon series,

$$J = L + S,\ L + S - 1,\ \ldots\ |L - S| \qquad (2.6)$$

In this type of situation, the spin orbit interaction is only a small perturbation on the energy level structure determined from diagonalization of $\hat{H}_C$. It is noteworthy to mention that the Russell-Saunders scheme works well only for light atoms (low atomic number). In the second case where $\hat{H}_C << \hat{H}_{SO}$ (*j-j* coupling scheme), the Russell-Saunders scheme fails as the spin-orbit coupling is large (heavy atoms or high atomic number). The individual spin and orbital momenta of the electrons are coupled into individual j values, after which, these momenta are combined in a grand total J [73]. However in the rare earths, both limiting cases are of approximately equal magnitude and the energy level calculations are more mathematically involved resulting in a situation called the *intermediate coupling scheme*.

2.2 Crystal Field

Crystal field theory is a model used to interpret the bonding between ligands and a metal ion. In this theory the bonding is assumed to be primarily electrostatic. The ligands are regarded to be negative point charges. The ligand electron pairs are not donated into orbitals of the central ion. Crystal field theory may therefore be regarded as the determination of the energy level and wavefunction modifications of the free ions due to the surrounding environment (crystalline lattice, glass network, etc).

Using the crystal field parameters, one can calculate the crystal field strength depending on the type of approximation used: strong field or weak field approximations [74]. Essentially, the crystal field is a quantitative measure of the interaction between the rare earth and the surrounding lattice. For lanthanides, the weak crystal field approximation is used as the crystal field potential is small in comparison to the spin-orbit interactions.

2.3 Term Symbols

A term symbol is used to convey certain information regarding some of the electronic properties of an atom. An example of a term symbol may be written as ${}^1D_2$ which is pronounced as a *singlet D two* or *one D two*. These numbers and letters in fact represent what is known as the term symbols and may be referred to as the ${}^S L_J$ notation. The term symbols give important information: (i) the total orbital angular momentum number (L) which has values of S, P, D, F, G, H, I, ...(in alphabetical order) corresponding to 0, 1, 2, 3, 4, 5, 6, ..., respectively; (ii) the multiplicity of the term (S) which is expressed as 2S+1 where S is the total spin angular momentum, and (iii) the total angular momentum quantum number (J) which may be expressed as shown in Equation 2.6 in section 2.1

2.4 Selection Rules

There are two requirements which need to be fulfilled for matter to absorb the electric field component of radiation: 1) energy matching must occur and 2) the energy transition in the molecule must be accompanied by a change in the electrical centre of the molecule in order that electrical work can be done on the molecule by the

electromagnetic radiation field. Selection rules summarize the requirements for the absorption of light by matter [75].

According to the selection rules, a possible transition is known as an "allowed" transition, whereas an impossible transition is known as a "forbidden" transition; however, the selection rules are set up for simple models and in many cases, many "forbidden" transitions are in fact observed. As the probability of a transition increases, so does the intensity of the emission or the absorption in that transition. It follows that a forbidden transitions gives absorption or emission of low intensity. Figure 2.1 shows the energy level diagram of the tripositive praseodymium ion. Certain transitions are not allowed within the various energy levels of Pr^{3+} as they are prohibited by the selection rules. Some of the spin-allowed transitions are discussed in detail in Chapter 4.

The electric dipole operator is given by $\sum_i er_i$ with the translation components being $\sum_i ex_i$, $\sum_i ey_i$, and $\sum_i ez_i$. Forming linear combinations of these components will form an irreducible tensor operator of the first order [76],

$$\mathbf{r}_1 = -\sum_i \frac{\mathbf{x}_i + \mathbf{i}\mathbf{y}_i}{2^{1/2}} \qquad (2.7)$$

$$\mathbf{r}_0 = -\sum_i \mathbf{z}_i \qquad (2.8)$$

$$\mathbf{r}_{-1} = -\sum_i \frac{\mathbf{x}_i - \mathbf{i}\mathbf{y}_i}{2^{1/2}} \qquad (2.9)$$

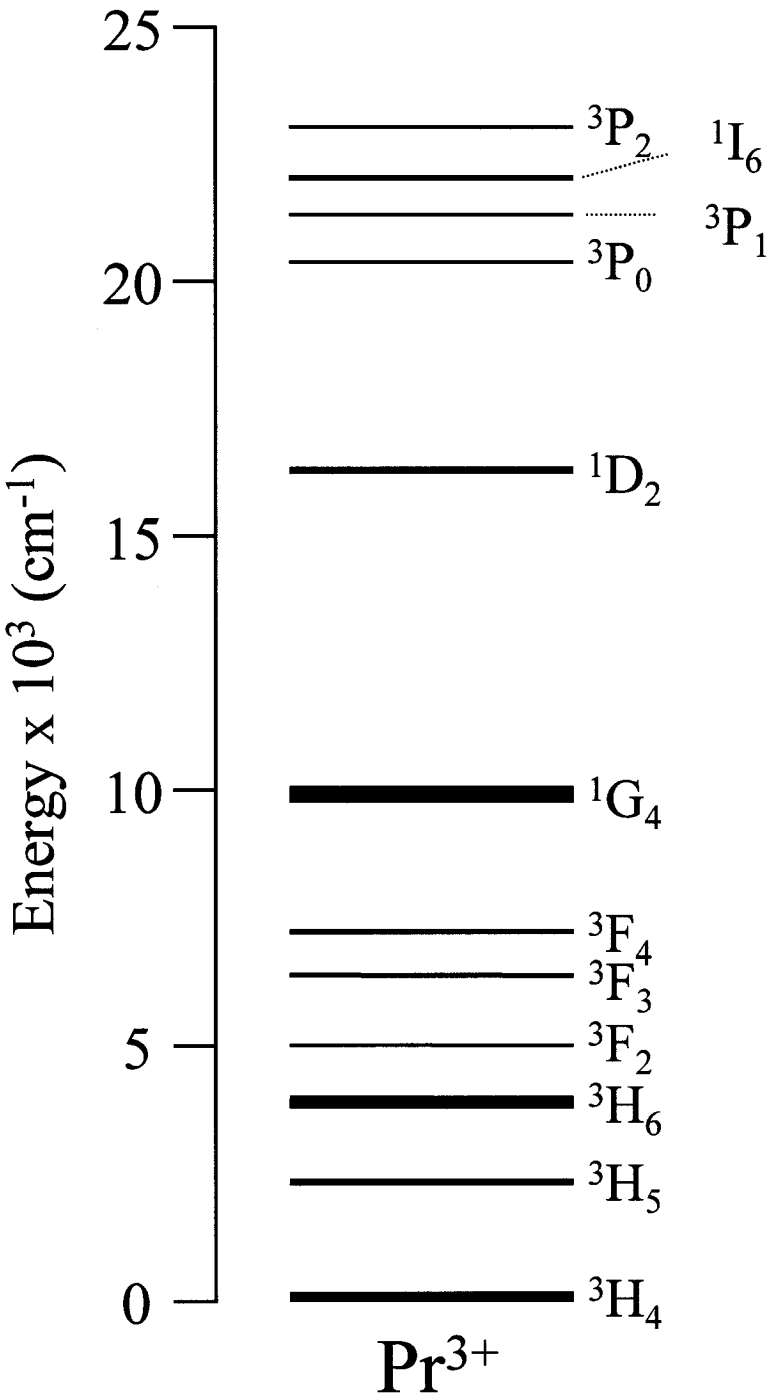

Figure 2. 1. Energy level diagram of the tripositive praseodymium ion.

These new components transform like basis functions for the representation D_{lu} (u is odd) of the three-dimensional rotation group.

Matrix elements $< \psi_f^{el} \mid r_\alpha \mid \psi_i^{el} >$ define whether a transition is spontaneous or induced. The products $r_\alpha \psi_i^{el}$ transform according to the following if $J_i \geq 1$,

$$D_1 \text{ x } D_{Ji} = D_{Ji}+1 + D_{Ji} + D_{Ji} - 1 \qquad (2.10)$$

$J_i = 0$, then

$$D_1 \text{ x } D_0 = D_1 \qquad (2.11)$$

Consequently, only J_f=1 is allowed, eliminating $J_f = 0 \rightarrow J_i = 0$.

Knowing that the electric dipole operator is an odd operator, the parity of the final state must be different from the parity of the original state in accord with Laporte's rule.

$$\Delta J = 0, \pm 1; \qquad J_i = 0 \mapsto J_f = 0$$
$$P_f \neq P_i \qquad (2.12)$$

In the Russell-Saunders approximation, eigenfunctions transform like the D_L x D_S representation. The dipole operator components transform like D_1 ($L = 1$, $S = 0$).

$$\Delta L = 0, \pm 1; \qquad L_i = 0 \mapsto L_f = 0$$
$$\Delta S = 0$$
$$P_f \neq P_i \qquad (2.13)$$

The magnetic dipole operator for one electron is given by the following:

$$\mu = -\frac{e}{2mc}(\mathbf{L} + 2\mathbf{S}) \qquad (2.14)$$

The first order irreducible tensor operator becomes:

$$\mu_1 = -\frac{e}{2mc}\frac{(\mathbf{L}_x + 2\mathbf{S}_x) + i(\mathbf{L}_y + 2\mathbf{S}_y)}{2^{1/2}} \qquad (2.15)$$

$$\mu_0 = -\frac{e}{2mc}(\mathbf{L}_z + 2\mathbf{S}_z) \qquad (2.16)$$

$$\mu_{-1} = -\frac{e}{2mc}\frac{(\mathbf{L}_x + 2\mathbf{S}_x) + i(\mathbf{L}_y + 2\mathbf{S}_y)}{2^{1/2}} \qquad (2.17)$$

These new components transform like basis functions for the representation D_{lg} (g is even) of the three-dimensional rotation group [76]. In contrast to the electric dipole operator, the magnetic dipole operator is an even operator. In the absence of an external field,

$$\Delta J = 0, \pm 1; \qquad J_i = 0 \mapsto J_f = 0$$
$$P_f = P_i \qquad (2.18)$$

In the Russell-Saunders couplings,

$$\Delta L = 0, \pm 1; \qquad L_i = 0 \mapsto L_f = 0$$
$$\Delta S = 0$$
$$P_f = P_i \qquad (2.19)$$

The rare earths ions' energy levels (in a crystal) are quite similar to those of the free ions [76]. The energy levels of an f^n configuration in a weak field depends on 3 components: (i) the $\mathbf{F}_2$, $\mathbf{F}_4$, and $\mathbf{F}_6$ Slater integrals, (ii) the spin orbit parameter ζ_{4f} and (iii) the crystal field strength. In rare earth ions, valid rules are determined by site symmetry. Moreover, due to the weakness of the crystalline fields, the selection rules of the free ion still are relevant. For magnetic and electric radiation,

$$J = 0, \pm 1; \qquad J = 0 \mapsto J = 0 \qquad (2.20)$$

Environmental perturbations allow the electric dipole transitions within an f^n configuration. Therefore, the local field symmetry at the site of the ion controls the selection rules.

2.5 Energy Transfer and Cross-Relaxation Processes

In the discussion of luminescence in Section 1.1, the process of absorption of a pump photon and emission was a single ion process; however, experimental evidence in the literature has suggested time and time again that many ions may contribute to the absorption or emission of a photon; hence, luminescence may occur through multiple processes and mechanisms such as energy transfer (ET) for example where an ion can de-excite by transferring its energy to a second ion in a radiationless manner. There are multiple processes by which ET may occur: (i) resonant energy transfer, (ii) phonon assisted energy transfer, (iii) step-wise upconversion, (iv) ion-pair absorption and (v) ion-pair emission [77-84]. Energy transfer processes (i) and (ii) will be discussed in greater detail in this section while step-wise upconversion (iii) is discussed in section 2.5.

In the classical resonant energy transfer process (i), two ions are involved, the donor and the acceptor ions (Figure 2.2a). Using a pump photon, ion I in ground state A_1 is raised to the excited state A_2. Following this process, ion I de-excites non-radiatively to its ground state, A_1, and transfers its energy to the acceptor ion II raising it from its ground state B_1 to the excited state B_2. In this classical example, there was no loss in the energy transfer as the energy gap (ΔE) separating $A_2 \rightarrow A_1$ was equal to the ΔE of $B_1 \rightarrow B_2$. Typically however, the ET process does not involve perfectly resonant states. A ΔE value of even 50-100 cm^{-1} would require the mediation of phonon energies available through the lattice vibrations. In the phonon-assisted energy ET process, ion I is excited in a similar fashion to resonant energy transfer; however, the difference in energy gap will require the emission or absorption of a system phonon (Figure 2.2b, c) [85]. It can therefore be stated that the energy transfer is further affected by the transfer wavelength and by the distance between the energy donor and energy acceptors in the system. All three mechanisms of energy transfer describe cross-relaxation processes where the ET occurs between resonant or closely resonant (phonon-mediated) transitions between a neighbouring pair of ions.

The transfer of energy from the donor to the acceptor is critical dictating the resultant luminescence. It is also critical in co-doped systems where the donor and acceptor ions are different ions most notable in the case of co-doping with ytterbium (Section 6.1).

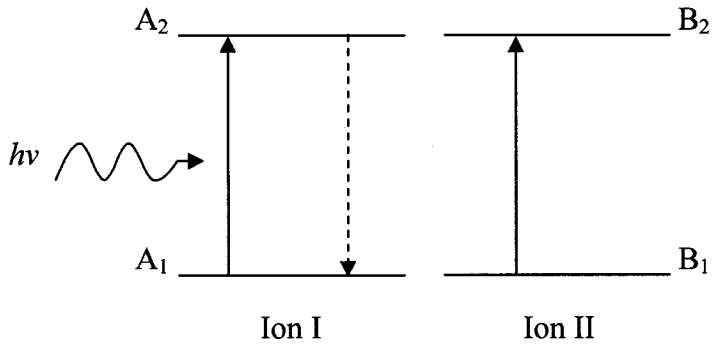

(a)

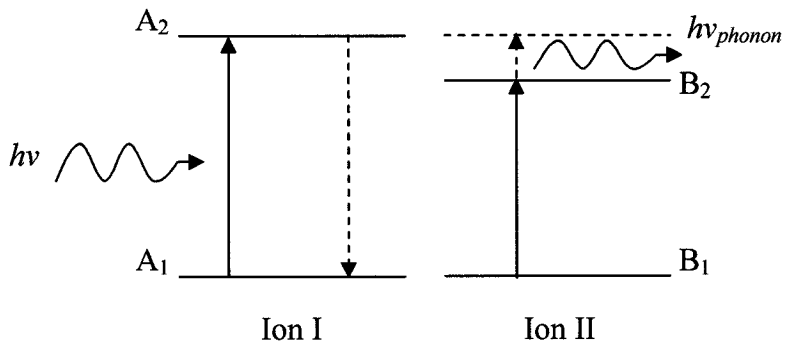

(b)

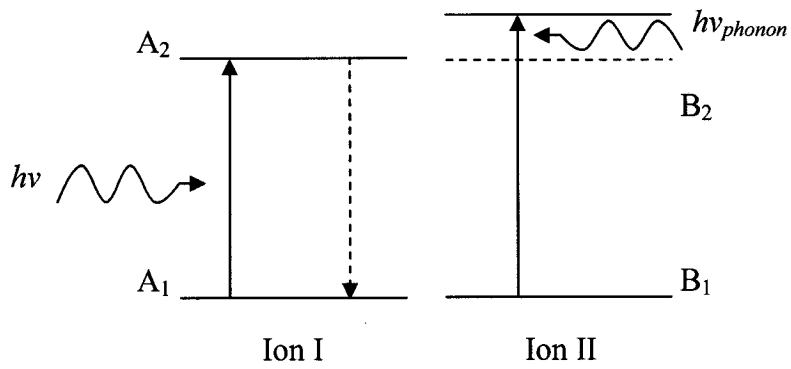

(c)

Figure 2. 2. Two-ion energy transfer processes showing (a) resonant energy transfer, (b) phonon-assisted energy transfer with emission of a phonon and (c) phonon-assisted energy transfer with absorption of a phonon.

2.6 Upconversion

Upconversion can be defined as a process where two or more low energy photons from the excitation source are converted into one photon of higher energy [86]. Upconversion may therefore be alternatively defined as a process in which a system relaxes through the emission of photons of higher energy than those it absorbs during excitation. For example two near-infrared (NIR) photons can be converted to one photon of visible emission. NIR-to-visible upconversion is an important process for the generation of visible light. If the upconversion process is efficient, it can in principle, provide an alternative method for converting laser radiation from low energy to high-energy photons. Trivalent rare-earth ions doped in various hosts are excellent candidates for upconversion [5]. The $4f^n$ electronic structures of these ions provide many long-lived intermediate levels that can be populated with infrared radiation as well as metastable, higher lying energy levels, that give rise to strong visible emission. The upconversion efficiency of rare earth ion doped hosts depends greatly on the non-radiative relaxation processes (quenching and multi-phonon relaxation) of the energy levels involved as well as the Boltzmann distribution of the electronic population.

Upconverting particles and especially upconverting nanoparticles are extremely attractive for display applications. Nanocrystals are attractive for a wealth of applications namely imaging and display devices where it has been previously shown that resolution is inversely related to the particle size [87, 88]. Current display devices rely mainly on micrometer-sized phosphors; consequently, the potential for higher resolution is greatly limited relative to their nanoparticle counterparts. Furthermore the implementation of nano-sized phosphors will surely have significant impact on the display-device size [89-

91]. The introduction of plasma displays has already ushered the movement towards more efficient and compact devices. A commonly available and relatively inexpensive semiconductor diode can be used to excite the upconverting nanoparticles which can produce the myriad of colours required for display and imaging applications. It is however important to highlight that upconverting materials are being evaluated for incorporation in many different technologies/fields and especially biomedicine. For example, using a solvothermal technique, Wang et al. [92] successfully prepared a novel biosensor for the detection of trace amounts of avidin based on fluorescence resonance energy transfer (FRET) (Figure 2.3). Upconversion luminescence was quenched in the presence of avidin with a linear dependence between the upconversion luminescence and the avidin concentration thereby indicating that the proposed biosensor was feasible.

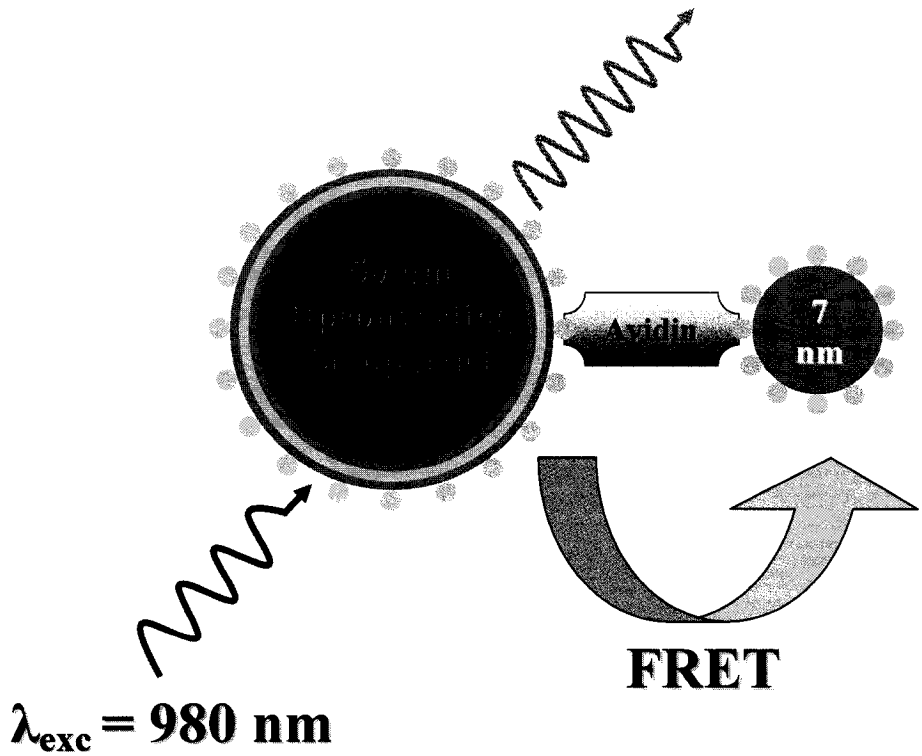

Figure 2. 3. Schematic of an upconversion FRET Assay.

Wang et al. [93] also published on using a co-doped Er^{3+}/Yb^{3+} in hexagonal phase β–$NaYF_4$ and demonstrated the ability, via magnetic separation techniques, to use co-doped nanoparticles systems in biological applications such as trace DNA detection.

Upconversion can occur via three distinct mechanisms: (i) excited state absorption (ESA), (ii) energy transfer upconversion (ETU) and (iii) photon avalanche (PA) [86, 94]. The three mechanisms are discussed in greater detail in sections 2.6.1 – 2.6.3. It is important to highlight that these mechanisms often occur simultaneously. It is therefore crucial to understand the differences between the different types of upconversion.

2.6.1 Excited State Absorption Upconversion

Excited state absorption (ESA) also known as sequential two-photon absorption can lead to upconversion excitation with a first photon populating an intermediate state, and a second photon pumping the upper laser level via excited state absorption (Figure 2.4a). Thus if the photons of hν have an energy resonant with the transition from ground state 1 to excited state 2, some of them are absorbed from ground state 1. Incident photons with energy resonant with the transition from state 2 to excited state 3 may be absorbed by one of the previously excited ions. Sequential photon upconversion is not concentration dependant. It follows that at low rare-earth dopant concentration, it is the mechanism of choice through which upconversion may occur.

Unlike the energy transfer upconversion (ETU) process which is discussed in section 2.6.2, there is no lengthening of the transition lifetimes associated with an ESA mechanism. This is due to the fact that the transition is populated by the rapidly incoming pump photons and not via an energy transfer from another ion. Hence, there is no expected change in the lifetimes of an ESA process.

2.6.2 Energy Transfer Upconversion

The ETU mechanism occurs via successive energy transfer from neighboring lanthanide ions which will firstly promote the ion to an intermediate excited state (Figure 2.4b) [86, 94]. A second energy transfer will follow and excitation to a higher state will occur followed by visible upconversion emission. An ETU process may also occur via cross-relaxation (CR) (Figure 2.4c) in a process by which the photons of the pump beam are absorbed by two rare-earth ions, in close proximity, raising both ions from the ground state to an intermediate excited state. An energy transfer process then promotes one of the ions to a higher energy excited state while the other ion relaxes to the ground state.

2.6.3 Photon Avalanche Upconversion

This process involves excited state absorption of the pump light as well as interionic cross-relaxation [95]. The first feature of this energy transfer process is that the pump wavelength is only resonant between a metastable state and a higher energy level. The second important feature of this process is that an excitation power threshold clearly separates two different regimes. Below the threshold point, the upconverted fluorescence intensity is weak and the sample is transparent to the pump beam. Above the threshold, the upconversion emission intensity increases by orders of magnitude, and pump light is consequently strongly absorbed. The mechanism in Figure 2.5 can be described by considering a pump photon that populates the metastable state of ion I (marked by an asterisk). This is followed by non-radiative decay to the intermediate excited state, 2. A second incoming pump photon raises the ion to the highest excited state, 4, which non-radiatively decays to level 3. Following this process, a cross relaxation process will

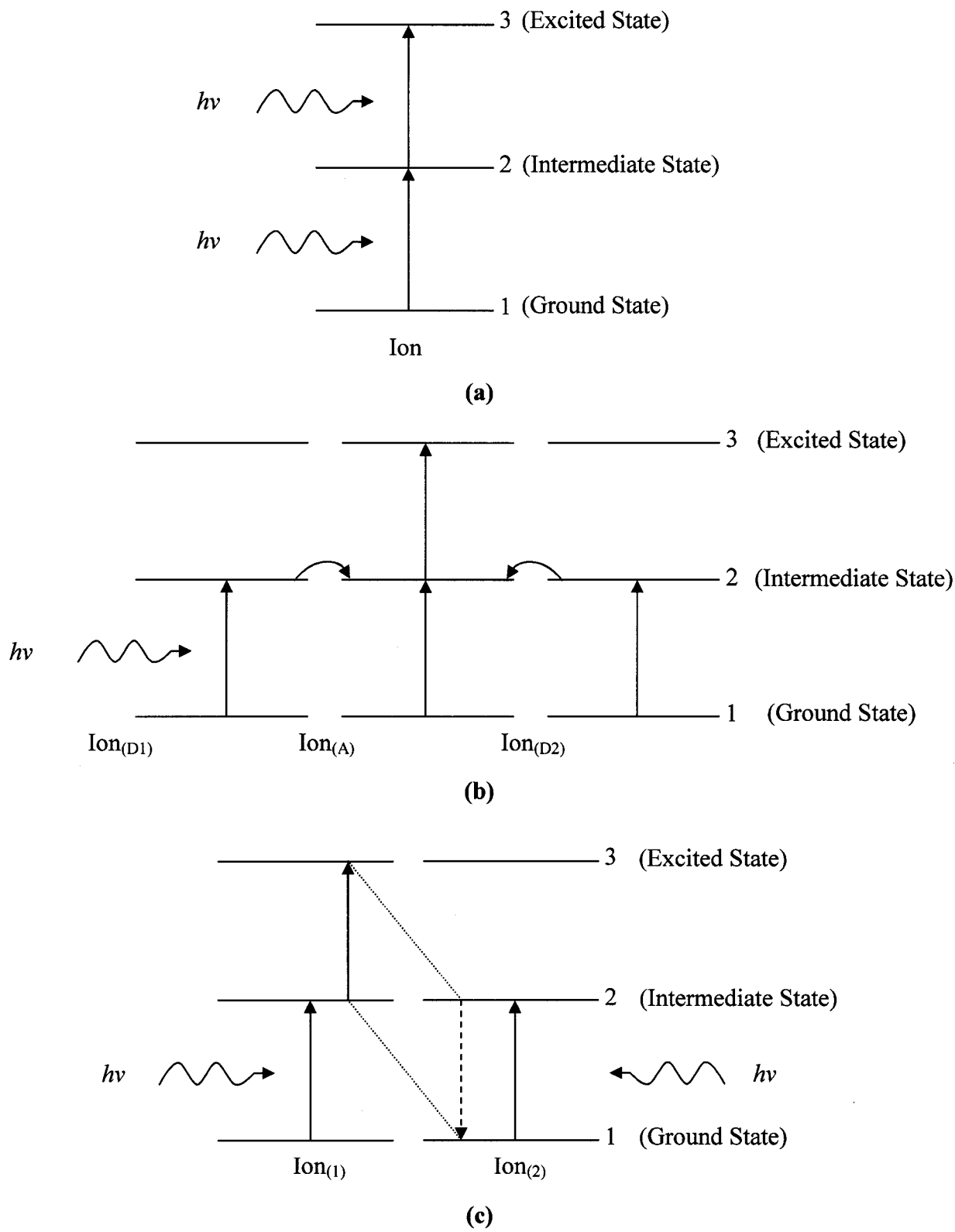

Figure 2. 4. Upconversion mechanisms: (a) excited state absorption (ESA), (b) energy transfer upconversion (ETU) and (c) energy transfer upconversion via cross-relaxation (CR) [6] (used with permission: F. Vetrone, Ph. D. Thesis, Concordia University (2005)).

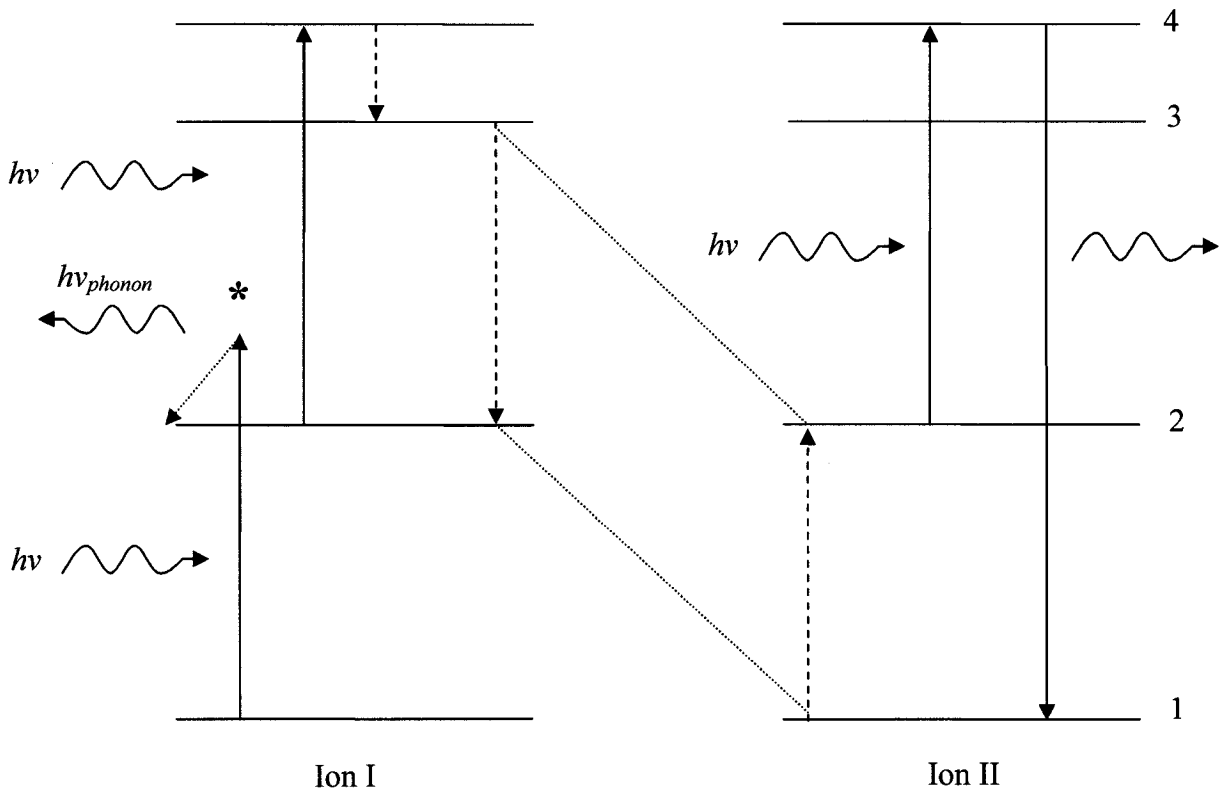

Figure 2. 5. Photon avalanche upconversion mechanism

relax the excited ion in 3 to excited state 2 and will excite a neighbouring ion (II) to intermediate excited state 2. At this stage of the mechanism, 2 ions are available in the intermediate excited state which can repeat through this process and results in 4, 16, 256....n^2 ions in the intermediate excited state. This "avalanche" of ions in the intermediate excited state will only occur once the threshold power is reached.

2.7 Multi-Phonon-Relaxation

In physics, a phonon is a quantized mode of vibration occurring in a rigid crystal lattice, such as the atomic lattice of a solid (glass or crystal). Phonons play a crucial role in the optical properties of the material as briefly discussed in Section 1.1 and 2.5. Phonons are a quantum mechanical equivalent of a special type of vibrational motion, known as "normal modes" in classical mechanics. In classical mechanics, normal modes of vibrations are said to occur when each part of a lattice oscillates with the same frequency. The connection between the atoms in a rigid system gives rise to what is known as "vibrational waves" since the displacement of the atoms from their equilibrium position coupled with their connectivity in the solid results in the propagation of the wave through the lattice [96-98]. A phonon can therefore be simply referred to as a lattice vibration. It follows that phonon-related processes exhibit a certain temperature dependence.

From a spectroscopic approach, relaxation to a lower lying level for an ion in the excited state to a lower lying intermediate excited state or the ground state may occur via non-radiative pathways. In the simplest case, the transition between the two levels is a direct process and upon occurrence the energy difference separating the levels is used to create a phonon of the same energy. This phonon then dissipates through the lattice [85].

The interactions with phonons induce transitions between the various crystal field levels in the system and hence result in a shortening of the lifetime of the transitions. Consequently, it will also result in the broadening of the spectral lines of the system.

Chapter III

3.1 Praseodymium-Doped Gadolinium Gallium Garnet (GGG) Bulk and Nanoparticles

The bulk (single crystal) gadolinium gallium garnet sample was doped with 1 mol% Pr^{3+} and was grown using the Czochralski technique. The crystal growth was carried out under an O_2 atmosphere [99, 100].

Cubic $Gd_3Ga_5O_{12}$ nanocrystals doped with either 0.1, 1, 5 or 10 mol% Pr^{3+} ($Gd_{2.97}Pr_{0.03}Ga_5O_{12}$) were prepared using a solution combustion (propellant) synthesis procedure according to the following reaction [101]:

$$3(1\text{-}x)Gd(NO_3)_3 + 5Ga(NO_3)_3 + 3xPr(NO_3)_3 + 3(NH_2NH)_2CO \rightarrow$$

$$(Gd_{1\text{-}x}Pr_x)_3Ga_5O_{12} + 24NO_2 + 6N_2 + 3CO_2 + 9H_2O \qquad (3.1)$$

XRD linewidth measurements in combination with TEM micrographs showed that this technique yields cubic GGG nanocrystals on the order of approximately 20 nm in diameter [102] (Figure 3.1). All nanocrystalline samples were kept in air without any further precaution.

Further details of the synthesis of the bulk and nanocrystals are summarized in Appendix A1.1 and A1.2.

Figure 3. 1. TEM Micrograph of gadolinium gallium garnet nanocrystals

3.2 Experimental Setup

Visible room temperature emission spectra (457.9 nm) were obtained using a Coherent Sabre Innova, 20 W cw argon ion laser. The laser line was tuned prior to spectra collection to ensure proper functionality and maximum power output. Emission Spectra were recorded using a Jarrell-Ash 1 meter Czerny-Turner double monochromator with a slit width of 150 μm. The gratings are mounted on a cosecant bar driven by a stepper motor with a step size of 0.01 cm^{-1}/step. A Hamamatsu R943-02 photomultiplier with a flat spectral response of 200-850 nm was used to monitor the spectral signal.

Background dark count rate was kept to below 10 counts per second via thermoelectric cooling. The photomultiplier signal was processed through a Stanford Research Systems SR440 preamplifier before being sent to the Stanford Research Systems SR400 gated photon counter equipped with a computer running the Stanford SR465 data collection software. The equipment setup is shown in Figure 3.2.

Infrared (IR) emission spectra were measured by exciting the sample with the 457.9 nm line of a Coherent Sabre Innova argon ion laser (20 W). The infrared emission spectra were recorded using a Jarrell-Ash ¾ meter monochromator in second order. The fluorescence signal was monitored using a North Coast EO-817P liquid nitrogen cooled germanium detector. The detector was filled with liquid nitrogen and allowed to cool for one hour prior to any analysis. A Stanford Research System SR510 lock-in amplifier equipped with a computer running the lock-in data acquisition software was used to analyze the detector signal.

A Coherent Sabre Innova argon ion laser (20 W) was used to pump a Spectra Physics 375 tunable dye laser. The Rhodamine 6G dye was used to obtain the

fluorescence spectra at the desired wavelength of 606.9 nm. The argon ion laser was also used to pump a Ti:Al_2O_3 laser (titanium sapphire laser, 980 nm). The dye laser and the Ti-sapphire laser were both used in the study of upconversion luminescence.

Lifetime curves were measured by modulating the cw 457.9, 606.9 and 980 nm excitation lines using a Stanford Research Systems SR540 optical chopper and obtained using the aforementioned data acquisition system.

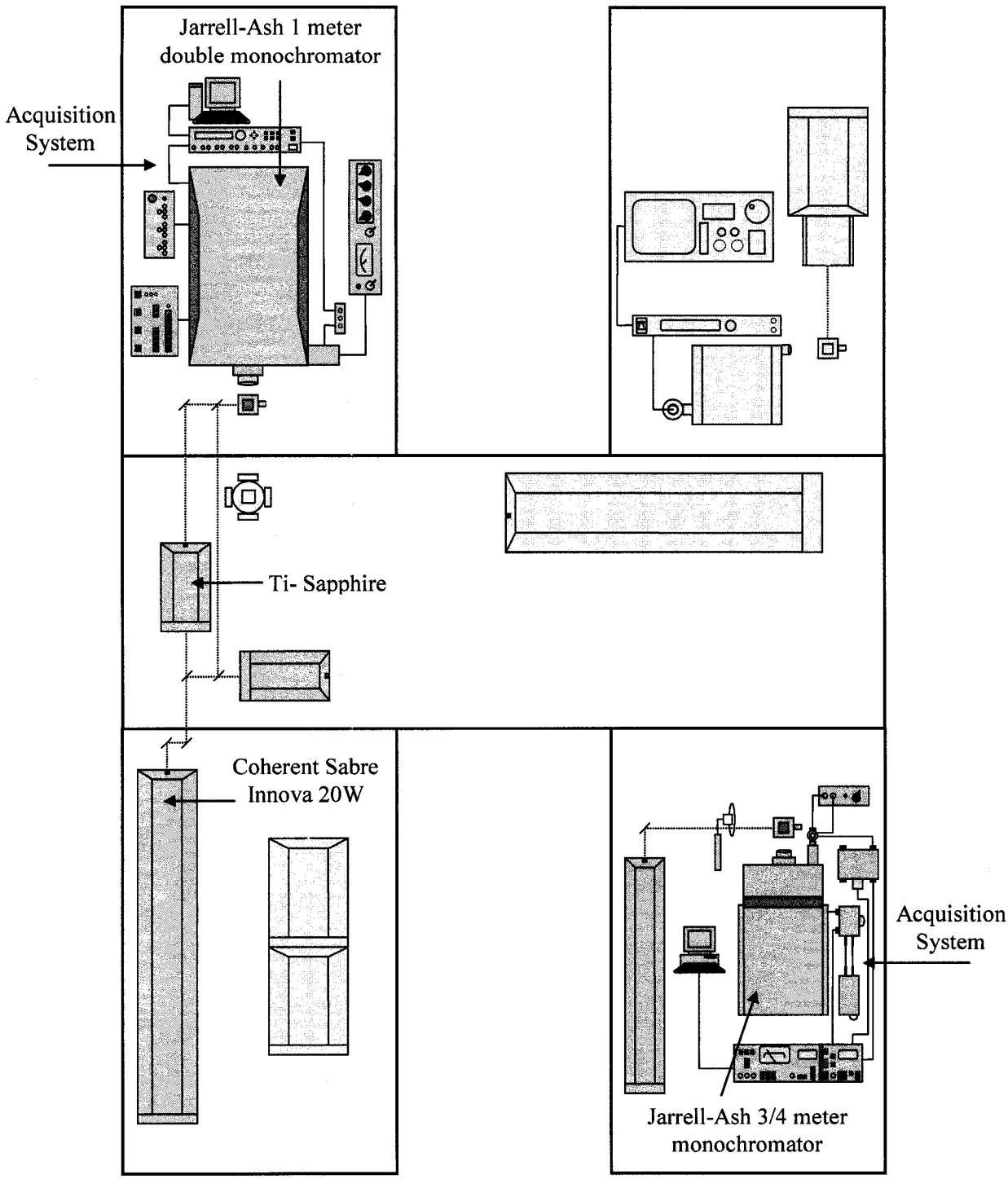

Figure 3. 2. Schematic of the equipment setup and arrangement [6] (used with permission: F. Vetrone, Ph. D. Thesis, Concordia University (2005)).

Chapter IV

4.1 Visible Room Temperature Emission of Singly-Doped Bulk and Nanocrystals

Following direct excitation into the $^1I_6$ level using a wavelength of 457.9 nm, blue/green, red and near infrared emission was observed for the 1 mol% Pr^{3+}-doped GGG nanocrystals and single crystal (Figure 4.1). The spectra are largely dominated by emission from the ^3P_J (J = 0, 1) and the $^1D_2$ levels. Blue/green emission centered at 473 nm and 487 nm was observed to originate from the $^3P_1 \rightarrow {}^3H_4$ and $^3P_0 \rightarrow {}^3H_4$ transitions, respectively. The $^3P_1$ state is populated primarily through thermalization from the $^3P_0$ energy level as the distance separating the two energy levels is comparable at room temperature. Green emission centered at 531 nm and 561 nm was attributed to the $^3P_1 \rightarrow {}^3H_5$ and $^3P_0 \rightarrow {}^3H_5$ transitions. Furthermore, red emission from the $^3P_1 \rightarrow {}^3H_6$, $^1D_2 \rightarrow {}^3H_4$, $^3P_0 \rightarrow {}^3H_6$, $^3P_0 \rightarrow {}^3F_2$ and $^3P_1 \rightarrow {}^3F_{3,4}$ transitions were centered at 596, 607, 617, 658 and 696 nm, respectively. Finally, NIR emission from the $^3P_0 \rightarrow {}^3F_3$ and $^3P_0 \rightarrow {}^3F_4$ transitions was observed at 712 nm and 740 nm, respectively. The observed transitions were assigned (Table 4.1) and are in accordance with the assignment of tripositive praseodymium transitions previously reported in the literature such as in the works of Balda [103-105], Yen [13], Meijerink [106] and Malinowski [107, 108].

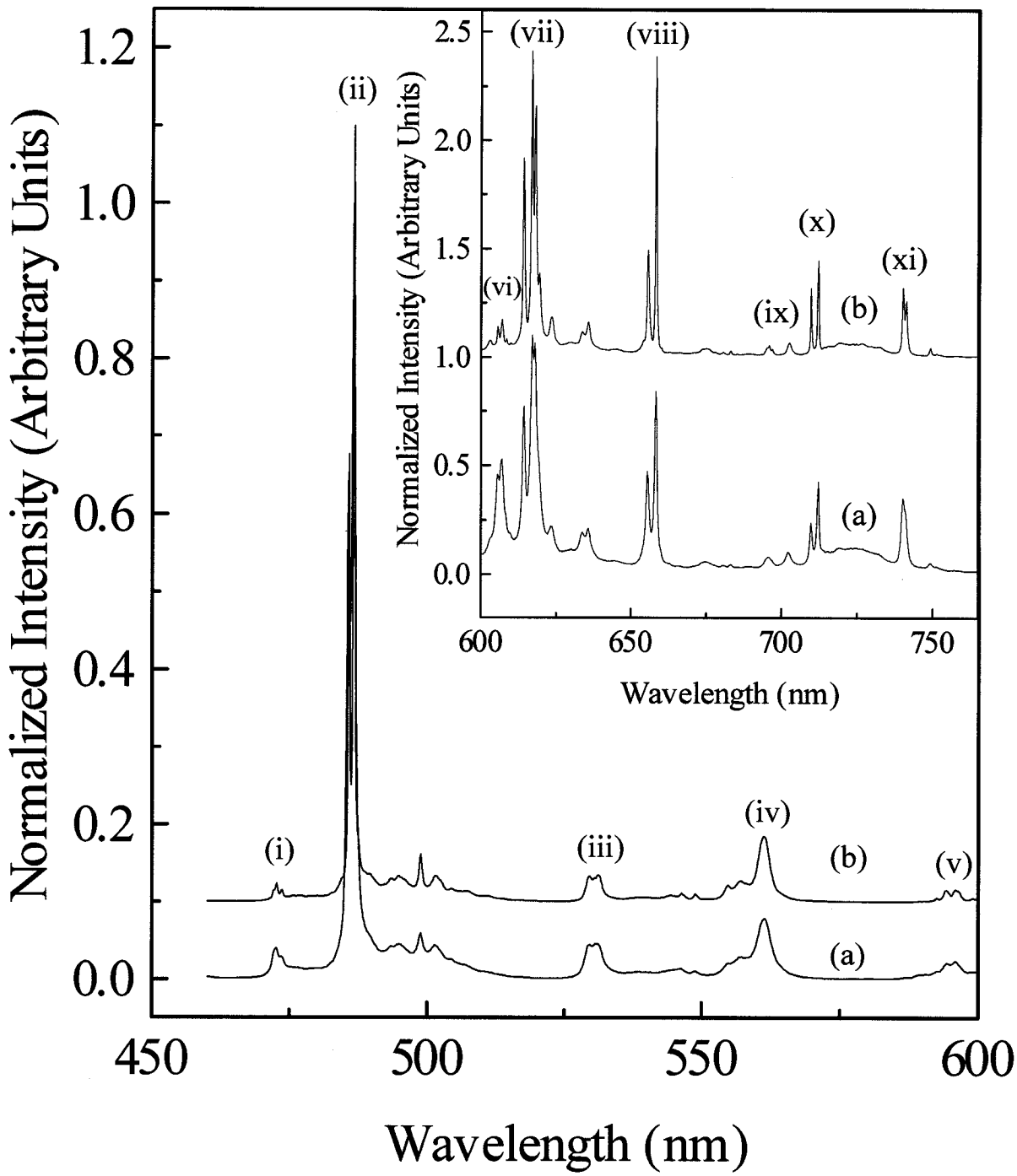

Figure 4. 1. Room temperature visible emission spectra (λ_{exc} = 457.9 nm) of GGG:Pr^{3+} (1%) (a) nanocrystals and (b) single crystal – (i) $^3P_1 \rightarrow {}^3H_4$, (ii) $^3P_0 \rightarrow {}^3H_4$, (iii) $^3P_1 \rightarrow {}^3H_5$, (iv) $^3P_0 \rightarrow {}^3H_5$, (v) $^3P_1 \rightarrow {}^3H_6$, (vi) $^1D_2 \rightarrow {}^3H_4$, (vii) $^3P_0 \rightarrow {}^3H_6$, (viii) $^3P_0 \rightarrow {}^3F_2$, (ix) $^3P_1 \rightarrow {}^3F_{3,4}$, (x) $^3P_0 \rightarrow {}^3F_3$, (xi) $^3P_0 \rightarrow {}^3F_4$.

Table 4. 1. Peak assignment for praseodymium transitions

Pr^{3+} Transition	Wavelength/Wavenumber (nm/cm^{-1})
$^3P_1 \rightarrow {}^3H_4$	472.67 / 21156
$^3P_0 \rightarrow {}^3H_4$	486.71 / 20546
$^3P_1 \rightarrow {}^3H_5$	531.22 / 18825
$^3P_0 \rightarrow {}^3H_5$	561.40 / 17813
$^3P_1 \rightarrow {}^3H_6$	596.00 / 16779
$^1D_2 \rightarrow {}^3H_4$	606.94 / 16476
$^3P_0 \rightarrow {}^3H_6$	616.83 / 16212
$^3P_0 \rightarrow {}^3F_2$	657.96 / 15198
$^3P_1 \rightarrow {}^3F_{3,4}$	695.92 / 14369
$^3P_0 \rightarrow {}^3F_3$	712.27 / 14040
$^3P_0 \rightarrow {}^3F_{3,4}$	740.11 / 13512

4.2 Infrared Emission

In contrast to the strong and predominantly blue visible emission upon excitation using a wavelength of 457.9 nm, weak IR emission, under the same excitation source, was observed for both the bulk and nano systems. The observed emission was attributed to the $^1D_2 \rightarrow {}^3H_6$, $^3F_2$ levels and the $^1D_2 \rightarrow {}^3F_{3,4}$ lower lying states (Figure 4.2). The weak IR emission was attributed to cross-relaxation and weak non-radiative decay due to low intrinsic phonon energy of the host; there is a minimal quantity of high energy phonons available through adsorption of hydroxyl and carbonate ions on the surface of the Pr^{3+}-doped gadolinium gallium garnet nanosystems. The $^1G_4$ energy level is typically populated via excitation into the $^1I_6$ level of Pr^{3+} using 457.9 nm followed by successive non-radiative decay processes to the lower lying $^3P_0$, $^1D_2$ intermediate excited states and finally the $^1G_4$ energy level.

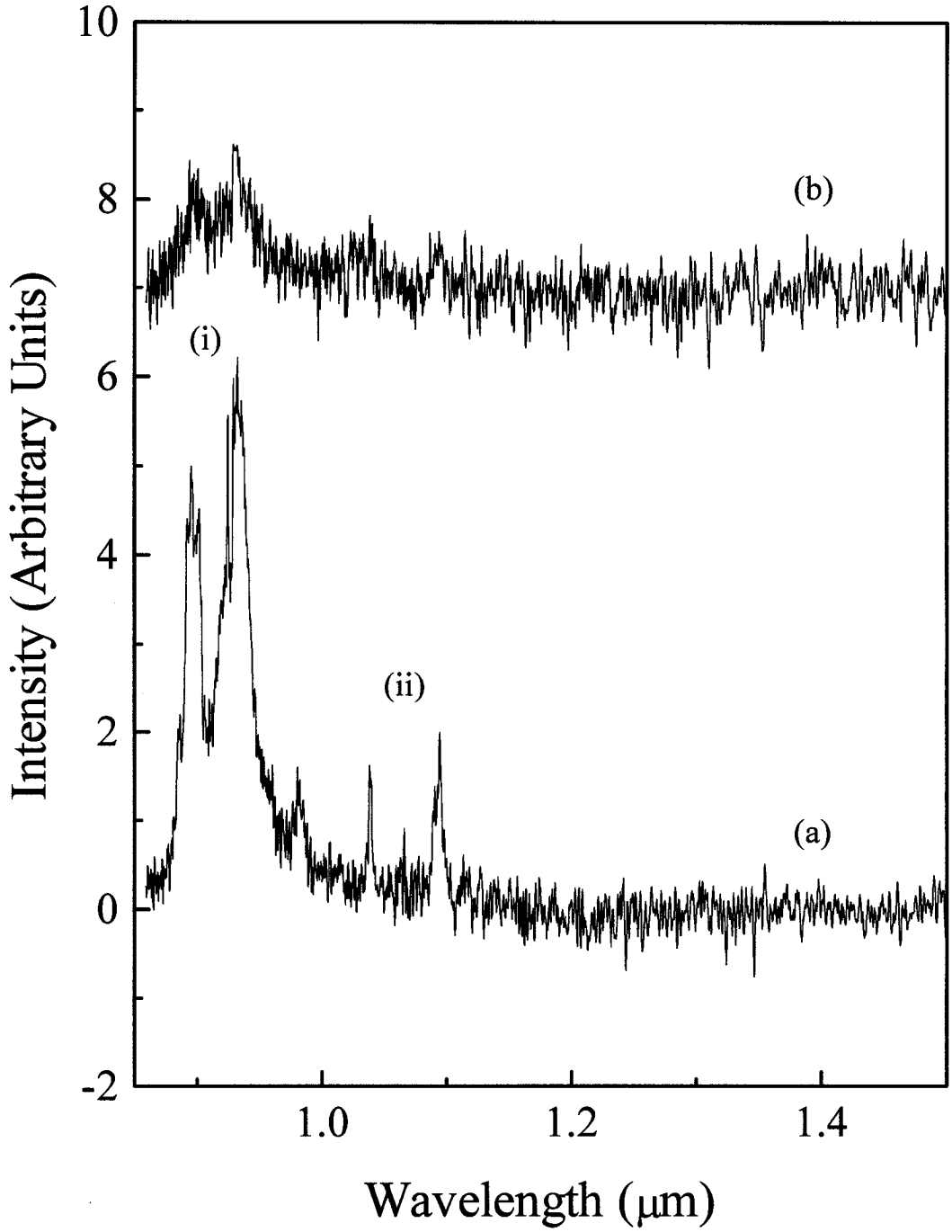

Figure 4. 2. IR Emission of Pr^{3+}-doped (a) bulk and (b) Nanocrystalline gadolinium gallium garnet. IR emission observed corresponds to the (i) $^1D_2 \rightarrow {}^3H_6$, $^3F_2$ and (ii) $^1D_2 \rightarrow {}^3F_{3,4}$ transitions.

As previously mentioned, the intrinsic phonon energy of GGG is 600 cm^{-1} and therefore would require approximately 6 phonons ($^3P_0 \rightarrow {}^1D_2$, ΔE = ~3500 cm^{-1}) to bridge the energy gap followed by approximately 10 phonons to bridge the $^1D_2 \rightarrow {}^1G_4$ gap (ΔE = ~6500 cm^{-1}). It follows that the probability of population of the $^1G_4$ energy level through multiphonon relaxation is relatively weak.

The $^1G_4$ energy level may be alternatively populated through cross-relaxation. The cross-relaxation process is favoured due to the quasi-similar energy gaps (ΔE) separating the various transitions of the tripositive praseodymium ion. In this case, following excitation into the $^1I_6$ level of Pr^{3+} using 457.9 nm followed by non-radiative decay to the lower lying $^3P_0$ level, a cross relaxation mechanism (Figure 4.3) may occur to populate the $^1G_4$ energy level. The mechanism may be expressed as $[^3P_0, {}^3H_4] \rightarrow [^1G_4, {}^1G_4]$. This may however be immediately followed by a subsequent cross-relaxation mechanism (also shown in Figure 4.3) which may be expressed as $[^1G_4, {}^1D_2] \rightarrow [^3H_6, {}^3P_0]$ thereby depopulating the $^1G_4$ energy level and re-populating the $^3P_0$ state. The ions in the $^1G_4$ intermediate excited state relax to the lower lying $^3H_6$ level while the ions present in the $^1D_2$ level are raised to the $^3P_0$ excited state.

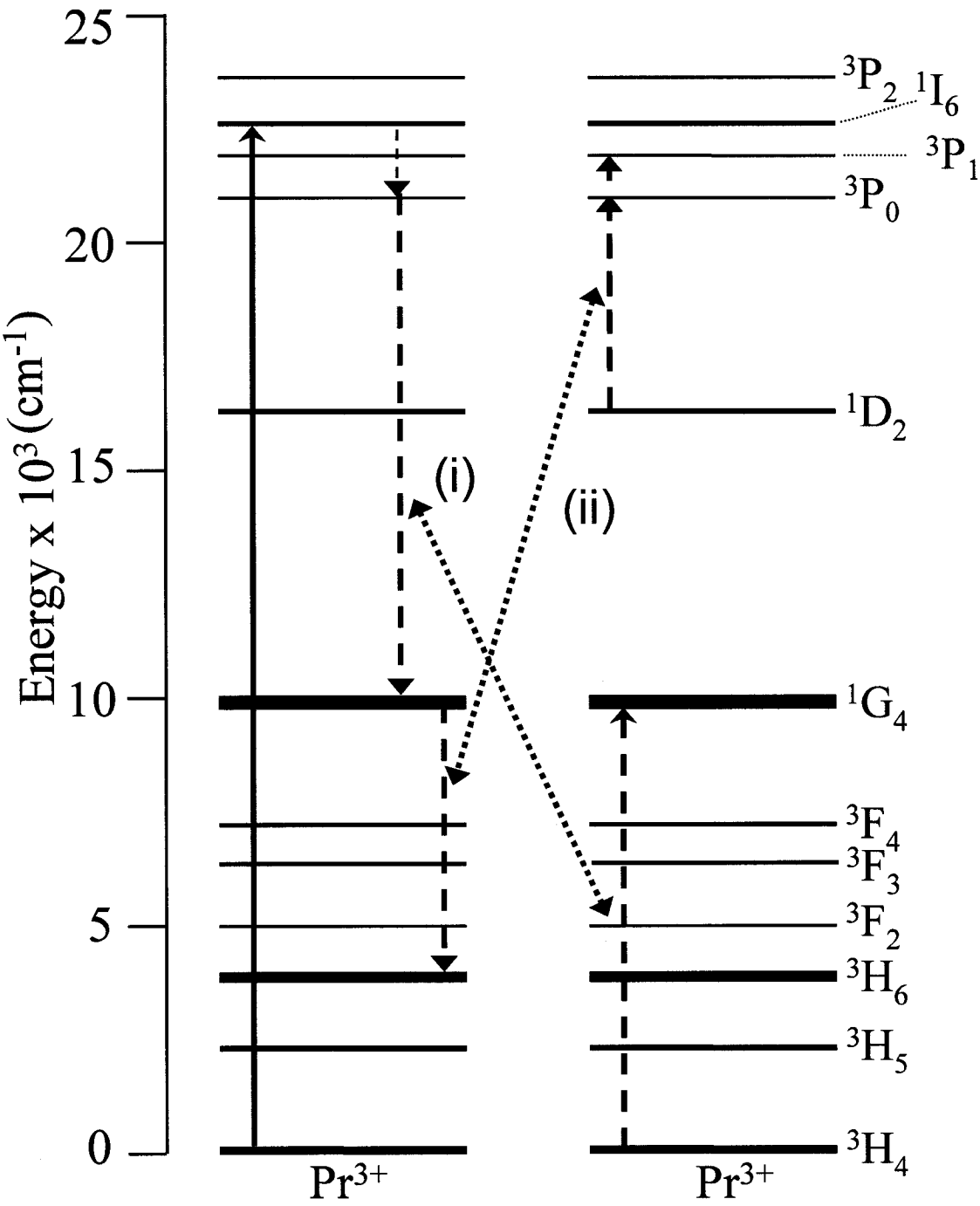

Figure 4. 3. Cross-relaxation mechanism responsible for (i) population of the $^1G_4$ energy level [$^3P_0$, $^3H_4$] → [$^1G_4$, $^1G_4$] and (ii) depopulation of the $^1G_4$ energy level [$^1G_4$, $^1D_2$] → [$^3H_6$, $^3P_0$].

4.3 Lifetime Measurements

Lifetime measurements following excitation using a wavelength of 457.9 nm for the 1 mol% Pr^{3+}-doped GGG single crystal and nanocrystals are reported in Table 4.2 and were determined by fitting the lifetime curves with a single exponential model. The lifetimes of the $^3P_0 \rightarrow {}^3H_4$ transition were found to be 18 and 24 μs for the nanocrystals and bulk sample, respectively (Table 4.2).

Table 4. 2. Lifetimes of 1% GGG:Pr^{3+} nanocrystals and single crystal following excitation using a wavelength of 457.9 nm.

Transition	**$Gd_3Ga_5O_{12}:Pr^{3+}$ Lifetimes (μs)**	
	Pr^{3+} Nanocrystals	**Pr^{3+} Single Crystal**
$^3P_0 \rightarrow {}^3H_4$	18	24
$^1D_2 \rightarrow {}^3H_4$	105	157

Previous work carried out on rare earth-doped cubic yttria nanocrystals showed a significant decrease of the lifetimes of the nanoparticles relative to the bulk (micrometer) material [47, 109]. This observation was attributed to highly efficient multiphonon relaxation in the nanocrystals due to adsorption of CO_2 and H_2O on the surface of the yttria nanoparticles, due to the high surface area of the porous material. The carbonate and hydroxyl ions provide for higher energy phonons (1500 and 3350 cm^{-1}, respectively). As a result, the efficiency of the non-radiative relaxation to lower lying levels increases tremendously as it requires fewer phonons to bridge the gap between the emitting state and the level right underneath it [110]. GGG nanocrystals on the other hand have been previously shown, using mid infrared (MIR) spectroscopy [111], to have little tendency for CO_2 and H_2O adsorption on the surface of the nanoparticles. As a result, the lifetimes

of the $^3P_0$ level for the nanocrystalline material and the single crystal are similar. On the other hand, at least six GGG phonons (maximum phonon energy of 600 cm^{-1}) are required to fill the gap between the $^3P_0$ and the next lower $^1D_2$ level. Therefore, the non-radiative decay probability significantly decreases for both the nanocrystalline and single crystal hosts. Hence, the lifetimes of the ^3P_J (J=0, 1) levels should be similar in both hosts, as experimentally observed.

The lifetime of the $^1D_2 \rightarrow {}^3H_4$ transition was measured to be 157 μs and 105 μs for the single crystal and the nanocrystals, respectively. The lifetime of the $^1D_2$ state therefore differed for both samples contrary to what was observed for the ^3P_J transitions. The $^1D_2 \rightarrow {}^3H_4$ transition is hypersensitive [12, 110, 112, 113] and thus induces a shortening of the lifetime in the nanocrystals. The optical properties (intensity and lifetime) of hypersensitive transitions are strongly affected by the environment and the ligand coordination. At the nano scale, a large fraction of the dopant ions is found on the surface relative to the center of the particle. Those dopant ions experience a different crystal field; they experience a more disordered environment with respect to the ions in the particle center [114]. Consequently, this likely contributes to the lowering of the Pr^{3+} site symmetry and a decrease in the lifetime. This is further supported by the ratio of emission intensities from the $^1D_2$ and $^3P_0$ levels to the $^3H_4$ ground state. The intensity ratio of the $^1D_2$ / $^3P_0$ emission in the single crystal was calculated to be 0.017, while in the nanocrystals, this value increases to 0.053. Furthermore, in the nanocrystalline material, the lifetime of the $^1D_2$ state is likely reduced due to cross-relaxation occurring between neighbouring Pr^{3+} ions through the $[^1D_2,{}^3H_4] \rightarrow [^1G_4,{}^3F_{3,4}]$ mechanism. This cross

relaxation mechanism is favoured due to the match in energy gap separating the involved states [12, 112, 115].

The differences in the crystal fields between the single crystal and the nanocrystals can also be observed from the emission spectra. The bands in the spectrum of the nanocrystals are slightly broadened compared to those in the emission spectrum of the bulk. The broadening occurs because the Pr^{3+} ions near the surface will experience a different crystal field than the ions buried inside the particle. The resulting emission spectrum is therefore a superposition of the different Pr^{3+} emissions and broadening is observed.

4.4 Visible Upconversion Emission

Following excitation in the $^1D_2$ level using a wavelength of 606.9 nm, blue/green upconverted emission was observed in the nanocrystalline and the single crystal samples (Figure 4.4). Upconverted emission was observed to originate from the $^3P_1 \rightarrow {}^3H_4$ and the $^3P_0 \rightarrow {}^3H_4$ transitions at 472 and 487 nm, respectively. In an effort to elucidate the operative upconversion mechanisms for the GGG:Pr^{3+} materials, a power dependence study was carried out. It has been previously shown in the literature that the upconverted luminescence (I_o) is proportional to the pump intensity (I_p) raised to a power n (where n = 1, 2, 3...). The value of n reflects the number of photons required to populate the emitting state and was determined from the slope of the plot of ln I_o versus ln I_p (Figure 4.5).

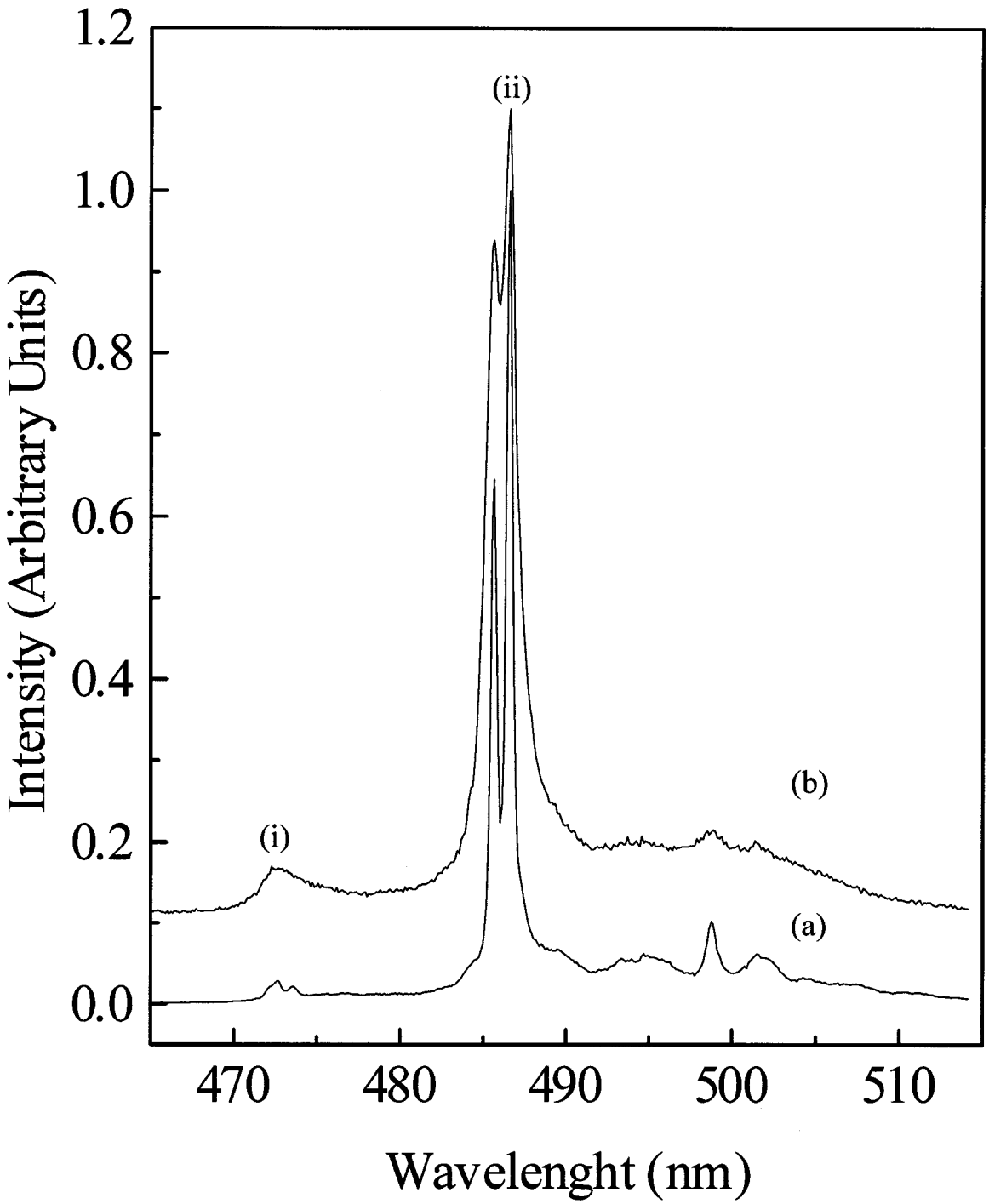

Figure 4. 4. Room temperature upconversion emission spectra (λ_{exc} = 606.9 nm) of GGG:Pr^{3+} (1%) (a) bulk and (b) nanocrystals – (i) $^3P_1 \rightarrow {}^3H_4$, (ii) $^3P_0 \rightarrow {}^3H_4$.

A linear regression fit was used and a slope value of 1.8 was obtained for the upconversion emission from the $^3P_0 \rightarrow {}^3H_4$ transition in the nanocrystals. Similarly, a slope of 2.2 was obtained for the upconverted emission from the $^3P_0 \rightarrow {}^3H_4$ energy level in the single crystal. This indicates that upconversion occurs via a 2-photon process for both samples.

Population of the $^3P_1$ and $^3P_0$ states can occur via two possible mechanisms namely excited state absorption (ESA) and energy transfer upconversion (ETU). Upconversion via a photon avalanche (PA) mechanism was not considered as no power threshold and thus no inflection point was observed during the power study. The lifetime of the $^3P_0 \rightarrow {}^3H_4$ transition upon excitation at 606.9 nm was measured for both samples. Lifetimes of 80 μs and 50 μs were observed for the single crystal and nanocrystals, respectively (Table 4.3).

Table 4. 3. Upconversion lifetimes for the $^3P_0 \rightarrow {}^3H_4$ transition in 1% GGG:Pr^{3+} nanocrystals and single crystal following excitation using a wavelength of 606.9 nm and 980 nm.

Excitation Wavelength (nm)	**$Gd_3Ga_5O_{12}:Pr^{3+}$ Lifetimes (μs)**	
	Pr^{3+} Nanocrystals	**Pr^{3+} Single Crystal**
606.9	50	80
980	22	-----

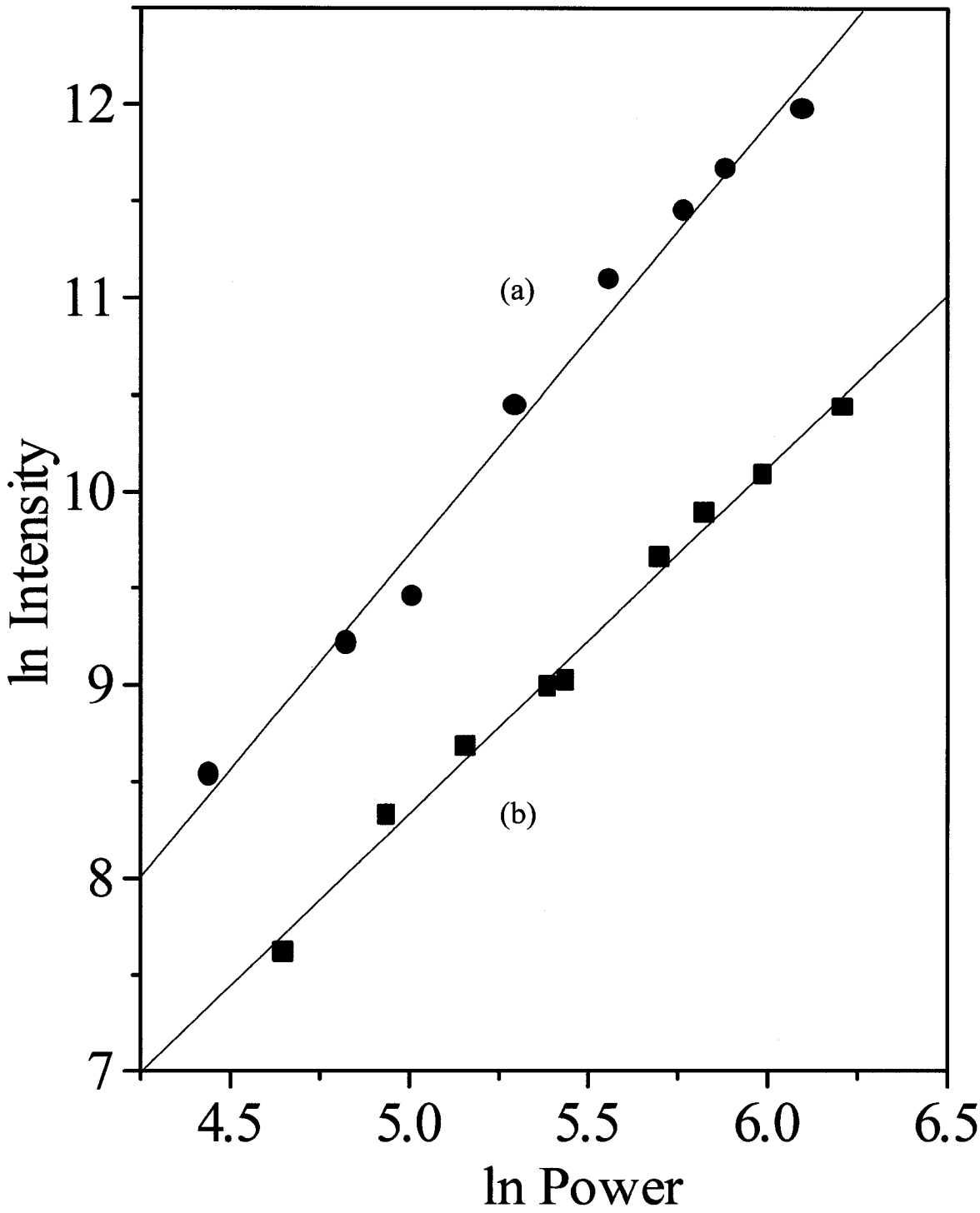

Figure 4. 5. Power dependence study for the upconversion emission of the $^3P_0 \rightarrow {}^3H_4$ transition (λ_{exc} = 606.9 nm) of GGG:Pr^{3+} (1%) (a) nanocrystals (slope = 1.8) and (b) single crystal (slope = 2.2).

This represents about a 2 or 3-fold increase for the nanocrystalline and the bulk samples, respectively, relative to the values obtained upon direct excitation using a wavelength of 457.9 nm. The lengthening of the lifetime is characteristic of an ETU mechanism. This occurs as the upconversion process is a two-ion process and is dependent on the lifetime of the intermediate state from which ET occurs. The contribution of an ESA mechanism should not be overlooked as upconversion is likely occurring through both competing mechanisms. Unlike the lifetimes measured after excitation at 457.9 nm, the upconversion lifetimes (λ_{exc} = 606.9 nm) of the single crystal and nanocrystals differ significantly and this is attributed to the cross relaxation mechanism occurring in the nanocrystals.

The proposed upconversion mechanisms at 606.9 nm are shown in Figure 4.6. In the ESA mechanism, a Pr^{3+} ion is raised to an intermediate excited state, the $^1D_2$ level. This is followed by non-radiative decay to the lower lying $^1G_4$ level and subsequently to the $^3F_3$ and $^3H_6$ states. A second pump photon then raises the ion to either the $^3P_2$ or the $^3P_0$ levels from which radiative emission was observed. In the ETU mechanism, excitation using a wavelength of 606.9 nm results in two neighbouring Pr^{3+} ions being raised to the $^1D_2$ intermediate excited state. One Pr^{3+} ion will non-radiatively decay to the lower lying $^3F_3$ and $^3H_6$ levels as previously mentioned for the ESA mechanism above after which it is excited to either the $^3P_2$ or $^3P_0$ levels through a non-radiative energy transfer from the second ion in the intermediate state.

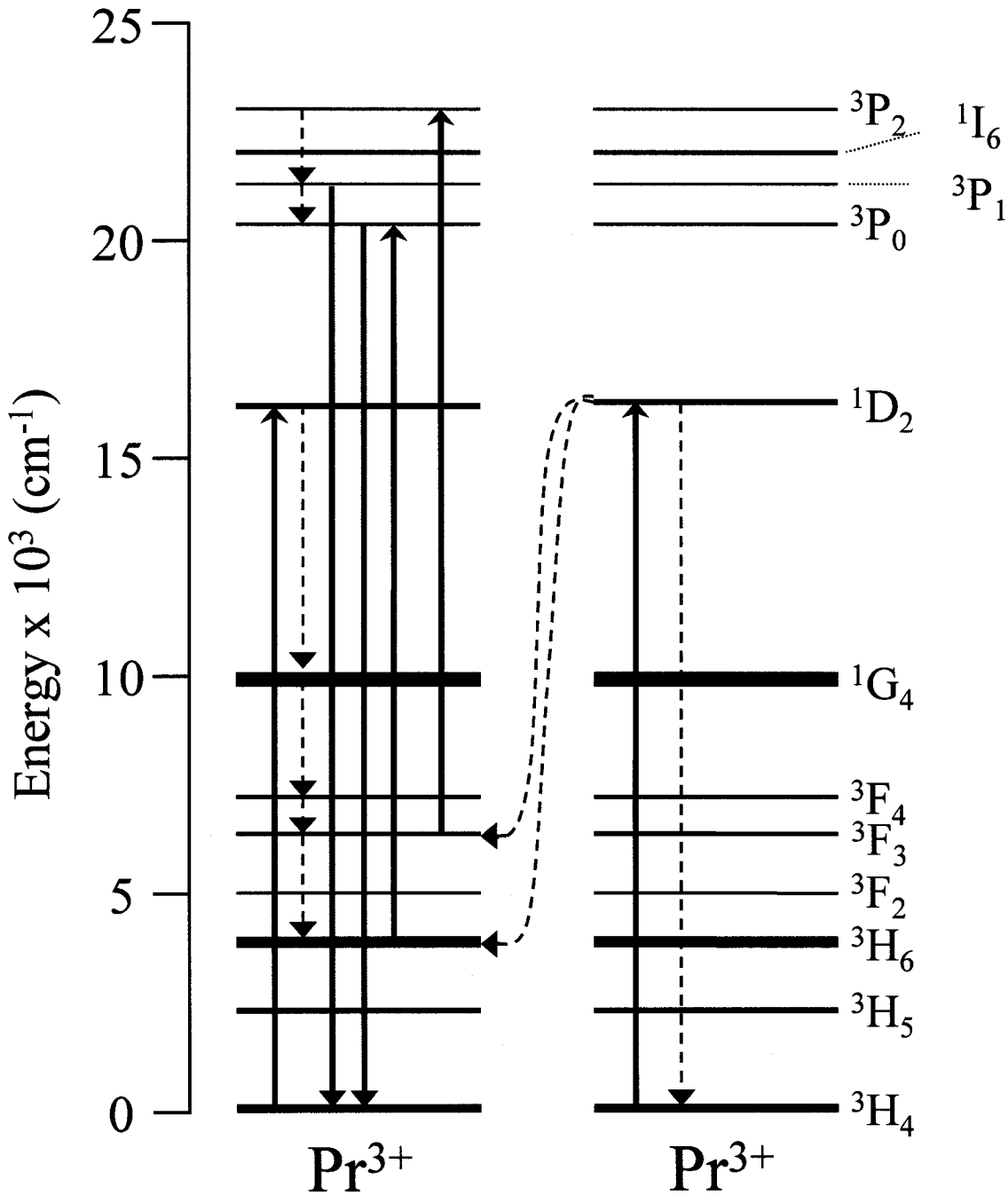

Figure 4. 6. Proposed upconversion mechanism using an excitation wavelength of 606.9 nm for the GGG:Pr^{3+} (1%) single crystal and nanocrystals – shown above are excited state absorption (ESA) and energy transfer upconversion (ETU) mechanisms.

The process of upconversion was further investigated for the GGG nanocrystals upon excitation into the $^1G_4$ state using a wavelength of 980 nm. The resultant upconversion spectrum was similar to that obtained after direct excitation at 457.9 nm showing emission from the $^3P_{0,1}$ levels to the various ^3F_J (J = 2, 3, 4) and $^3H_{J'}$ (J' = 4, 5, 6) states, as well as emission from the $^1D_2$ energy level to the $^3H_4$ ground state (Figure 4.7). A power study was carried out and a linear regression fit was used and a slope value of 2.2 was obtained for the upconversion emission from the $^3P_0 \rightarrow {}^3H_4$ transition in the nanocrystals (Figure 4.8).

This indicates that upconversion was occurring once again through a 2-photon mechanism. The lifetime for the upconversion emission from the $^3P_0$ state was fitted using a single exponential function and a value of 22 μs was obtained. The upconversion lifetime was similar to that obtained upon direct excitation at 457.9 nm. The observed similarity in the lifetime measurements suggests that ESA is the predominant mechanism involved in the upconversion process. It should be noted that a relatively weaker upconversion, following excitation with 980 nm, was observed in the single crystal. The proposed upconversion mechanism, at 980 nm, is shown in Figure 4.9. In the ESA mechanism, the $^1G_4$ intermediate excited state of the Pr^{3+} ion state is populated by a 980 nm photon after which a second pump photon then raises the ion to the $^3P_0$ level resulting in the observed emission. The ESA mechanism is a resonant process and thus it is possible that there may be a small shift in the crystal field Stark components in the nanocrystals such that ESA is resonant in this material and not in the single crystal.

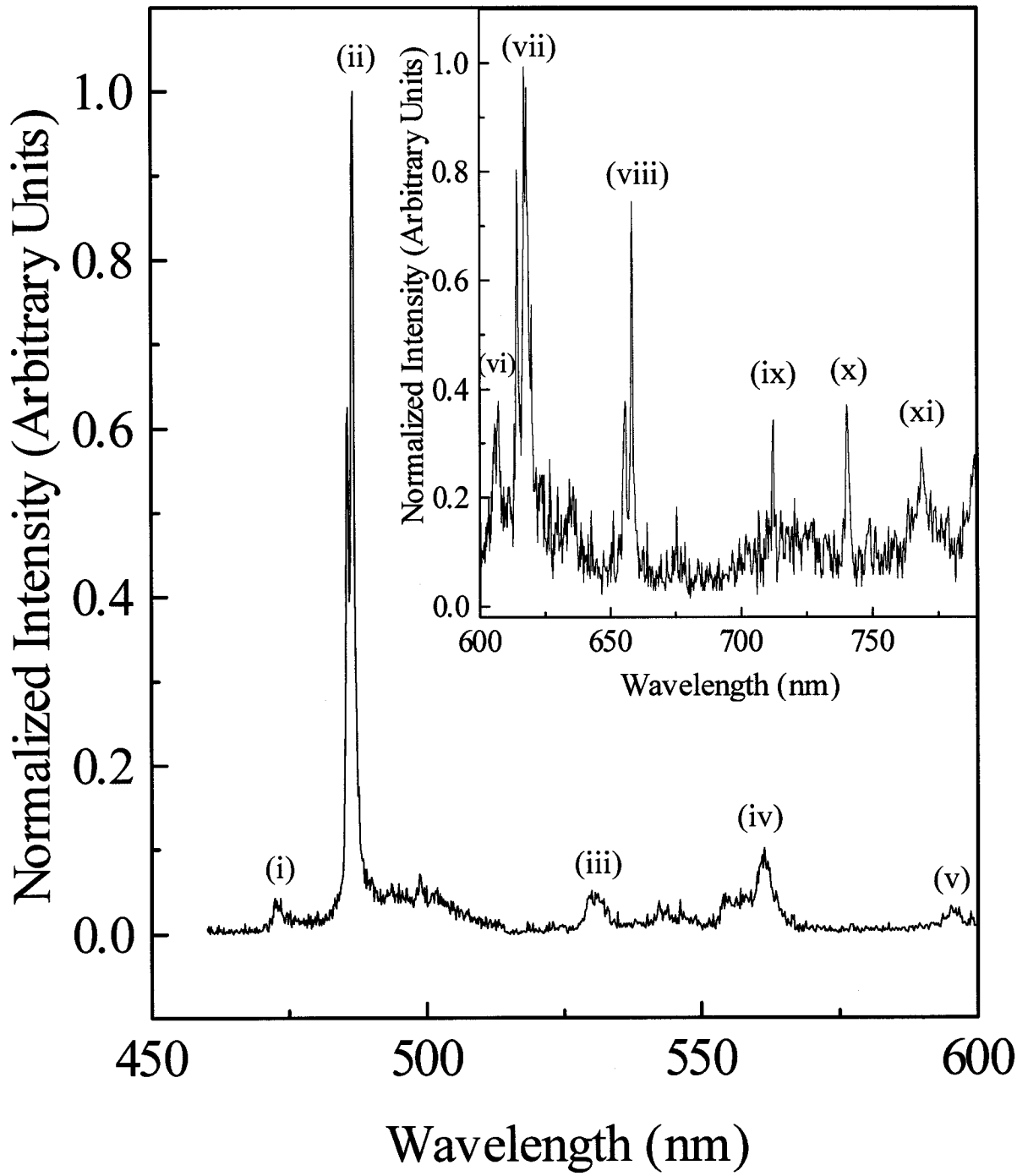

Figure 4. 7. Room temperature upconversion emission spectrum (λ_{exc} = 980 nm) of GGG:Pr^{3+} (1%) nanocrystals – (i) $^3P_1 \rightarrow {}^3H_4$, (ii) $^3P_0 \rightarrow {}^3H_4$, (iii) $^3P_1 \rightarrow {}^3H_5$, (iv) $^3P_0 \rightarrow {}^3H_5$, (v) $^3P_1 \rightarrow {}^3H_6$, (vi) $^1D_2 \rightarrow {}^3H_4$, (vii) $^3P_0 \rightarrow {}^3H_6$, (viii) $^3P_0 \rightarrow {}^3F_2$, (ix) $^3P_1 \rightarrow {}^3F_{3,4}$, (x) $^3P_0 \rightarrow {}^3F_3$, (xi) $^3P_0 \rightarrow {}^3F_{3,4}$.

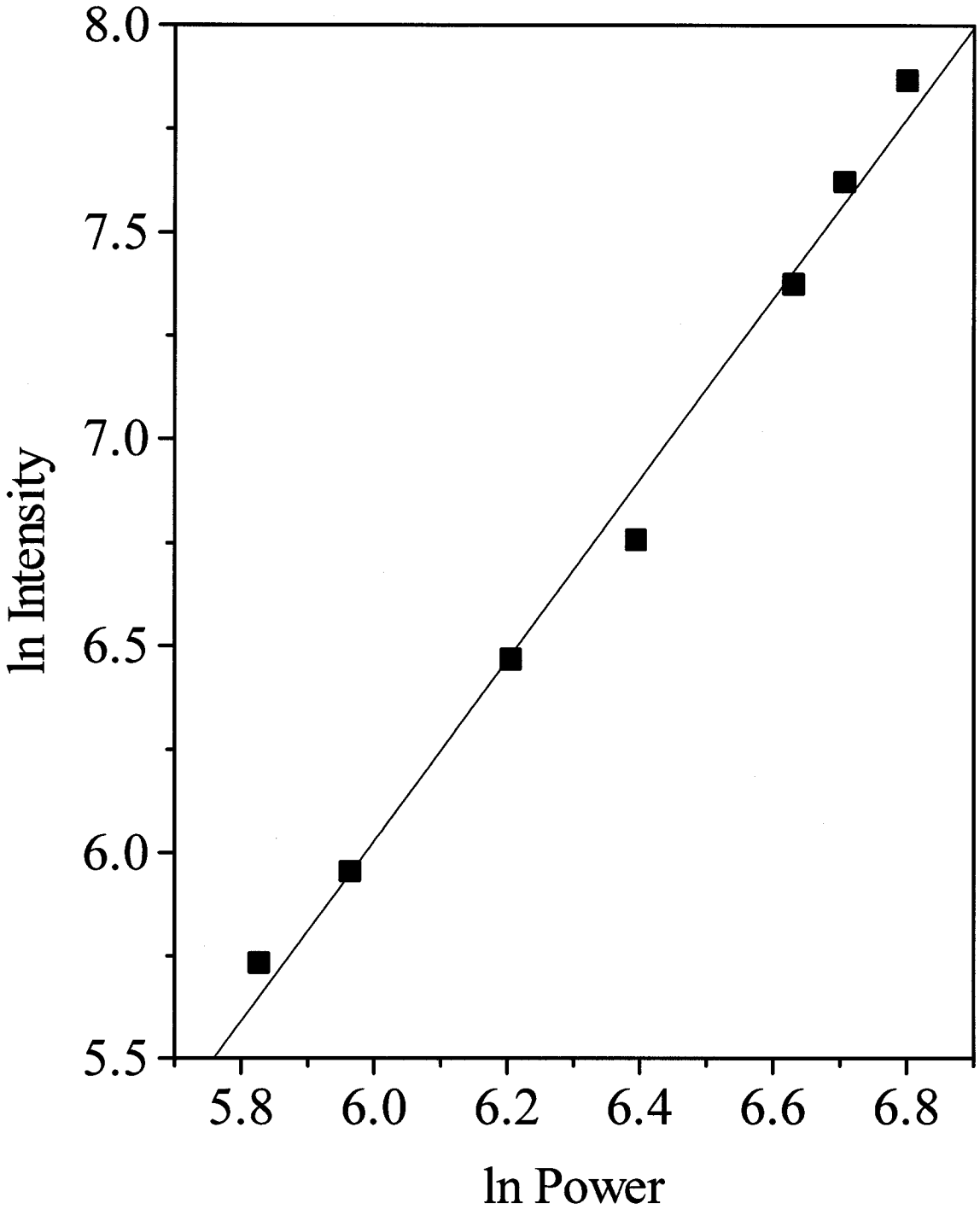

Figure 4. 8. Power dependence study for the upconversion emission of the $^3P_0 \rightarrow {}^3H_4$ transition (λ_{exc} = 980 nm) of GGG:Pr^{3+} (1%) nanocrystals.

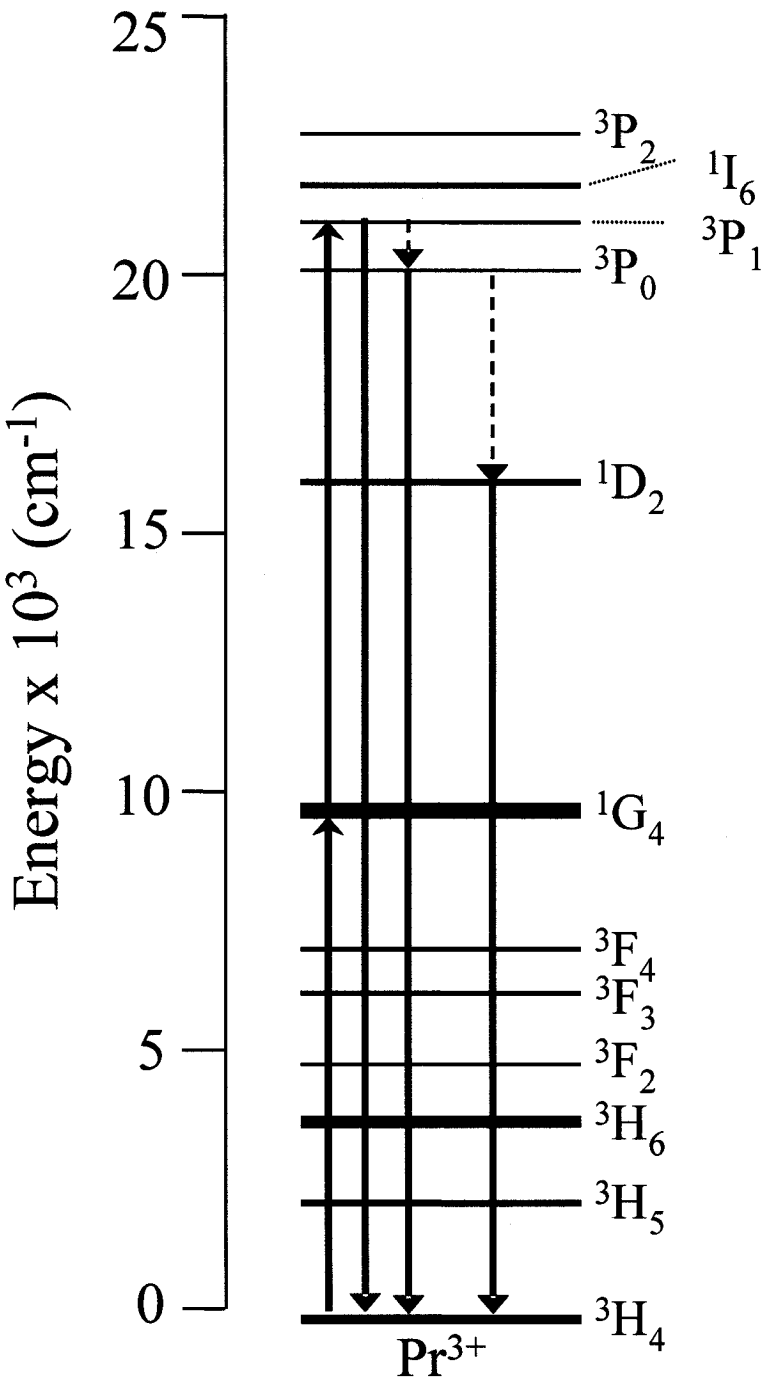

Figure 4. 9. Proposed upconversion mechanism using an excitation wavelength of 980 nm for the GGG:Pr^{3+} (1%) nanocrystals – shown above is the excited state absorption (ESA) mechanisms.

Chapter V

5.1 Effect of Dopant Concentration on the Visible Room Temperature Emission of Singly-Doped Nanocrystals

The optical properties of the nanocrystals were investigated as a function of dopant concentration in the system. Following direct excitation using a wavelength of 457.9 nm ($^1I_6$ energy level), blue/green, red and NIR emission was observed for the Pr^{3+}-doped GGG nanocrystals (Figure 5.1). All four samples largely exhibit dominant blue/green emission from the ^3P_J (J = 0, 1) energy levels. The resultant spectra were similar to those observed for the bulk and nanocrystalline samples discussed in Chapter 4.1. Peak assignment is consistent with that reported in Table 4.1.

Further evaluation of the raw un-normalized data reveals that the $^3P_0 \rightarrow {}^3H_4$ emission intensity decreases with increasing praseodymium concentration The $^3P_0 \rightarrow {}^3H_4$ emission quenching may occur via three different processes: (i) multiphonon relaxation (MPR) and the subsequent population of the $^1D_2$ level, (ii) cross relaxation mechanism between Pr^{3+} ion pairs in the $^1D_2$ and $^1G_4$ levels or (iii) energy migration to quenching sites [9]. The first term is independent of dopant ion concentration and hence cannot be attributed to the observed optical properties. Furthermore, the gap separating the $^3P_0$ and $^1D_2$ states (~3500 cm^{-1}) would require 6 phonons to bridge the gap making this a weak contributor to the $^3P_0$ emission quenching. One potential mechanism for the cross relaxation could be $[^3P_0, {}^3H_4] \rightarrow [^3H_6, {}^1D_2]$ (Figure 5.2), because the energy mismatch amounts to ~ 100 cm^{-1}.

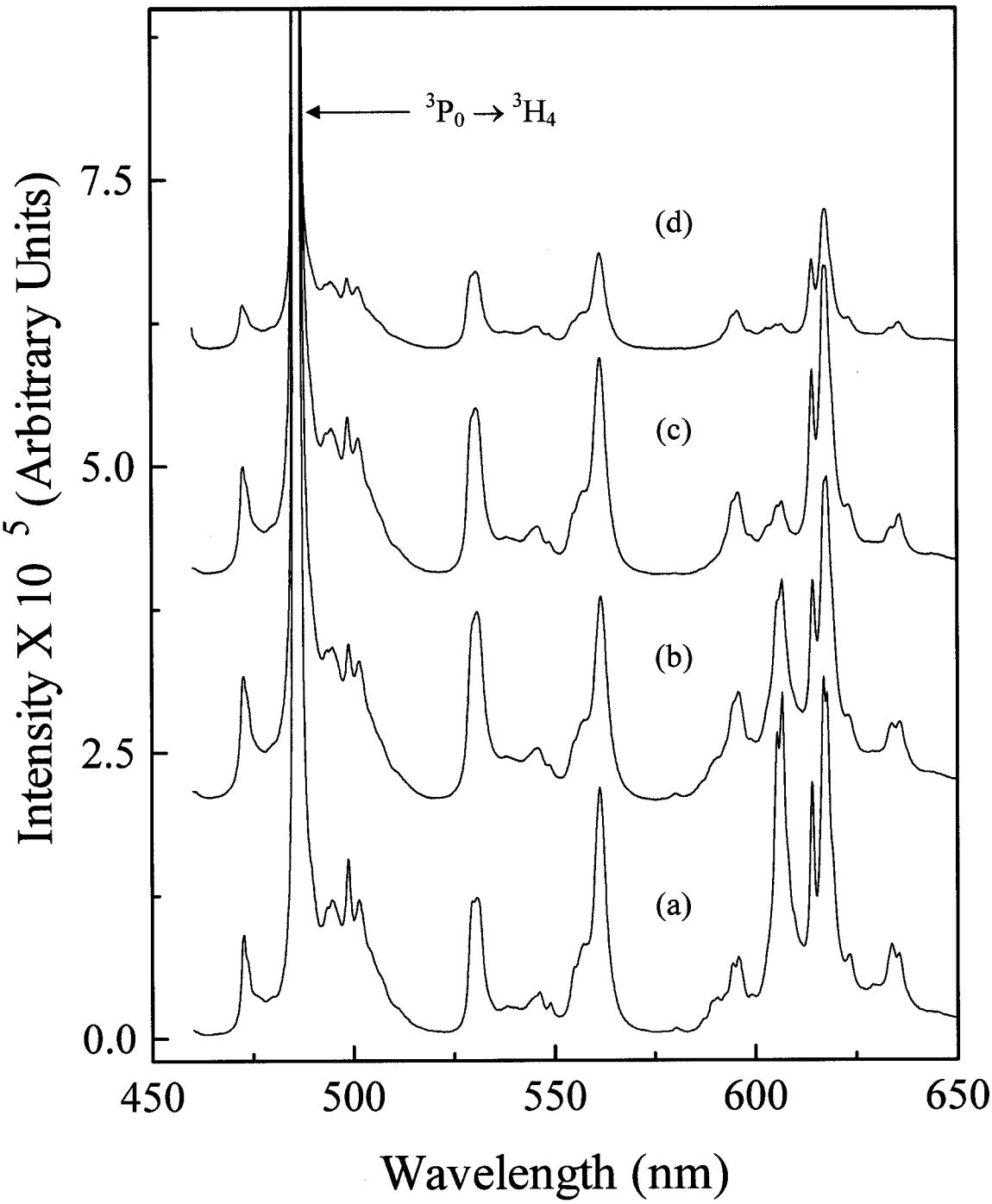

Figure 5. 1. Room temperature visible emission spectra (λ_{exc} = 457.9 nm) of GGG at (a) 0.1, (b) 1, (c) 5 and (d) 10 mol% Pr^{3+}.

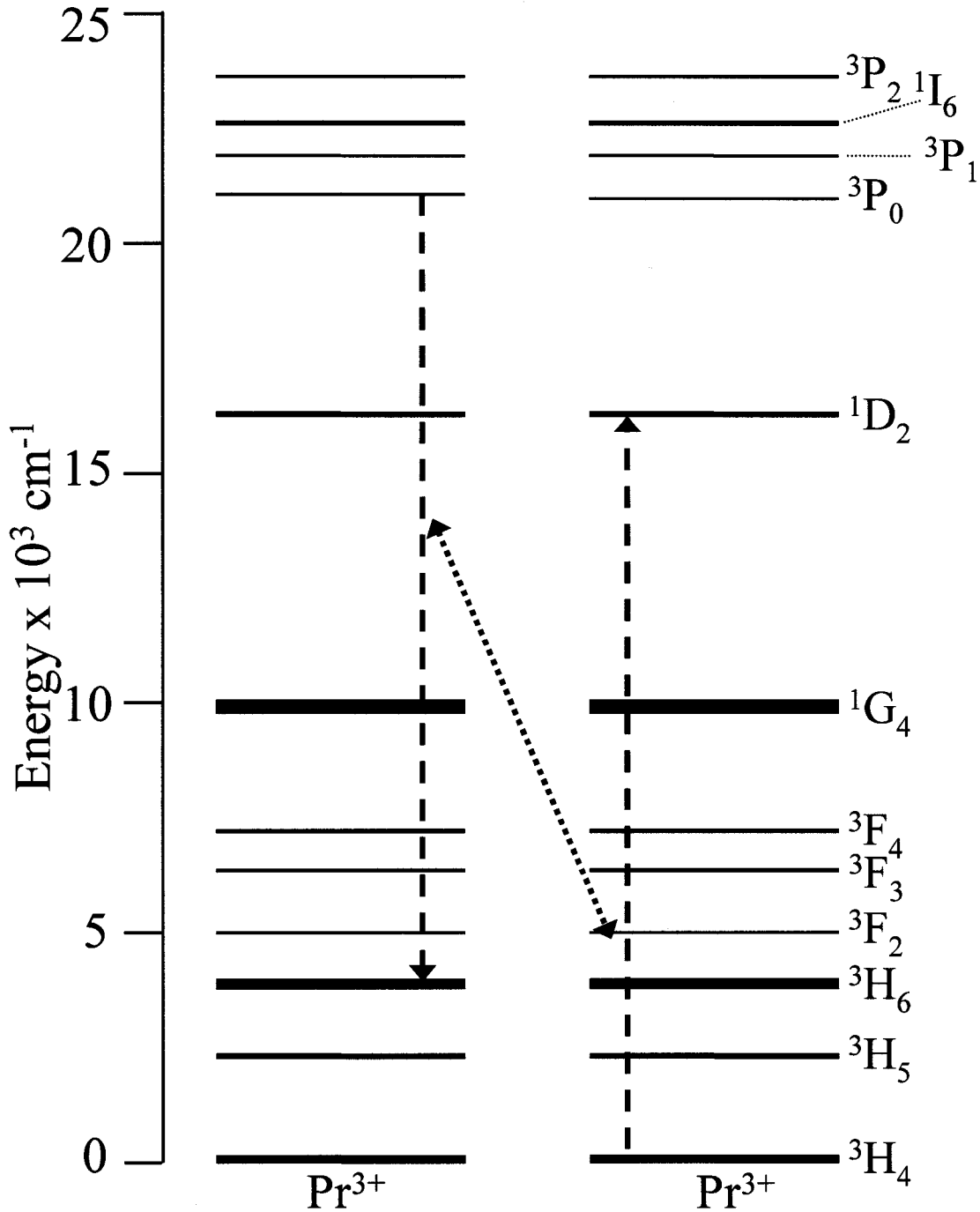

Figure 5. 2. $[^3P_0, {}^3H_4] \rightarrow [^3H_6, {}^1D_2]$ cross-relaxation mechanism populating the $^1D_2$ energy level.

This mechanism would however imply that an increase in the $^1D_2$ emission would be expected; however, as this level is populated by the proposed mechanism, it can be easily depopulated via the $[^1D_2, {}^3H_4] \rightarrow [^1G_4, {}^3F_{3,4}]$ pathway. What is in fact observed is a decrease in intensity for the $^1D_2$ peak to the lower lying ground state ($^3H_4$). This decrease was attributed to efficient cross relaxation mechanisms which are enhanced by the increase in the dopant ion concentration. Work by Chen et al. [116] showed an increase in emission intensity for the $^3P_0$ and $^1D_2$ states with increasing Pr^{3+} content but only up to 0.3 mol%, after which a decrease in the emission intensity was observed for $^1D_2$ state and 3 mol% for the $^3P_0$ state. Chen et al. also reported that almost total fluorescence quenching was observed for the $^1D_2$ state at 10 mol%. The exponential decrease in emission quenching noted for the $^1D_2$ state suggests that concentration quenching is much more significant for this state relative to the $^3P_0$ counterpart and likely depends on the distance separating neighbouring Pr^{3+} ions which surpasses a critical separation distance (~10Å) [11]. Efficient concentration quenching of the $^1D_2 \rightarrow {}^3H_4$ emission may therefore occur via the $[^1D_2, {}^3H_4] \rightarrow [^1G_4, {}^3F_{3,4}]$ mechanism [117] (Figure 5.3). This cross relaxation mechanism is plausible due to the match in energy gap separating the involved states [113]. Any energy mismatch can be likely bridged using one intrinsic phonon energy of the system. Consequently, this becomes a very highly probable occurrence in the nanosystem.

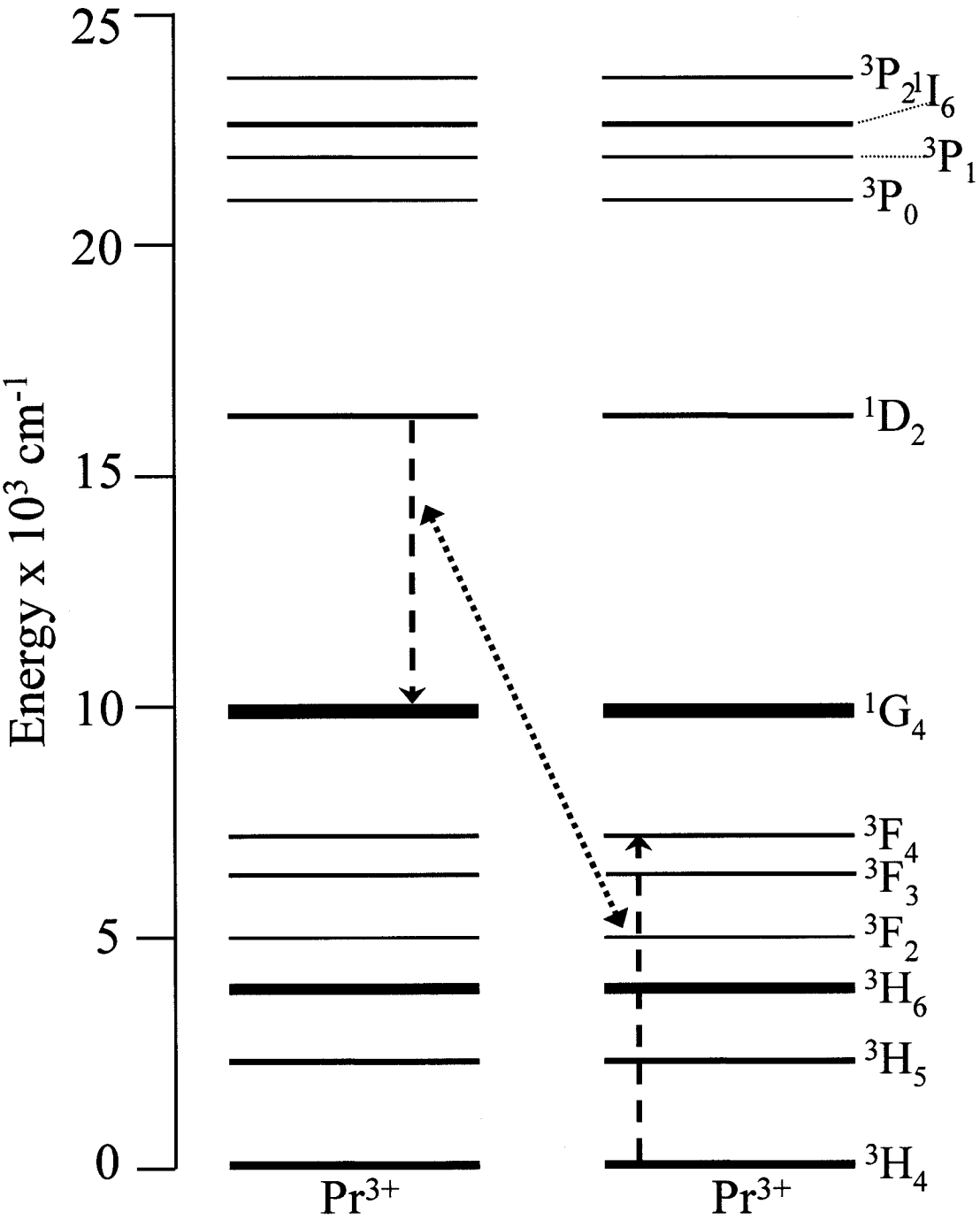

Figure 5. 3. Concentration quenching of the $^1D_2 \rightarrow {}^3H_4$ emission via the $[^1D_2, {}^3H_4] \rightarrow [^1G_4, {}^3F_{3,4}]$ cross-relaxation mechanism.

5.2 Lifetime Measurements

Lifetime measurements (Figure 5.4) following excitation using a wavelength of 457.9 nm for the 1% Pr^{3+}-doped nanocrystals are reported in Table 5.1.

Table 5. 1. Effective lifetimes (τ_{eff}) of Pr^{3+} energy levels for the Pr^{3+}-doped GGG nanocrystalline samples.

Level	Sample			
	0.1 mol%	**1 mol%**	**5 mol%**	**10 mol%**
$^3P_0 \rightarrow {}^3H_4$	32	18	7	2
$^1D_2 \rightarrow {}^3H_4$	280	110	11	3

The lifetimes could not be fit using a single exponential function and were treated using the Nakazawa equation [118] (Equation 5.1).

$$\tau_m = \frac{\int_0^\infty t\, I(t)dt}{\int_0^\infty I(t)dt} \qquad \textbf{(5.1)}$$

The Nakazwa equation [119] provides a means of the calculation of the effective decay time, τ_{eff}. The effective decay time can be viewed as an "average" lifetime which accounts for the many different processes (radiative and non-radiative) that may occur through out the lanthanide-doped system.

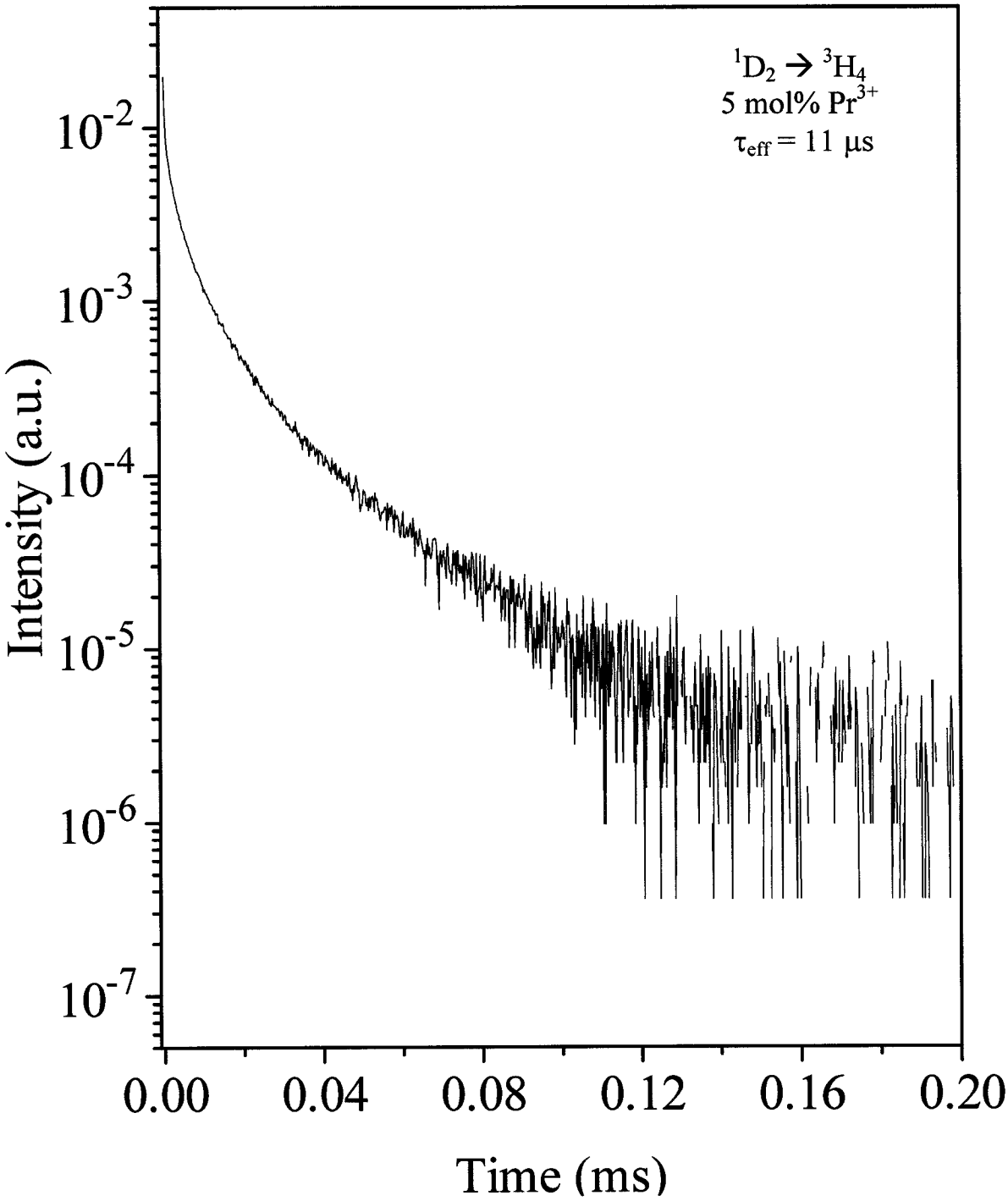

Figure 5. 4. Lifetime of the $^1D_2 \rightarrow {}^3H_4$ transition in 5 mol% doped GGG:Pr^{3+} (λ_{exc} = 580 nm, λ_{em} = 607 nm).

The Nakazwa equation accounts for cooperative luminescence due to the Ln^{3+}-Ln^{3+} interactions in the system. Competing mechanisms such as non-radiative energy transfer, as well as cross-relaxation within a given system will occur between neighbouring ions. It follows that as the concentration of the ions increases, the distance separating the ions will decrease accordingly. The probability of having a greater number of neighbouring ions will therefore increase. At this point, the probability of these competing mechanisms (competing with visible luminescence) increases dramatically and can have a substantial effect on the transition lifetimes. For example, cross-relaxation or multi-phonon relaxation typically results in the shortening of the lifetime. This occurs as the energy level of a given lanthanide will depopulate faster than it can visibly emit. The same is observed in concentration quenching where the successive radiationless energy transfer steps will depopulate the various excited states of a tripositive lanthanide ion leading to the eventual quenching of the luminescence. In contrast, some energy transfer processes such as those required in energy transfer upconversion (ETU) can cause a prolongation in the lifetime. The rate limiting step in the ETU process rests on the successful and slower energy transfer step from one ion to its neighbour to a specific energy level.

Using an excitation wavelength of 457.9 nm, the non-exponential lifetimes of the Pr^{3+}-doped GGG nanoparticles, are associated with the occurrence of concentration quenching, cross-relaxation as well as multi-phonon relaxation mechanisms, albeit a minor contribution of the latter due to the low phonon energies of the system. The lifetimes of the ^3P_J (J = 0, 1) levels were found to vary between 32 to 2.3 μs for the 0.1 mol% to 10 mol% dopant concentration. This is in agreement with the proposed

cross-relaxation mechanism. There are no expected significant differences in the lifetimes measurements of the $^3P_0$ and $^3P_1$ states as this was attributed to their rapid thermalization at room temperature. In contrast, the $^1D_2 \rightarrow {}^3H_4$ transition lifetime varied from 280 μs (0.1 mol% Pr^{3+}) to 3.0 μs (10 mol%). Essentially at 10 mol%, there is almost a complete quenching of the $^1D_2$ emission as was reflected in the transition lifetime and shown in Figure 5.5 for purpose of clarity. Emission from the $^1D_2$ state is nonetheless detectable, albeit weak, via population through the $[^3P_0, {}^3H_4] \rightarrow [^3H_6, {}^1D_2]$ mechanism as the quenching is not complete (see Figure 5.2). It is noteworthy to mention that even at < 1 mol% concentration, the non-radiative mechanisms are in effect, although less effective compared to higher dopant-containing systems. In the work of Chen et al. [116] and Naik et al. [120], concentration quenching occurred as low as 0.3 mol% and almost complete quenching of the $^1D_2 \rightarrow {}^3H_4$ emission in fact occurred at 10 mol% praseodymium concentration.

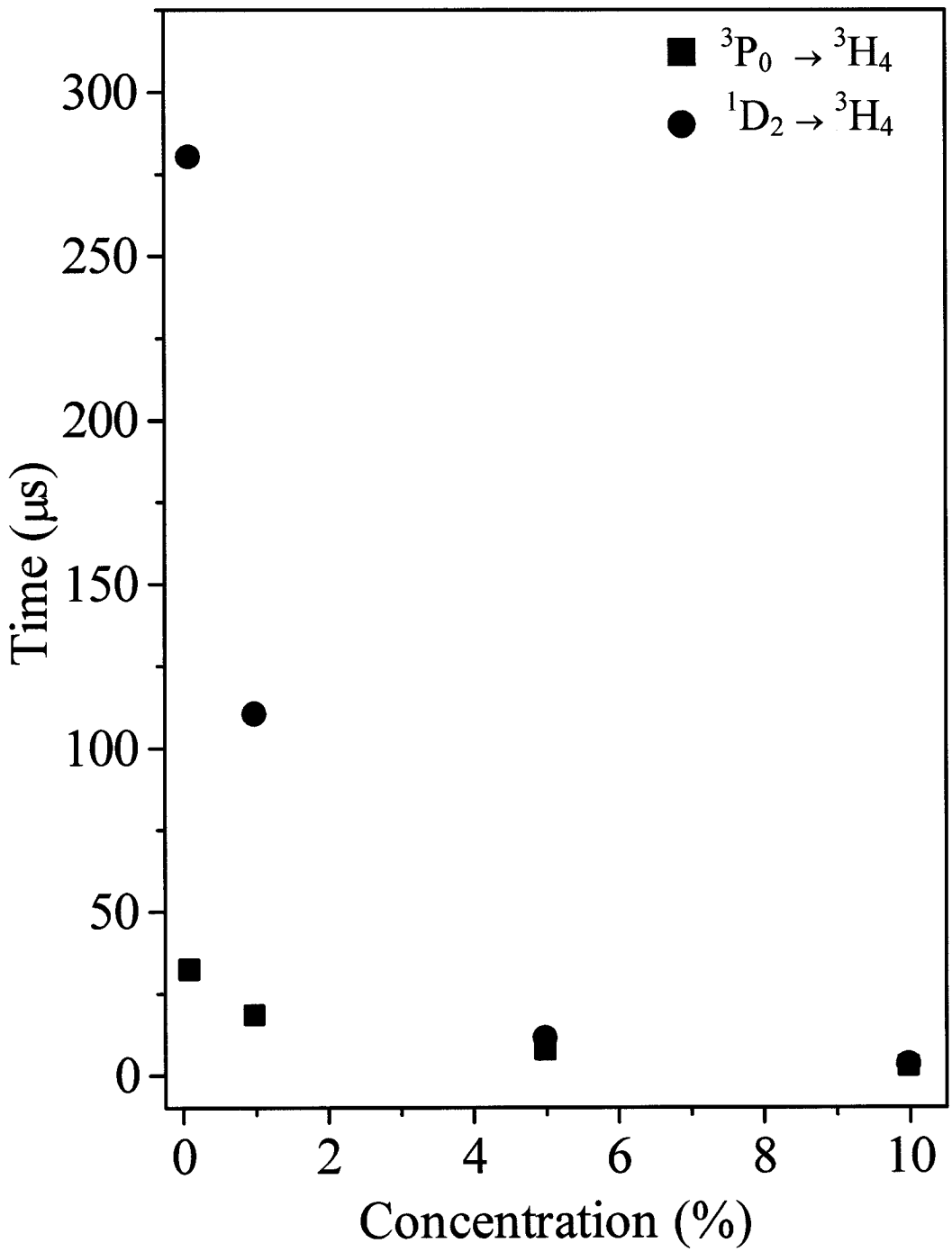

Figure 5. 5. Effective lifetimes (τ_{eff}) of Pr^{3+} energy levels for the $^3P_0 \rightarrow {}^3H_4$ and $^1D_2 \rightarrow {}^3H_4$ transitions in 0.1 – 10 mol% Pr^{3+} doped GGG nanocrystals.

5.3 Non-Equivalent Praseodymium Sites

In a high-dopant concentration system, the interactions between the ions cannot be ignored and may have drastic effects on the luminescence lifetimes of the various transitions of the system. As the concentration increases, so does the energy transfer within the system. In the system, it is expected that both resonant and non-resonant energy transfer may occur with the latter occurring between an optically excited donor and an acceptor in the ground state. In the case of an excited acceptor ion, the process becomes known as upconversion [121].

Expressions for the various multipolar electrostatic or ion-ion exchange processes were developed by Förster [78] and Dexter [77], as well as Inokuti and Hirayama [122]. The Inokuti-Hirayama (IH) model may be applied to the lifetime measurements to describe energy transfer processes in which the transfer process from donor to acceptor is significantly faster than the diffusion amongst donors. Inokuti and Hirayama proposed that it is possible to express the emission intensity, due to energy transfer processes arising from electric-multipolar interactions, according to the following expression,

$$\Phi(t) = A\exp\left[-kt - \alpha(kt)^{3/S}\right] \tag{5.2}$$

where $\phi(t)$ refers to the luminescence intensity at time t, A is the luminescence intensity at $t = 0$ and kt is the intrinsic lifetime of the donors in the absence of acceptors. The remaining two variables are α and S. The former is used to describe the probability of energy transfer while the latter describes the type of interactions. Table 5.2 summarizes the values of S.

Table 5. 2. S-values for the interactions using the Inokuti-Hirayama model.

Interaction	S-value
Dipole-Dipole (D-D)	6
Dipole-Quadrupole (D-Q)	8
Quadrupole-Quadrupole (Q-Q)	10

The lifetime measurements were treated using the IH model and Equation 5.2; however, a good fit could not be obtained. Hence it was not possible to determine the exact nature of the interactions occurring between the ions responsible for the energy transfer mechanism in the system (D–D, D–Q or Q–Q).

These observations do not imply the absence of ET in the system as this process is strongly supported by the visible luminescence and lifetime measurements. It is however likely that the improper fits are due to the presence of non-equivalent praseodymium sites within the GGG host. Work by Lupei et al. [123, 124] and others [125-128] has suggested that lanthanide ions in a garnet may not necessarily occupy one crystallographic site, which would lead to a symmetric perturbation of the crystal field (CF). Occupation of satellite sites may occur with it leading to an asymmetric perturbation of the CF. Even at low concentrations, there is a small probability of having ensembles or pairs of ions in the nearest crystallographic sites. It follows that as the dopant concentration increases, so does the probability of the occurrence and existence of such pairs. The asymmetric perturbation of the crystal field can lead to several effects such as: (i) rise of residual degeneracy of the energy levels thereby resulting in the lowering of the symmetry, (ii) shifts of the energy levels (several to tens of cm^{-1}) which can modify the gaps between

the crystal field levels, (iii) modifications of the selection rules where normally forbidden electric-dipole transitions are allowed, (iv) modification of the transition probabilities which can result in the enhancement or disappearance of certain transitions and finally (v) modification of the electron-phonon interactions which can strongly alter the temporal behaviour of the emissions of both donor and acceptor ions in the system. Consequently, the lifetimes are affected as they are strongly tied to the transition probabilities [123].

In GGG, tripositive praseodymium is known to enter the dodecahedral c-site and substitute for Gd^{3+}. The ion possesses D_2 symmetry in the c-site. It is however possible that the ion enters a minority site caused by crystal defects or even the a-site and substitute for gallium ions. In the a-site, Pr^{3+} ions would be surrounded by a trigonally distorted octahedron of O^{2-} ions and possess C_{3i} symmetry. An investigation of the emission spectra collected for 0.1-10 mol% Pr^{3+}-doped nanocrystals (λ_{exc} = 457.9 nm) suggests the likely presence of a second Pr^{3+} site (Figure 5.6). This is supported by the change of emission intensity ratio of the minority site (M) relative to the principle site (N) of Pr^{3+} ions (Table 5.3). Analysis was carried out for the $^3P_0 \rightarrow {}^3H_4$ peak.

Table 5. 3. Ratio of the emission intensity of minority site (M) to principal site N (486.58 nm, $^3P_0 \rightarrow {}^3H_4$) in 0.1-10 mol% Pr^{3+}-doped GGG nanocrystals.

M Site (nm)	**M / N Emission Intensity Ratio**			
	0.1 mol%	**1 mol%**	**5 mol%**	**10 mol%**
M, 485.67	0.693	0.709	0.743	0.733

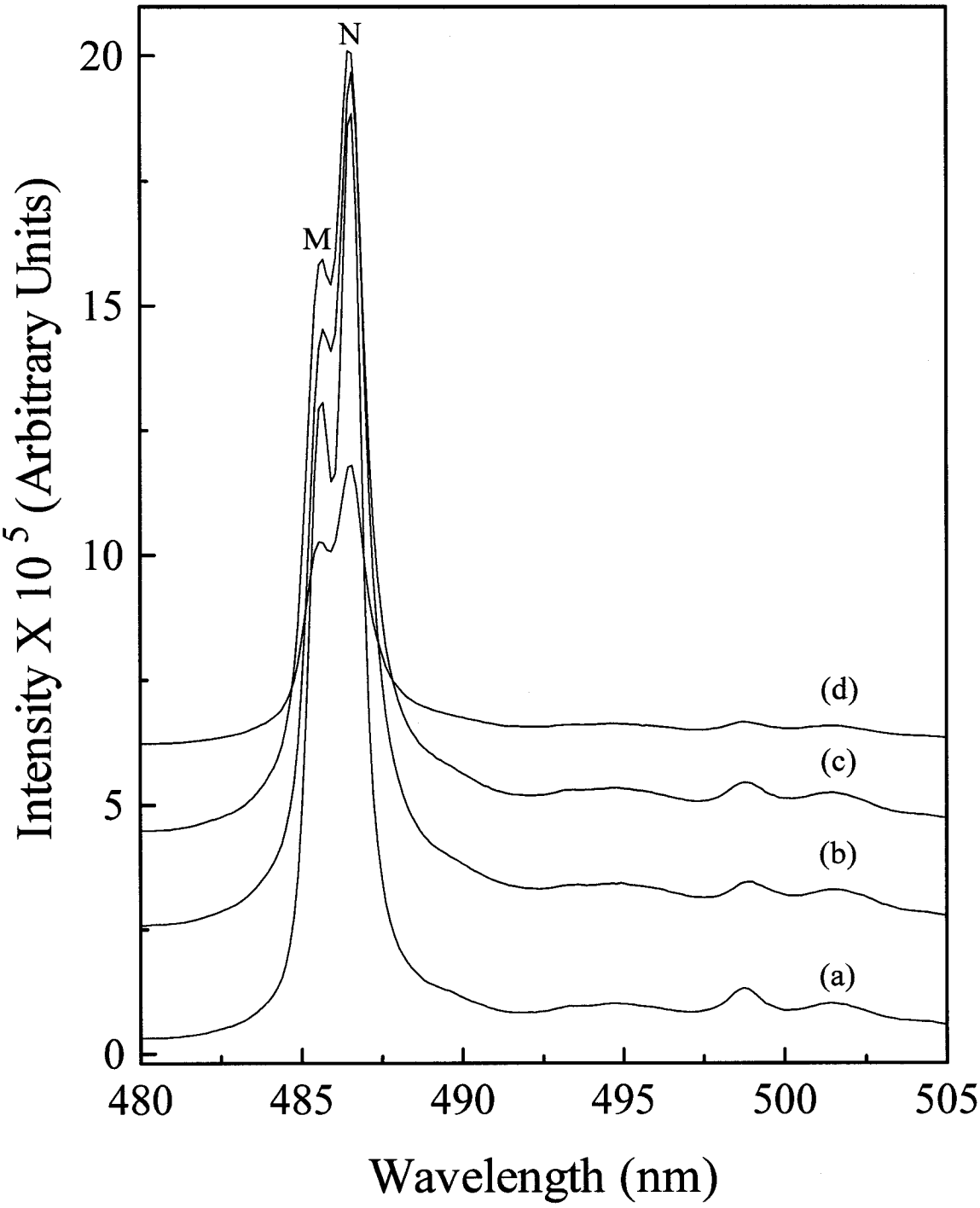

Figure 5. 6. Principal (N) and minority (M) Pr^{3+} sites for the $^3P_0 \rightarrow {}^3H_4$ transition in GGG nanocrystals at (a) 0.1, (b) 1, (c) 5 and (d) 10 mol% Pr^{3+}.

As the dopant concentration increases in the GGG host, the M/N emission intensity ratio increases accordingly since the probability of the ion substituting in the secondary site will also increase. It is noteworthy to mention that the emission of the minority site remains significantly lower than that of the principal site. Further studies will be required to confirm the presence of a secondary site including transition lifetime measurement and analysis; this will ensure that the observed emission at M is due to the presence of a non-equivalent Pr^{3+} site and not due to the next stark level of the $^3H_4$ ground state.

5.4 Visible Upconversion Emission

Upconversion emission following selective excitation into the $^1D_2$ state using a wavelength of 606.9 nm where blue/green emission was observed in a 1 mol% doped Pr^{3+} GGG sample was previously discussed in Chapter 4. The emission bands centered at 473 nm and 487 nm were observed to originate from the $^3P_1 \rightarrow {}^3H_4$ and $^3P_0 \rightarrow {}^3H_4$ transitions, respectively. The upconversion emission normalized to the $^3P_1 \rightarrow {}^3H_4$ energy level is shown in Figure 5.7 for the 0.1 and 1 mol% Pr^{3+}-doped nanocrystals.

Analysis of the transition lifetimes of the 0.1 mol% and 1 mol% doped samples suggests that the lifetime increases to 108 μs and 50 μs for the 0.1 mol% and 1 mol% Pr^{3+}-doped samples, respectively (Table 5.4).

Table 5. 4. Lifetimes of GGG:Pr^{3+} nanocrystals following excitation using a wavelength of 606.9 nm.

Transition (nm)	**$Gd_3Ga_5O_{12}:Pr^{3+}$ Lifetimes (μs)**			
	0.1%	**1%**	**5%**	**10%**
$^3P_0 \rightarrow {}^3H_4$ (486.7)	108	50	30	27

This represents a 2-4 fold increase in the lifetimes relative to excitation using 457.9 nm. The lengthening of the lifetime is characteristic of an energy transfer upconversion (ETU) mechanism. This occurs as the upconversion process is a two-ion process and is dependent on the lifetime of the intermediate state from which ETU occurs. It is likely that upconversion is also occurring through an excited state absorption (ESA) mechanism which competes, to a lesser extent, with ETU (see Chapter 4).

As the concentration of praseodymium increased in the host, the $^3P_0 \rightarrow {}^3H_4$ peak intensity was observed to decrease following 606.9 nm pumping. At 5 and 10 mol%, weak emission intensities were observed. The transition lifetimes at 5 and 10 mol% were determined to be 30 and 27 μs (Table 5.4), respectively. The lifetime of the $^3P_0 \rightarrow {}^3H_4$ emission, after 606.9 nm excitation, approaches the lifetime measured after 457.9 nm excitation. Cross-relaxation efficiency increases exponentially as the dopant concentration increases (concentration quenching). This is accompanied by an exponential decrease in the lifetime of the transition (Figure 5.8). The interionic distances between donor and acceptor ions (Pr^{3+}-Pr^{3+}) significantly decrease as the concentration increases which allows for a more efficient and probably quenching mechanism [11, 116].

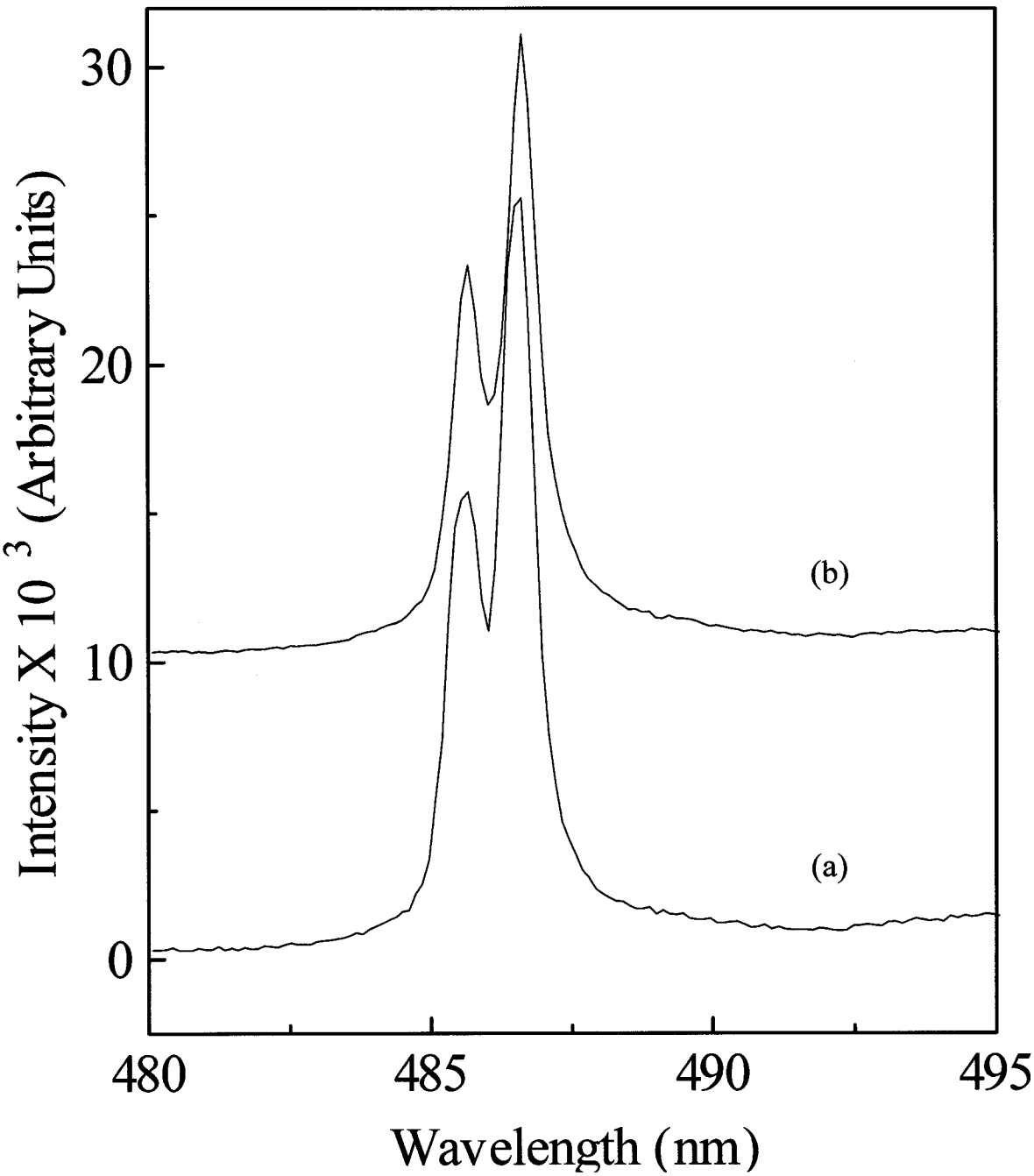

Figure 5. 7. Room temperature upconversion emission spectra (λ_{exc} = 606.9 nm) for the $^3P_0 \rightarrow {}^3H_4$ transition of GGG:Pr^{3+} at (a) 0.1 and (b) 1 mol%.

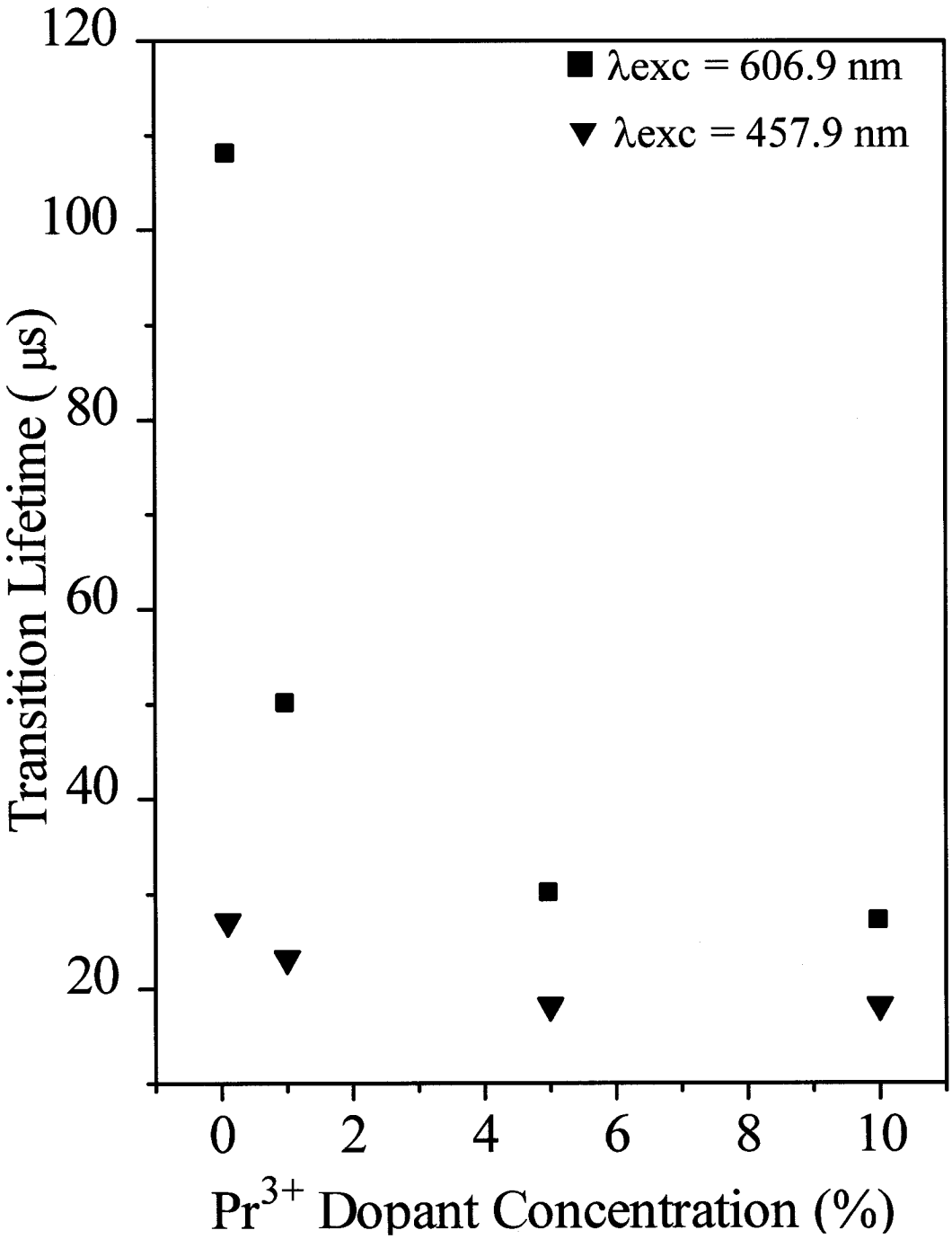

Figure 5. 8. Decrease in the transition lifetime for the for the $^3P_0 \rightarrow {}^3H_4$ transitions as a function of excitation wavelength.

Chapter VI

6.1 The Sensitizer/Activator Relationship – Co-doping with Ytterbium

The effect of co-doping with ytterbium has been well documented in the literature. Ytterbium has been used in combination with other lanthanide ions in glasses and crystals (including nanocrystals) for many years [70, 129-161]. Tripositive ytterbium is an ideal ion for co-doping materials since it possesses only one excited state, which can be easily excited using a wavelength of 980 nm (Figure 6.1), a convenient wavelength as many commercial diodes are readily available. Moreover, the excited state of the Yb^{3+} ion has a much higher absorption cross-section than many of the excited states of other lanthanides with similar energies rendering the upconversion/energy transfer processes much more efficient. Co-doping with ytterbium also allows for upconversion processes (at 980 nm) to occur in certain situations where it is not possible in a singly doped system (Tb^{3+}-Yb^{3+} co-doped systems) The inclusion of ytterbium with certain lanthanides allows the scientist to target specific luminescent properties otherwise rather difficult or impossible in a singly-doped system.

Ytterbium plays an essential role in energy transfer upconversion (ETU) processes. During an ETU process, and when specifically using a 980 nm excitation source, the ytterbium ion is raised from the $^2F_{7/2}$ ground state to its single $^2F_{5/2}$ excited state. Another pump photon will also raise the lanthanide ion to an intermediate excited state located at a ΔE of approximately 10200 cm^{-1} (980 nm).

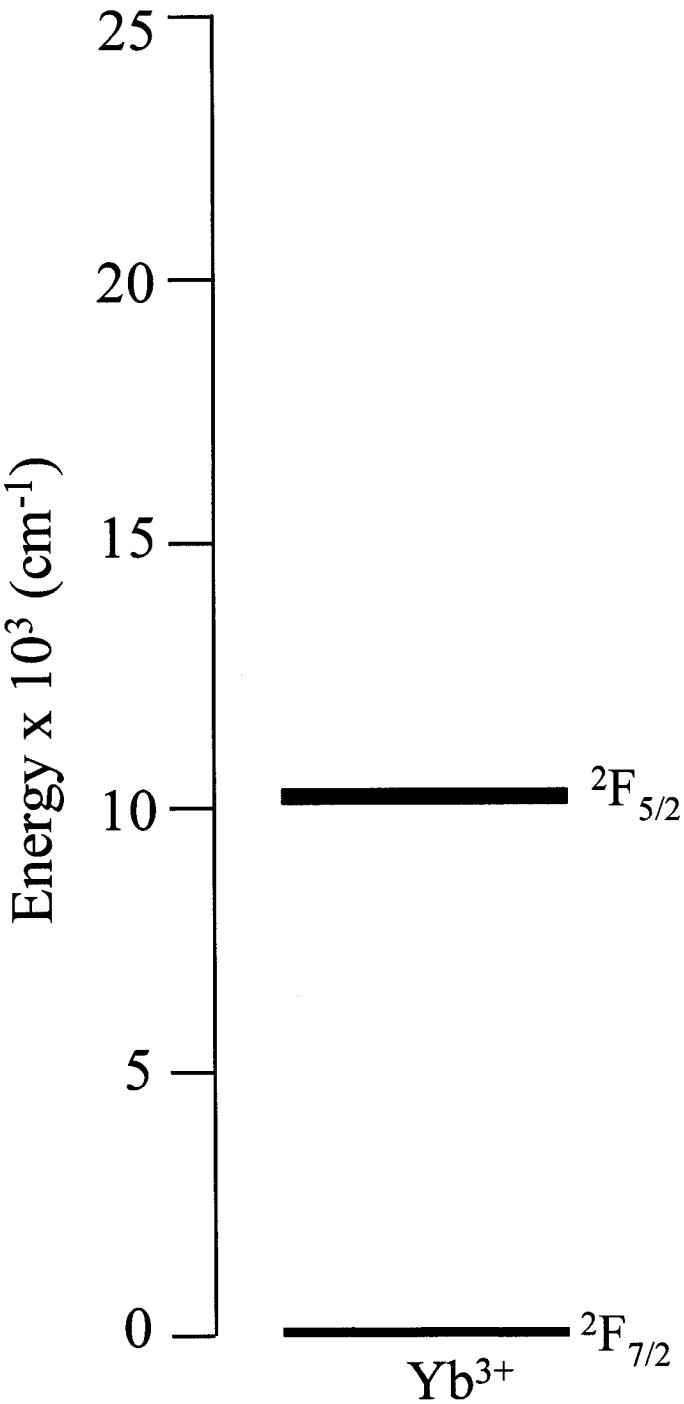

Figure 6. 1. Energy level diagram of the tripositive ytterbium ion.

Subsequently, the energy of the excited ytterbium ion is transferred, non-radiatively, to the neighbouring lanthanide co-dopant ion raising it to a higher excited state while the ytterbium ion returns to the ground state.

6.2 Room Temperature visible Emission in Co-Doped Samples

The co-doped nanocrystals were synthesized using a fixed concentration of the activator ion, praseodymium, which was set at 1 mol%. The concentration of the ytterbium activator ion was varied from 1- 10 mol%. Following direct excitation using a wavelength of 457.9 nm ($^1I_6$ energy level), blue/green, red and near infrared emission was observed for the Pr^{3+}-doped GGG nanocrystals (Figure 6.2). As was observed with the singly-doped nanocrystals, the co-doped counterparts also exhibit dominant blue/green emission from the ^3P_J (J = 0, 1) energy levels to lower lying levels.

While the emission intensity decreased with increasing dopant concentration in the singly-doped nanoparticles for only certain transitions ($^3P_0 \rightarrow {}^3H_4$, $^1D_2 \rightarrow {}^3H_4$), this was not observed in the co-doped system. In the case of the latter, the emission intensity was observed to decrease non-discriminately for all transitions with increasing ytterbium concentration especially at 10 mol% Yb^{3+} concentration where the $^1D_2 \rightarrow {}^3H_4$ red emission is practically extinct. Blue and green emission ^3P_J (J = 0, 1) emission also decreases significantly; however, is not extinct. In the previous chapter, the decrease in intensity observed for certain transitions was attributed to radiationless energy transfer phenomena, most notably cross-relaxation between neighbouring ions. The probability of this energy transfer increased significantly as the praseodymium concentration in the system increased.

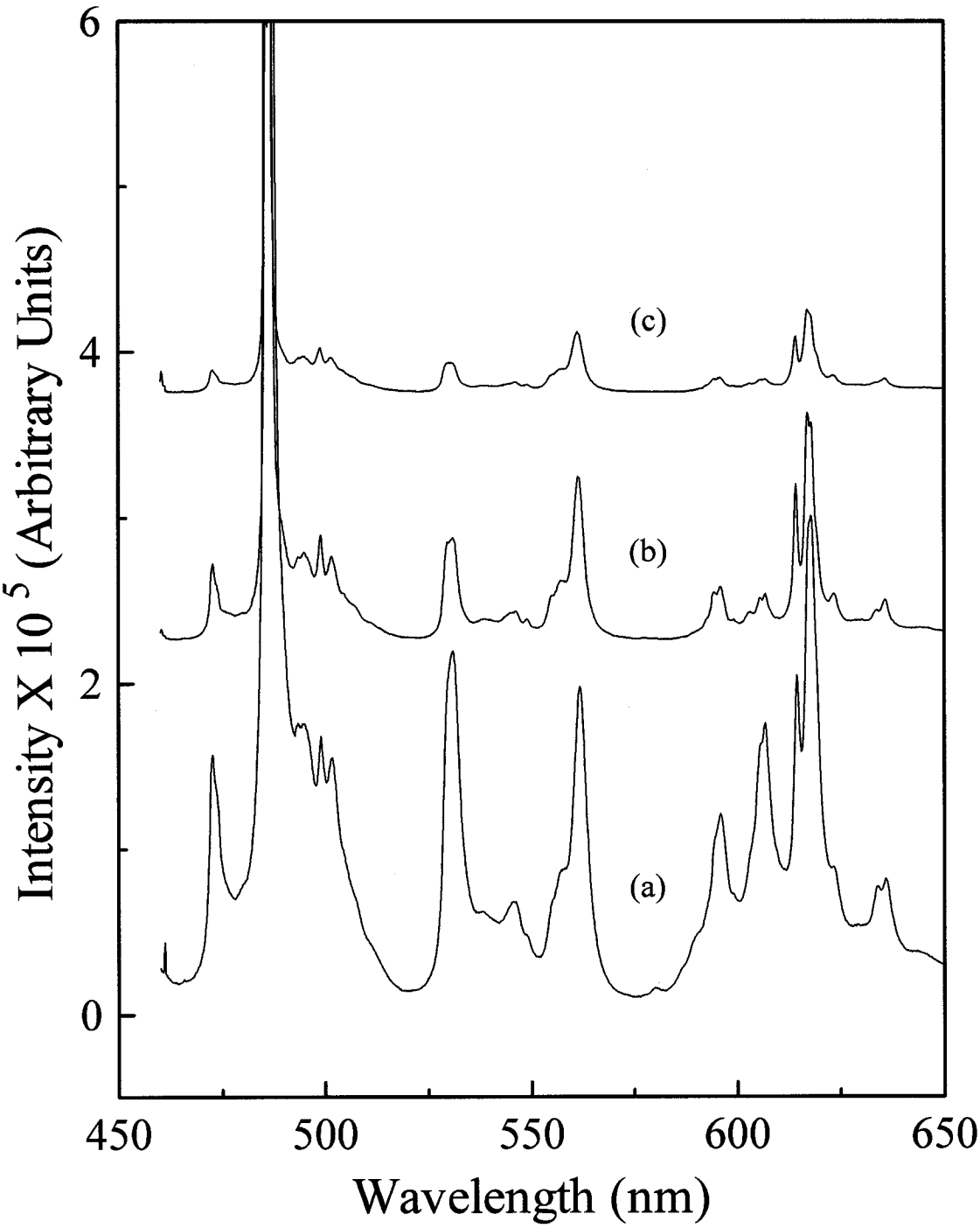

Figure 6. 2. Room temperature visible emission spectra (λexc = 457.9 nm) of 1 mol% Pr^{3+}-doped GGG nanocrystals co-doped with (a) 1, (b) 5, and (c) 10 mol% Yb^{3+}.

In the co-doped system, the tripositive praseodymium concentration was maintained at 1 mol%. While this would certainly account for cross-relaxation between neighbouring ions, it does not suffice to explain the decrease with increasing Yb^{3+} concentration in the system. The decrease in the emission intensity must therefore arise from the presence of ytterbium in the nanosystem.

As previously discussed in section 2.4, ET between a pair of ions may occur between resonant energy levels or through phonon assistance where phonon energy may mediate the energy transfer. Energy transfer is affected by the transfer wavelength and by the distance between the energy donor and energy acceptors in the system. The effect of the distance between the donor and the acceptor is greatly pronounced as the concentration of the ytterbium is increased; however, of even greater importance is the transfer wavelength. If the donor ion cannot transfer its energy of a certain wavelength (calculated through the energy gap separating the states) to a suitable acceptor, then energy transfer will not occur. It follows that the decrease in the emission intensity must correspond to a quasi match between the Pr^{3+} and Yb^{3+} ions. Inspection of the energy level diagrams of praseodymium and ytterbium reveals that indeed an ET process may occur between the two ions. The single level of ytterbium, the $^2F_{5/2}$, is at a comparable separation energy from the ground state (~1 μm or 10000 cm^{-1}) which is similar to praseodymium's $^1G_4$ energy level. Upon excitation using a wavelength of 457.9 nm, the Pr^{3+} ion is raised to the $^1I_6$ energy level. Subsequently the ion non-radiatively decays to the lower lying $^3P_1$ and $^3P_0$ energy levels. The ΔE separating the $^3P_0$ and $^1G_4$ levels is similar to that separating the $^1G_4$ and $^3H_4$ ground state. Therefore, in a singly-doped system, cross-relaxation would be expected to occur as shown in Figure 6.3.

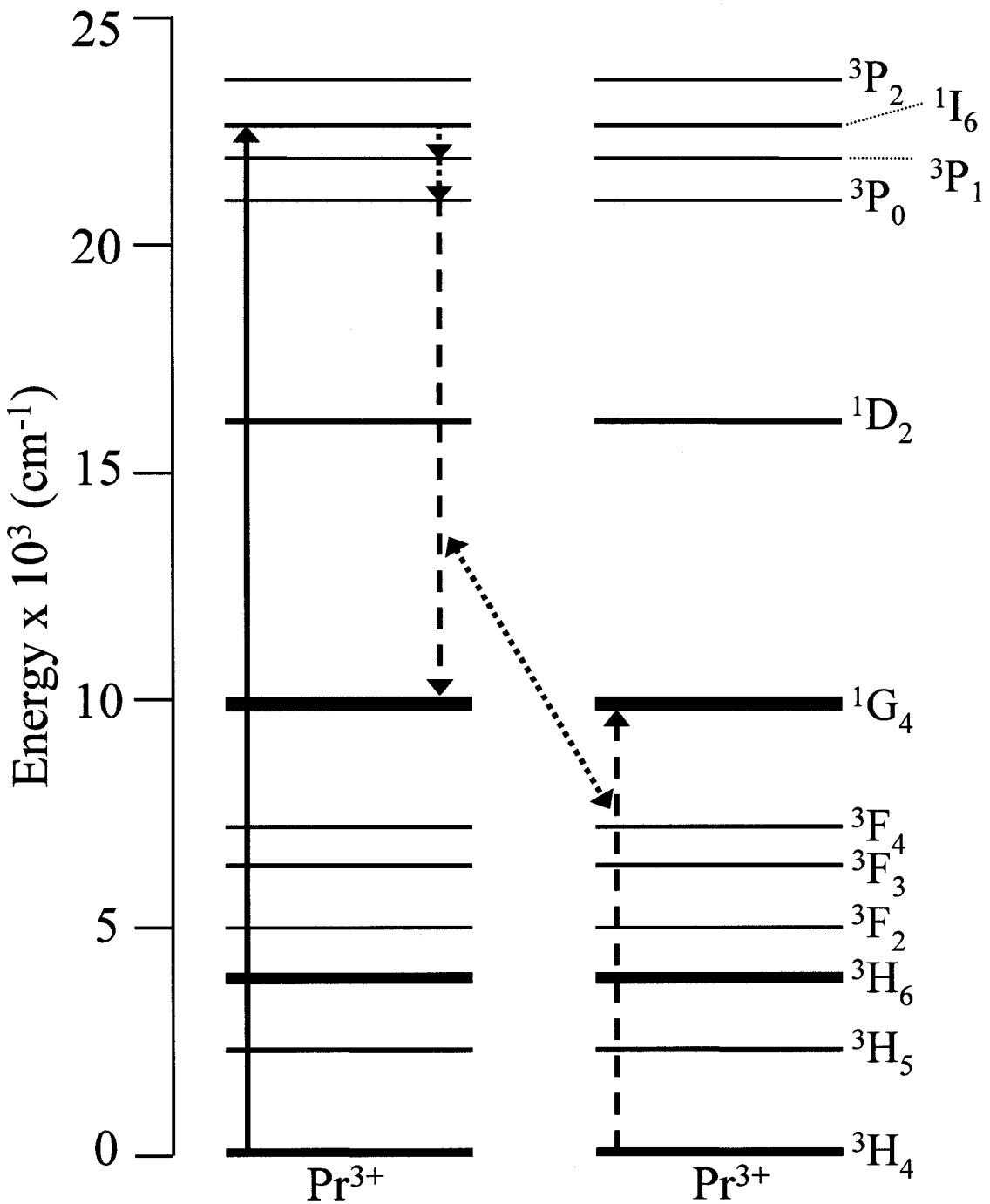

Figure 6. 3. Concentration quenching via the $[^3P_0, ^3H_4] \rightarrow [^1G_4, ^1G_4]$ cross-relaxation mechanism.

The proposed mechanism, $[^3P_0, {}^3H_4] \rightarrow [^1G_4, {}^1G_4]$, would involve a cross-relaxation of the ion in the $^3P_0$ state to the $^1G_4$ energy level which would transfer its energy to a neighbouring ion in the ground state raising the latter from the $^3H_4$ to $^1G_4$ energy level. In the case of a co-doped system where the activator concentration is maintained fixed, the CR mechanism can be modified as shown in Figure 6.4. Therefore it is written as follows: $[^3P_0, {}^2F_{7/2}] \rightarrow [^1G_4, {}^2F_{5/2}]$ where $^2F_{7/2}$ and $^2F_{5/2}$ are the ground and excited state of Yb^{3+}, respectively.

A second method of populating the $^2F_{5/2}$ excited state of Yb^{3+} involves successive non-radiative decay steps from the $^3P_0 \rightarrow {}^1D_2 \rightarrow {}^1G_4$ energy level via multiphonon relaxation followed by direct ET to ytterbium. Multiphonon relaxation from the $^3P_0$ to the $^1D_2$ level requires ~7 intrinsic phonons of GGG while a second relaxation to the lower lying $^1G_4$ energy level would require ~10 intrinsic phonons. The probability of population via this mechanism would likely be low as the total number of phonons required would be approximately 17.

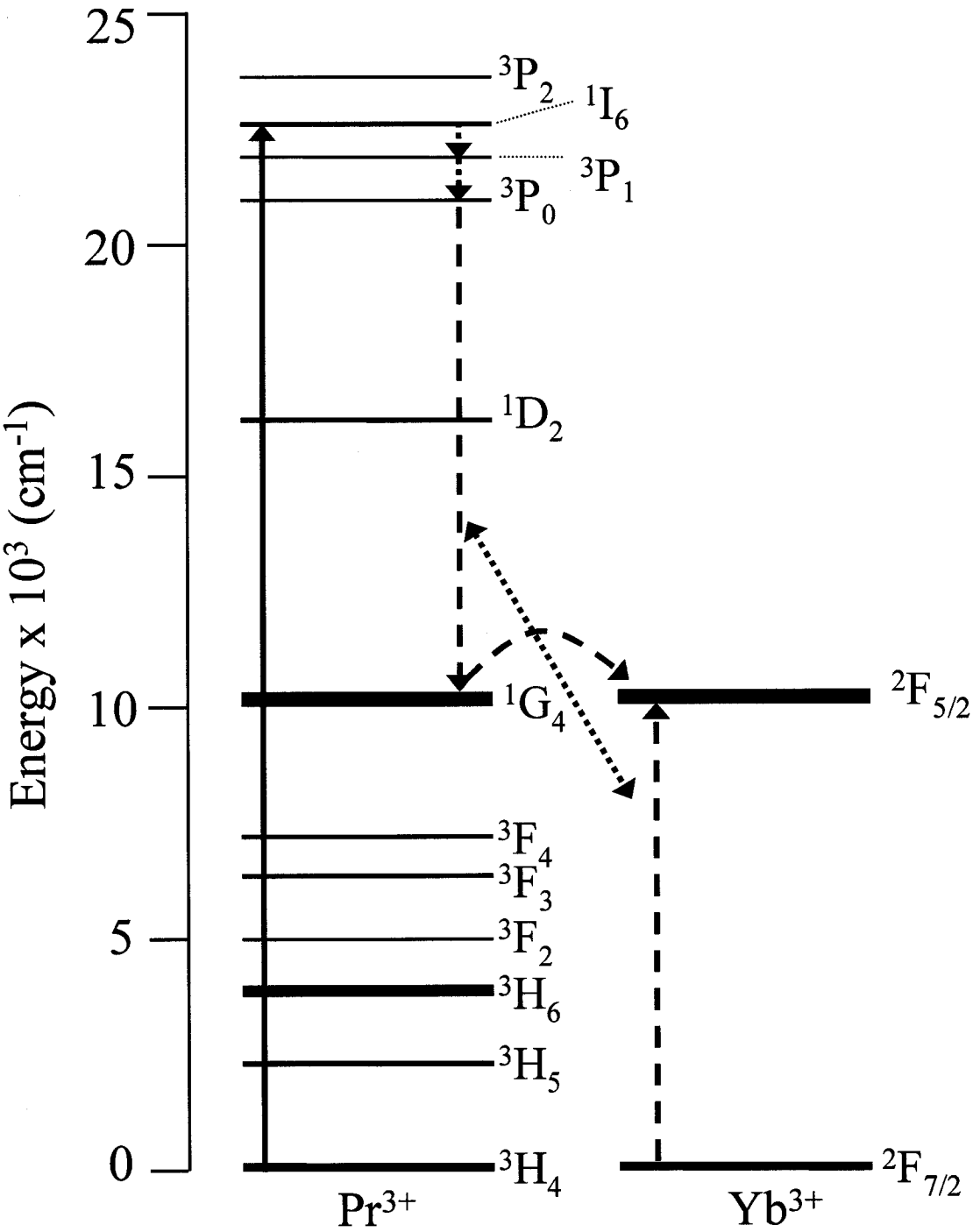

Figure 6. 4. Mechanism of energy transfer in 1 mol% Pr^{3+}-doped GGG nanocrystals co-doped with 1-10 mol% Yb^{3+}. Shown above is the energy transfer from Pr^{3+} to Yb^{3+}.

6.3 Lifetime Measurements

An investigation of the lifetime of the $^3P_0 \rightarrow {}^3H_4$ transition observed upon 457.9 nm excitation was carried out to confirm the proposed energy transfer via cross-relaxation mechanism. The results are summarized in Table 6.1 below,

Table 6. 1. Lifetimes of GGG: 1 mol% Pr^{3+}, xYb^{3+} nanocrystals following excitation using a wavelength of 457.9 nm.

Transition (nm)	**$Gd_3Ga_5O_{12}$:1 mol% Pr^{3+}, xYb^{3+} Lifetimes (μs)**		
	1%	**5%**	**10%**
$^3P_0 \rightarrow {}^3H_4$ (486.7)	50	30	27

The lifetime measurements could not be fitted using a single exponential function, which is not surprising given that visible emission and non-radiative ET are occurring concomitantly. Initial analysis of the lifetimes reveals that the lifetimes of the $^3P_0 \rightarrow {}^3H_4$ transition decrease as a function of ytterbium concentration in the system. This was expected since a similar trend was observed as the dopant concentration increased in the singly-doped system. Concentration quenching and cross-relaxation resulted in a rapid depopulation of the energy levels. These observations also support the mechanism proposed in Figure 6.4.

A comparative analysis of the 1 mol% Pr^{3+}-singly doped nanocrystals with the 1 mol% Pr^{3+}-1 mol% Yb^{3+} co-doped counterpart reveals that there is a lengthening of the lifetime of the $^3P_0 \rightarrow {}^3H_4$ transition. The lifetime increases from 32 μs (singly-doped) to 50 μs (co-doped). If energy transfer is solely occurring between Pr^{3+}-Yb^{3+}, based on the decrease in luminescence intensity, then lifetimes shorter than 32 μs would be expected.

The increase in the lifetime therefore suggests that energy transfer must also be occurring from ytterbium to praseodymium. In fact, this would suggest an ET cycle between the two neighbouring ions in the nanocrystalline host. The proposed mechanism is shown in Figure 6.5.

6.4 Visible Upconversion Emission

Using an excitation wavelength of 980 nm, visible upconversion emission was observed upon selective excitation into the $^1G_4$ energy level of praseodymium in the co-doped nanosystems. Visible upconversion emission emanating from the $^3P_{0,1}$ levels to the various ^3F_J (J = 2, 3, 4) and $^3H_{J'}$ (J' = 4, 5, 6) states, as well as emission from the $^1D_2$ energy level to the $^3H_4$ ground state was observed. The resultant spectrum was similar to that obtained using an excitation wavelength of 457.9 nm (Figure 6.6). The upconversion emission intensity of the co-doped samples was approximately 3-fold more intense relative to the singly-doped nanoparticles excited under the same conditions (Figure 6.7), a testament to the use of a sensitizer such as ytterbium with a high absorption cross-section.

Lifetime measurements carried out at λ_{exc} = 980 nm show a lengthening of the lifetime which could not be fitted using a single exponential function and was determined to be 206 μs. This value represents a 4-fold increase relative to the lifetime at λ_{exc} = 457.9 nm where a value of 50 μs was obtained. A power study was carried out where the natural log of the pump power was plotted versus the natural log of the emission intensity. A linear regression fit was used and a slope value of 2.09 was obtained for the upconversion emission from the $^3P_0 \rightarrow {}^3H_4$ transition in the nanocrystals (Figure 6.8).

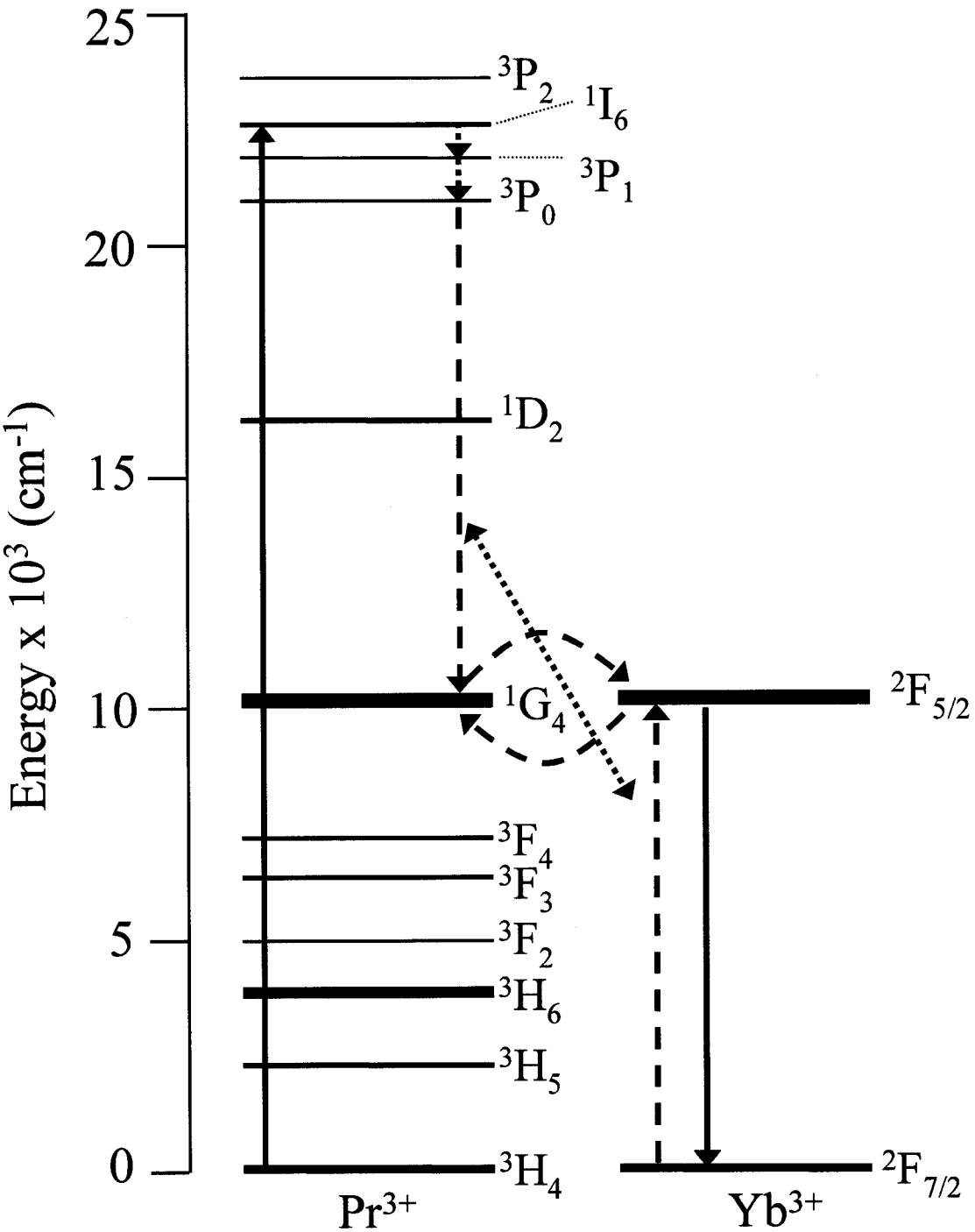

Figure 6. 5. Mechanism of energy transfer in 1 mol% Pr^{3+}-doped GGG nanocrystals co-doped with 1-10 mol% Yb^{3+}. Shown above is the energy transfer cycle from Pr^{3+} to Yb^{3+} and vice versa.

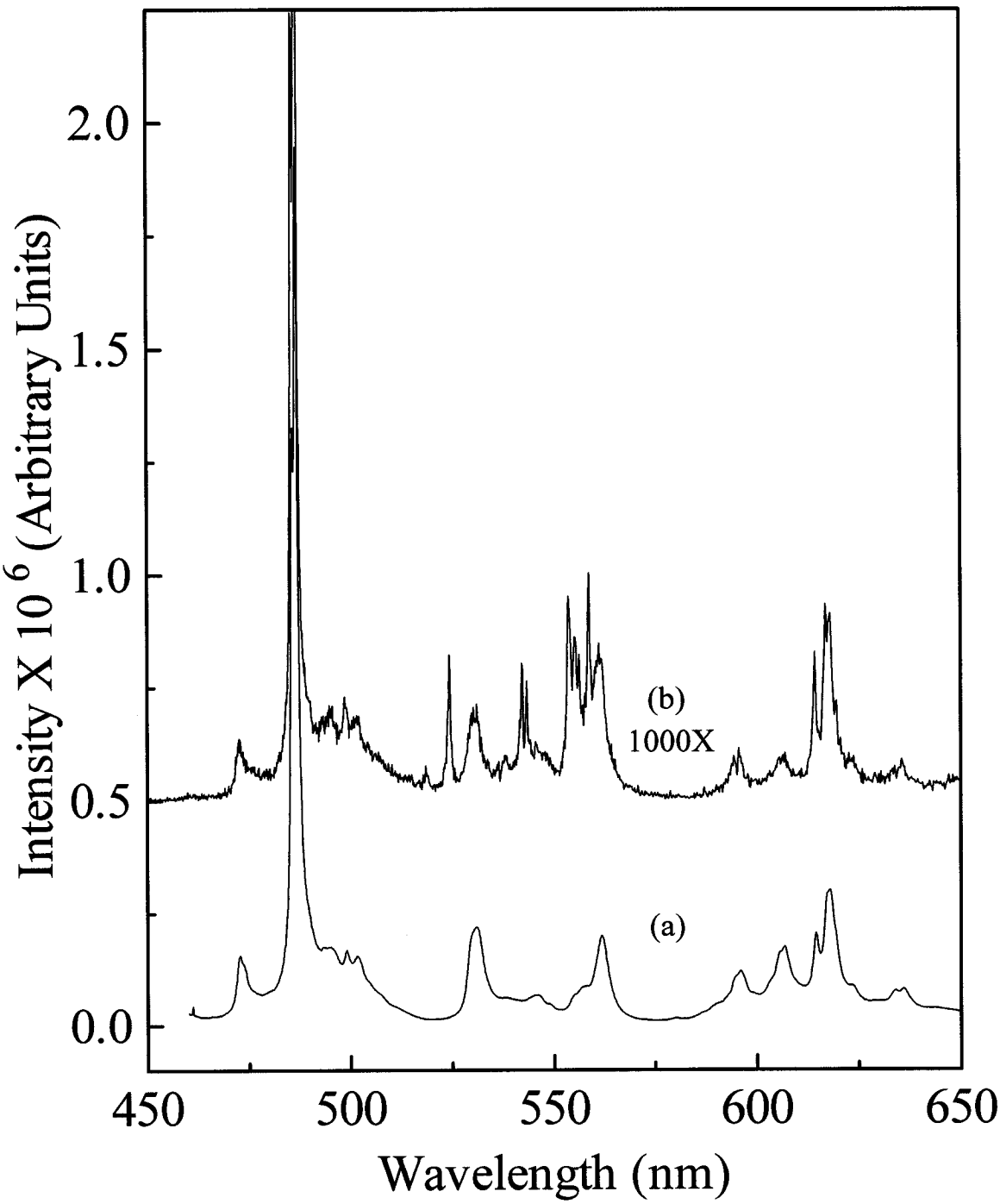

Figure 6. 6. Upconversion emission of co-doped Pr^{3+}/Yb^{3+} GGG nanocrystals (1 mol%) using an excitation wavelength of (a) 457.9 nm and (b) 980 nm (magnified a 1000X).

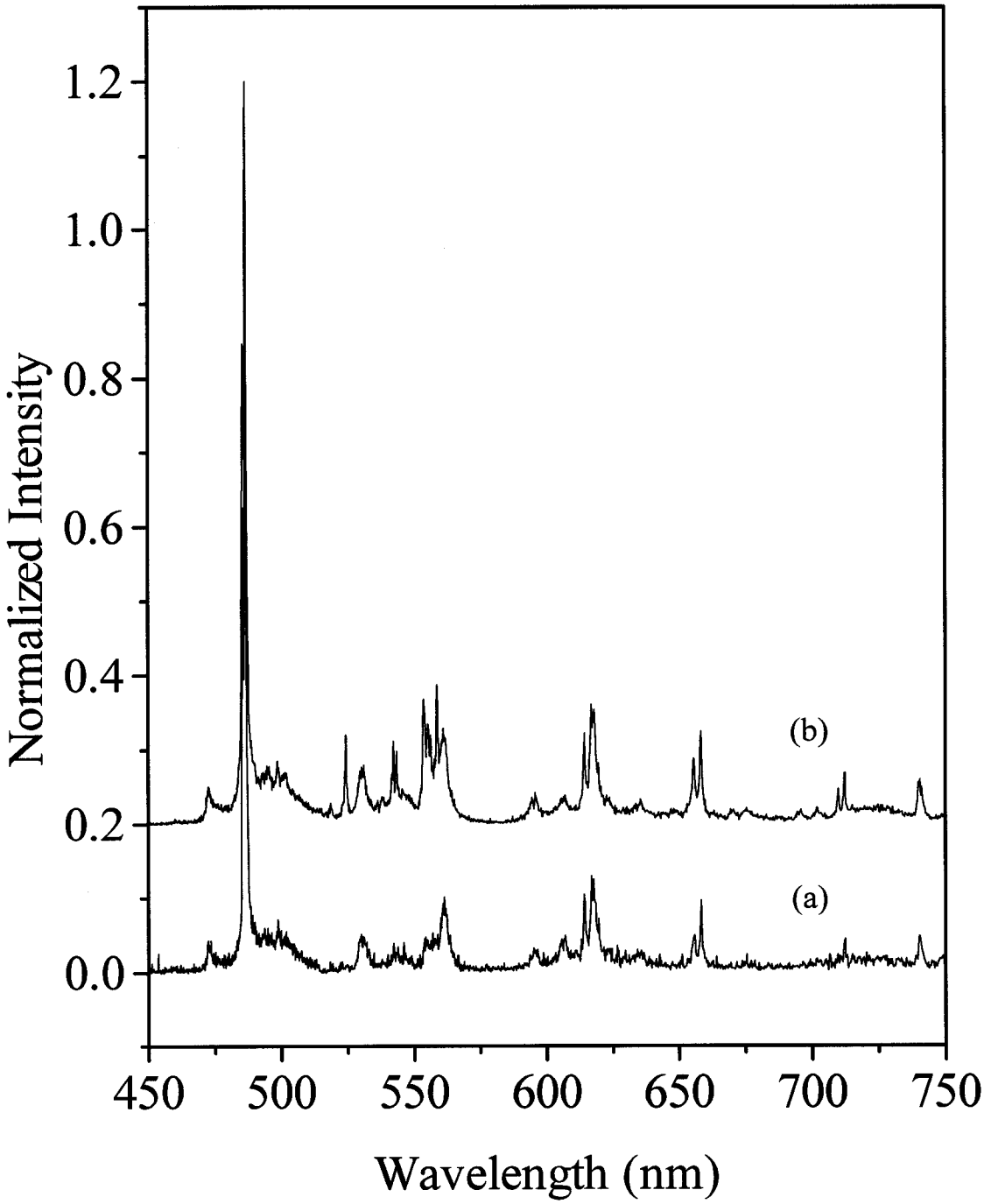

Figure 6. 7. Upconversion emission (λ_{exc} = 980 nm) for (a) singly-doped 1 mol% Pr^{3+} and (b) co-doped 1 mol% Pr^{3+}/ 1 mol% Yb^{3+}.

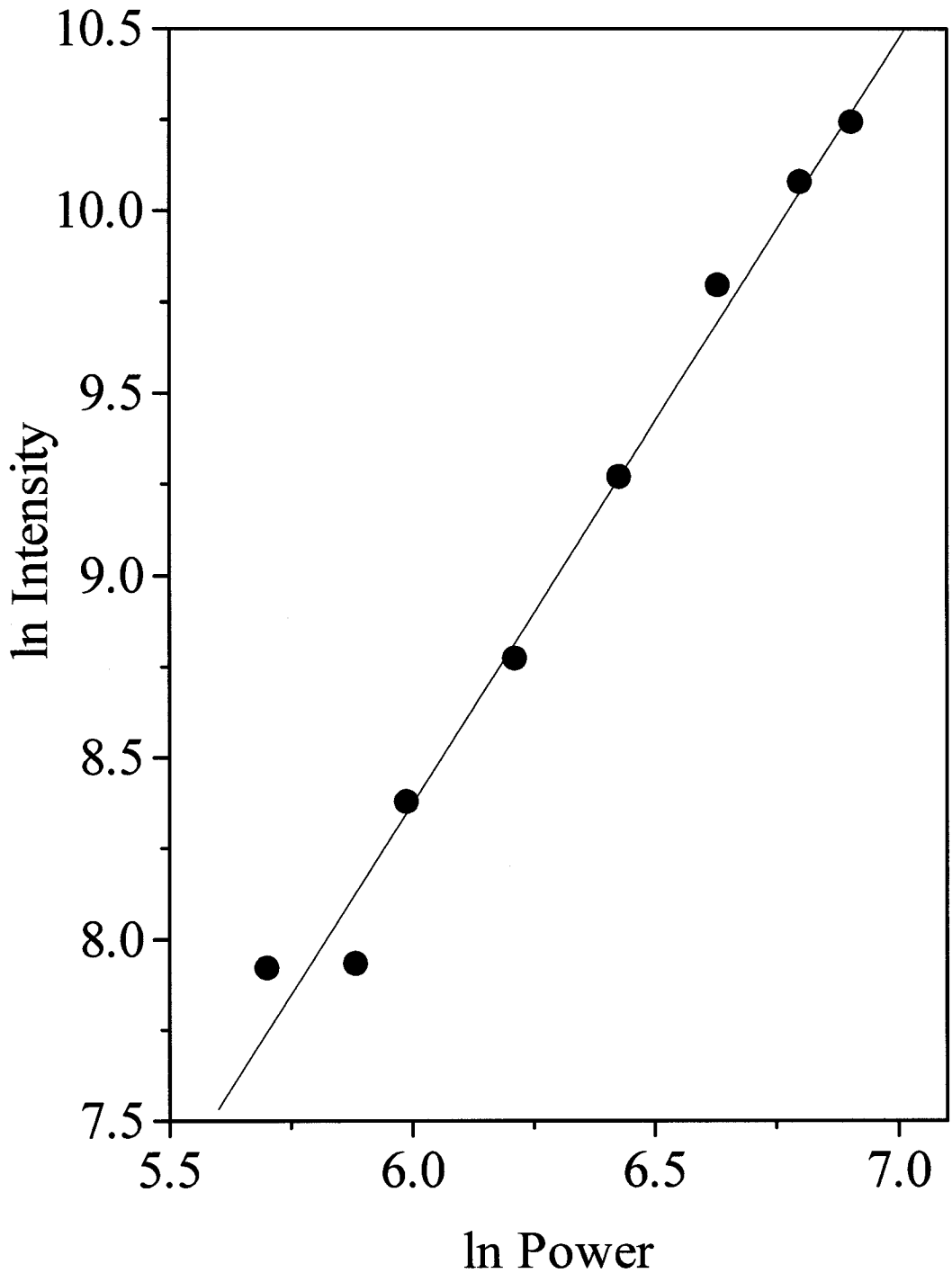

Figure 6. 8. Power dependence study for the upconversion emission of the $^3P_0 \rightarrow {}^3H_4$ transition (λ_{exc} = 980 nm) of Pr^{3+}/ Yb^{3+} (1 mol%) GGG nanocrystals.

The lengthening of the lifetime supports an ETU mechanism (Figure 6.9) where the incoming pump photon raises both a praseodymium and ytterbium ions to their respective excited states, namely the $^1G_4$ and $^2F_{5/2}$, states respectively. This is followed by a non-radiative energy transfer from the neighbouring ytterbium ion, which raises the ion to the $^3P_1$ and $^3P_0$ energy levels and upconversion emission will ensue. It is noteworthy to mention that an ESA mechanism is likely occurring albeit to a lesser extent. The effect of ESA cannot be ignored where two pump photons will sequentially populate the $^1G_4$ level first and subsequently the $^3P_1$ and $^3P_0$ energy levels.

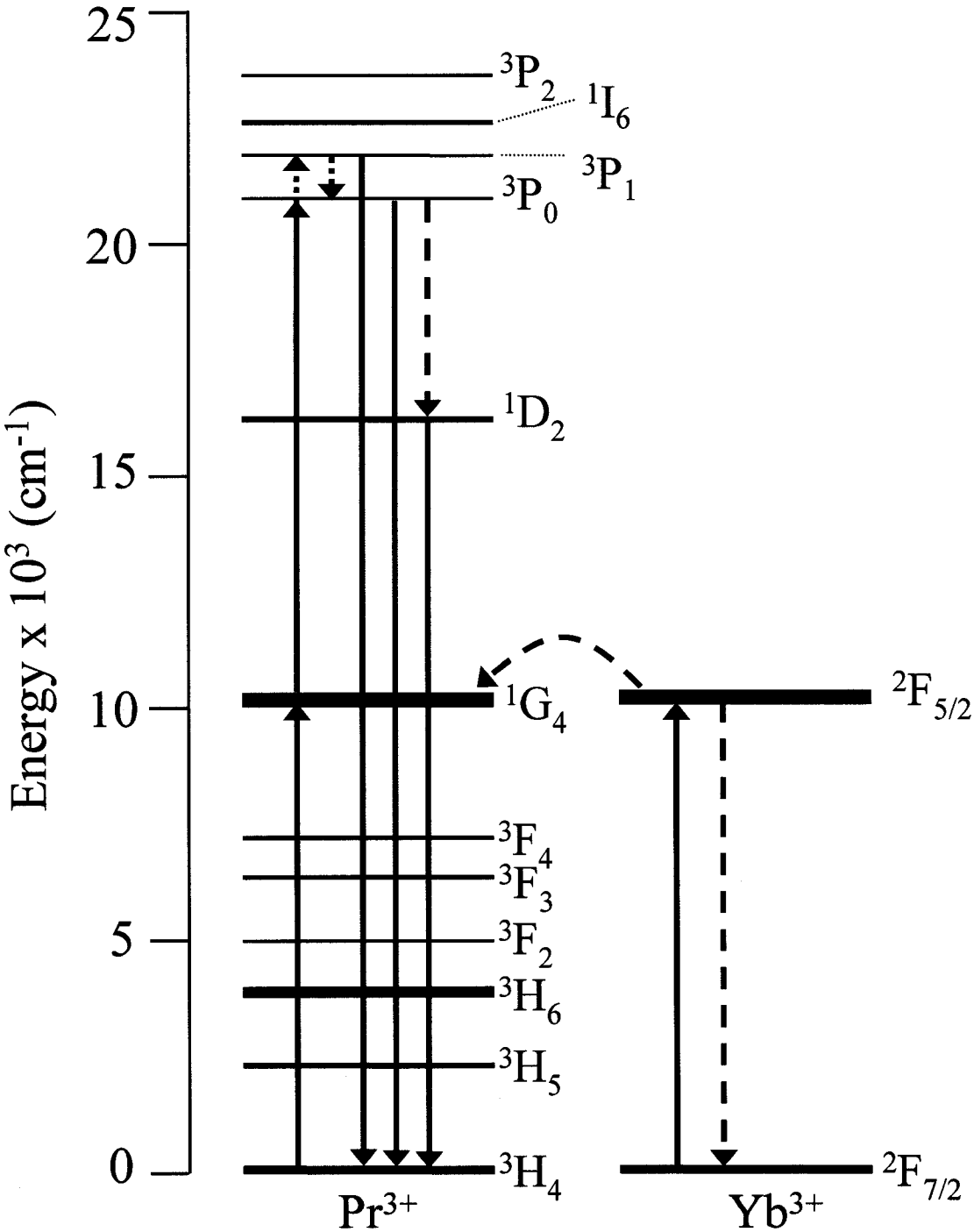

Figure 6. 9. Proposed upconversion mechanism for 1 mol% Pr^{3+}/ (1-10 mol%) Yb^{3+} co-doped GGG nanocrystals.

Chapter VII

Conclusions

In this thesis, we have investigated the optical properties of singly-doped tripositive praseodymium in a gadolinium gallium garnet (GGG) bulk (single crystal) and nanocrystalline hosts. The effect of co-doping with ytterbium has also been investigated and was reported.

Both bulk and nanocrystalline GGG doped with 1 mol% Pr^{3+} showed similar emission spectra upon 457.9 nm excitation. Moreover, energy transfer upconversion, after excitation in the $^1D_2$ energy level using a wavelength of 606.9 nm, was observed in both bulk and nanocrystalline samples. Upconversion emission was however more intense in the bulk system. Blue/green and red upconversion emission via ESA was observed following excitation at 980 nm. The transition lifetimes were critical in elucidating the mechanism of upconversion. Upconversion following excitation at 606.9 nm predominantly occurs through an energy transfer upconversion mechanism in the single crystal and nanocrystals as evidenced by the increase in the $^3P_0$ transition lifetime. Upconversion following excitation at 980 nm predominantly occurs through an excited state absorption mechanism as no increase in the $^3P_0$ transition lifetime was observed.

Increasing the rare earth concentration resulted in a marked decrease in the emission intensity emanating from the $^3P_{0,1}$ and $^1D_2$ levels to the lower lying intermediate state. This was attributed to efficient cross-relaxation (CR) energy transfer processes which efficiently de-populate the intermediate excited states of Pr^{3+} and de-excite the ion to the ground state. Typical operative CR processes include: $[^3P_0, {}^3H_4] \rightarrow [^3H_6, {}^1D_2]$ and $[^1D_2, {}^3H_4] \rightarrow [^1G_4, {}^3F_{3,4}]$. Upconversion emission at 0.1, 1, 5 and 10 mol% was also

observed using an excitation wavelength of 606.9 or 980 nm and occurred via ET and ESA, respectively.

The non-exponential lifetimes coupled with an in-depth evaluation of the emission spectra suggested the presence of minority sites within the GGG host. The increase in emission intensity at the minority site relative to the principle site, with increasing dopant concentration, suggests the likelihood of the existence of non-equivalent Pr^{3+} sites in the GGG host.

While the incorporation of the sensitizer ion resulted in a decrease of emission intensity (λ_{exc} = 457.9 nm) with increasing Yb^{3+} concentration, the upconversion emission intensity increased 3-fold relative to the singly-doped nanocrystalline system. Upconversion (λ_{exc} = 980 nm) was observed to occur via an ET mechanism as supported by the lifetime of the $^3P_0 \rightarrow {}^3H_4$ transition. Back transfer from the praseodymium to the ytterbium ion was observed based on the lengthening of the lifetime of the praseodymium transitions (λ_{exc} = 457.9 nm). This back transfer is facilitated and probable due to the similarity of the energy gaps separating the $^1G_4$ and $^2F_{5/2}$ excited states of the praseodymium and ytterbium ions, respectively and their respective ground states.

The research on GGG:Pr^{3+} presented in this thesis doesn't show tripositive praseodymium to be an efficient upconverter; however, it has been extremely useful to investigate the various mechanisms of upconversion and promote a further understanding of the associated radiative and non-radiative components.

Chapter VIII

Future Work

No work is complete without pondering future work to be conducted in an effort to further understand the studied system.

It would be of great interest to evaluate the effect of temperature on the luminescence properties of the praseodymium-doped nanocrystals most notably with respect to upconversion luminescence. The system temperature plays a critical role in multi-phonon relaxation and thermalization processes and hence will affect the luminescence properties of the material accordingly. Furthermore, it was proposed that the CR processes are mediated via the intrinsic phonons of GGG and so, it would be of benefit to evaluate the various cross-relaxation mechanisms of the system as a function of temperature likely spanning 4K to 373K.

In addition, the differences in the optical properties of the material in the bulk and nanophase suggests that the optical properties of the material should be studied as a function of the particle size. This would allow for a detailed understanding of the particle size effects and would allow for the tailoring of specific particle dimensions for corresponding technological applications. The optical properties vary drastically with the particle size and hence, applications in the display industry and biomedical field for example, will require specific dimensions suitable for the end result.

Furthermore, it would be of interest to develop a study investigating optimum concentrations of dopant in the systems to target efficient upconversion luminescence. This would entail a design of experiments where systems of various concentrations are synthesized until key sensitizer and activator concentrations are identified.

Lastly, a detailed study would be required to further prove the presence of non-equivalent Pr^{3+} sites in the system. At least one site has been identified; however, there remains a possibility that a second site may exist. X-ray powder diffraction studies would be critical to try to identify reflections which are uncommon to the *Ia*3*d* space group. Furthermore, a detailed study of the lifetimes of the minority sites could be crucial in divulging further information regarding the non-equivalent sites. The ions present in minority sites would be expected to have different lifetimes relative to the ions located in the principal site of the GGG host.

Chapter IX

References

1. *Luminescence*. M. Nic, J. Jirat, B. Kosata, Eds., IUPAC Compendium of Chemical Terminology (ICT Prague, Prague, ed. 2nd, 1997), vol. 68.
2. G. C. Pimentel, R. D. Spratley, *Understanding Chemistry* (Holden-Day, San Francisco, 1971).
3. S. Cotton, *Lanthanide and Actinide Chemistry*, Inorganic Chemistry: A Textbook Series (John Wiley & Sons, New York, 2006).
4. R. L. Carlin, *Magnetochemistry* (Springer, New York, 1986).
5. G. H. Dieke, *Spectra and Energy Levels of Rare Earth Ions in Crystals* (Interscience, New York, 1968).
6. F. Vetrone, Ph. D. Thesis, Concordia University (2005).
7. *The Columbia Encyclopedia*. (Columbia University Press, New York, 2006).
8. *Handbook of Chemistry & Physics*. D. R. Lide, Ed. (CRC Press, LLC, New York, ed. 87th Edition, 2006).
9. R. Balda, J. Fernández, I. S. d. Oscáriz, M. Voda, A. J. García, N. Khaidukov, *Phys. Rev. B* **59**, 9972 (1999).
10. C. D. M. Donegá, G. J. Dirksen, H. F. Folkerts, A. Meijerink, G. Blasse, *J. Phys. Chem. Solids* **56**, 267 (1995).
11. Y. V. Malyukin, A. A. Masalov, P. N. Zhmurin, N. V. Znamenski, E. A. Petrenko, T. G. Yukina, *Phys. Stat. Sol. (b)* **240**, 655 (2003).
12. B. Savoini, J. E. M. Santiuste, R. Gonzalez, *Phys. Rev. B* **56**, 5856-5865 (1997).
13. X. Wu, W. M. Dennis, W. M. Yen, *Phys Rev B* **50**, 6589-6595 (1994).
14. U. Bockelmann, *Phys Rev B* **42**, 8947 (1990).
15. U. Bockelmann, 105 (1992).
16. U. Bockelmann, *Phys Rev B* **46**, 15574 (1992).
17. U. Bockelmann, *Solid State Electronics* **37**, 1109 (1994).
18. O. Brandt, *Phys Rev B* **41**, 12599 (1990).
19. O. Brandt, *Phys Rev B* **44**, 8043 (1991).
20. Y. Tang, *Appl Phys Lett* **63**, 497 (1993).
21. Y. Tang, *Solid State Commun* **85**, 199 (1993).
22. P. Wang, *Appl Phys Lett* **61**, 946 (1992).
23. P. Wang, *J Appl Phys* **74**, 5907 (1993).

24. P. Wang, *Surf Sci* **305**, 585 (1993).

25. P. Wang, *Appl Phys Lett* **64**, 1526 (1994).

26. P. Wang, *Phys Rev B* **50**, 1604 (1994).

27. J. Uldrich, D. Newberry, *Next Big Thing Is Really Small: How Nanotechnology Will Change the Future of Your Business,* (2003).

28. G. E. Fryxell, Y. Lin, H. Wu, K. M. Kemner, *Studies in Surface Science and Catalysis,* A. Sayari and M. Jaroniec (eds), Elsevier, **141**, 583-590 (2003).

29. G. E. Fryxell, J. Liu, S. Mattigod, *Mater. Tech.* **14**, 188-191 (1999).

30. S. V. Mattigod, X. Feng, G. E. Fryxell, J. Liu, M. Gong, *Sep. Sci. Technol.* **34**, 2329-2345 (1999).

31. S. V. Mattigod, G. E. Fryxell, R. J. Serne, K. E. Parker, F. M. Mann, *Radiochim. Acta* **91**, 539-545 (2003).

32. S. V. Mattigod, R. Skaggs, G. E. Fryxell, *9th Annual Industrial Wastes Technical and Regulatory Conference, 2003 Industrial Wastes Conference Water Environment Federation* (2003).

33. W. Yantasee, Y. Lin, G. E. Fryxell, B. J. Busche, J.C. Birnbaum, *Sep. Sci. Technol.* **38**, 3809-3825 (2003).

34. J. A. Capobianco, F. Vetrone, J. C. Boyer, A. Speghini, M. Bettinelli, *J. Phys. Chem. B* **106**, 1181-1187 (2002).

35. J. A. Capobianco, F. Vetrone, T. D'Alesio, G. Tessari, A. Speghini, M. Bettinelli, *Phys. Chem. Chem. Phys.* **2**, 3203-3207 (2000).

36. G. De, W. Qin, J. Zhang, J. Zhang, Y. Wang, C. Cao, Y. Cui, *Solid State Commun* **137** (2006).

37. G. De, W. Qin, J. Zhang, J. Zhang, Y. Wang, C. Cao, Y. Cui, *J. Lumin.* **119-120**, 258-263 (2006).

38. T. Hirai, T. Hirano, I. Komasawa, *J. Colloid Interface Sci.* **253**, 62-69 (2002).

39. T. Hirai, T. Orikoshi, I. Komasawa, *Chem. Mater.* **14**, 3576-3583 (2002).

40. M. Kottaisamy, K. Horikawa, H. Kominami, T. Aoki, N. Azuma, T. Nakamura, Y. Nakanishi, Y. Hatanaka, *J. Electrochem. Soc.* **147**, 1612-1616 (2000).

41. A. B. Kutsenko, J. Heber, S. E. Kapphan, R. Demirbilek, R. I. Zakharchenya, *Phys. Stat. Sol. (c)* **2**, 685-688 (2005).

42. J. M. Luiz, E. B. Stucchi, N. Barelli, *Eur. J. Solid State Inorg. Chem.* **33**, 321-329 (1996).

43. D. Matsuura, *Appl. Phys. Lett.* **81**, 4526-4528 (2002).

44. R. S. Meltzer, W. M. Yen, H. Zheng, S. P. Feofilov, M. J. Dejneka, B. M. Tissue, H. B. Yuan, *J. Lumin.* **94&95**, 217-220 (2001).

45. H. Song, B. Sun, T. Wang, S. Lu, L. Yang, B. Chen, X. Wang, X. Kong, *Solid State Commun* **132**, 409-413 (2004).

46. H. Song, H.-P. Xia, B.-J. Sun, S.-Z. Lu, Z.-X. Liu, L.-X. Yu, *Chin. Phys. Lett.* **23**, 474-477 (2006).

47. F. Vetrone, J. C. Boyer, J. A. Capobianco, A. Speghini, M. Bettinelli, *J. Phys. Chem. B* **107**, 1107-1112 (2003).

48. F. Vetrone, J. C. Boyer, J. A. Capobianco, A. Speghini, M. Bettinelli, *J Appl Phys* **96**, 661-667 (2004).

49. F. Vetrone, J.-C. Boyer, J. A. Capobianco, A. Speghini, M. Bettinelli, *Chem. Mater.* **15**, 2737-2743 (2003).

50. L. D. d. Vila, E. B. Stucci, M. R. Davolos, *J. Mater. Chem.* **7**, 2113-2116 (1997).

51. D. K. Williams, B. Bihari, B. M. Tissue, J. M. McHale, *J. Phys. Chem. B* **102** (1998).

52. H.-S. Yang, S. P. Feofilov, D. K. Williams, J. C. Milora, B. M. Tissue, R. S. Meltzer, W. M. Dennis, *Physica B* **263-264**, 476-478 (1999).

53. S. Daniele, L. G. Hubert-Pfalzgraf, *Mater. Lett.* **58**, 1989-1992. (2004).

54. J. Gomes, A. M. Pires, O. A. Serra, *J Fluoresc* **16**, 411-421 (2006).

55. A. Madubuonu, H. Drings, R. Roewer, H.-E. Schaefer, *Phys. Stat. Sol. A* **203**, R64-R65 (2006).

56. A. V. Murugan, A. K. Viswanath, V. Ravi, B. A. Kakade, V. Saaminathan, *Appl. Phys. Lett.* **89**, 123120/123121-123120/123123 (2006).

57. H. Pedersen, L. Ojamaee, *Nano Lett.* **6**, 2004-2008 (2006).

58. F. Vetrone, J.-C. Boyer, J. A. Capobianco, in *Handbook of Luminescence, Display Materials, and Devices* H. S. Nalwa, L. S. Rohwer, Eds. (2003) pp. 141-186.

59. F. Vetrone, J.-C. Boyer, J. A. Capobianco, A. Speghini, M. Bettinelli, *J. Mater. Res.* **19**, 3398-3407 (2004).

60. F. Vetrone, J.-C. Boyer, J. A. Capobianco, A. Speghini, M. Bettinelli, *Nanotech.* **15**, 75-81 (2004).

61. X. Wang, G. Shan, K. Chao, Y. Zhang, R. Liu, L. Feng, Q. Zeng, Y. Sun, Y. Liu, X. Kong, *Mater. Chem. Phys.* **99**, 370-374 (2006).

62. Y. Zhang, J. Chen, L. Hu, W. Liu, *Mater. Lett.* **60**, 2302-2305 (2006).

63. D. S. Gill, A. A. Anderson, R. W. Eason, T. J. Warburton, D. P. Shepherd, *Appl. Phys. Lett.* **69**, 10-12 (1996).

64. D. Sugak, A. Matkovskii, A. Durygin, A. Suchocki, I. Solskii, S. Ubizskii, K. Kopczynski, Z. Mierczyk, P. Potera, *J. Lumin.* **82**, 9-15 (1999).

65. D. Hreniak, W. Strek, *J. Alloy Compd* **341**, 183-186 (2002).

66. C.-H. Lu, H.-C. Hong, R. Jagannathan, *J. Mater. Sci. Lett.* **21**, 1489-1492 (2002).

67. J. McKittrick, L. E. Shea, C. F. Bacalski, E. J. Bosze, *Displays* **19**, 169-172 (1999).

68. L. E. Shea, J. McKittrick, O. A. Lopez, *J. Am. Ceram. Soc* **79**, 3257-3265 (1996).

69. H.-L. Li, X.-J. Liu, R.-J. Xie, Y. Zeng, L. P. Huang, *J. Am. Ceram. Soc.* **89**, 2356-2358 (2006).

70. F. Pandozzi, F. Vetrone, J.-C. Boyer, R. Naccache, J. A. Capobianco, A. Speghini, M. Bettinelli, *J. Phys. Chem. B* **109**, 17400-17405 (2005).

71. M. Pang, J. Lin, *J. Cryst. Growth* **284**, 262-269 (2005).

72. B. Henderson, G. F. Imbusch, *Optical Spectroscopy of Inorganic Solids* (Oxford Science Publications, Oxford, 1989).

73. D. L. Andrews, *Lasers in Chemistry* (Springer, Berlin, ed. Third Edition, 1997).

74. P. Kabro, Ph.D. Thesis, Concordia University (1997).

75. R. S. Drago, *Physical Methods in Chemistry* (W.B. Saunders Company, Philadelphia, 1977).

76. B. DiBartolo, *Optical Interactions in Solids* (John Wiley & Sons, Inc, New York, 1968).

77. D. L. Dexter, *J. Chem. Phys.* **21**, 836 (1953).

78. T. H. Förster, *Ann. Physik* **2**, 55 (1948).

79. R. Orbach, *Optical Properties of Ions in Solids*. B. DiBartolo, Ed. (Plenum Press, New York, 1975).

80. R. Reisfeld, *Struct Bond* **30**, 68 (1976).

81. R. K. Watts, *Optical Properties of Ions in Solids*. B. DiBartolo, Ed. (Plenum Press, New York, 1975).

82. J. C. Wright, *Topics in Applied Physics*. F. K. Fong, Ed. (Springer-Verlag, Berlin and New York, 1976).

83. D. L. Dexter, *Phys Rev* **126**, 1962 (1962).

84. T. Förster, *Modern Quantum Chemistry*. O. Sinanoglu, Ed. (Academic Press, New York, 1965).

85. S. Hüfner, *Optical Spectra of Transparent Rare Earth Compounds* (Academic Press, New York, 1978).

86. F. Auzel, *C. R. Acad. Sci. (Paris)* **262**, 1016 (1966).

87. B. M. Tissue, *Chem. Mater.* **10**, 2837-2845 (1998).

88. D. K. Williams, H. Yuan, B. M. Tissue, *J. Lumin.* **83-84**, 297-300 (1999).

89. A. P. Alivisatos, *J. Phys. Chem.* **100**, 13226-13239 (1996).

90. T. Hase, T. Kano, E. Nakazawa, H. Yamamoto, *Adv. Electron. Electron Phys.* **79**, 271-373 (1990).

91. C. Xu, B. A. Watkins, R. E. Sievers, X. Jing, P. Trowga, C. S. Gibbons, A. Vecht, *Appl. Phys. Lett.* **71**, 1643-1645 (1997).

92. L. Wang, R. Yan, Z. Huo, L. W. J. Zeng, J. Bao, X. Wang, Q. Peng, Y. Li, *Angew. Chem.* **117**, 6208-6211 (2005).

93. L. Wang, Y. Li, *Chem. Commun.*, 2557-2559 (2006).

94. M. F. Joubert, S. Guy, B. Jacquier, *Phys. Rev. B* **48**, 10031 (1993).

95. M. F. Joubert, *Opt. Mater.* **11** (1999).

96. *McGraw-Hill Encyclopedia of Science and Technology.* (The McGraw-Hill Companies, Inc., New York, 2005).

97. D. Pines, *Elementary Excitations in Solids* (W. A. Benjamin, New York: , 1963).

98. *Die Kunst of Phonons.* T. Paszkiewicz, K. Rapcewicz., Eds. (Plenum, New York, 1994).

99. J. A. Capobianco, N. Raspa, A. Monteil, M. Malinowski, *J. Phys.: Condens. Matter* **5**, 6083-6090 (1993).

100. N. Raspa, Ph. D., Concordia University (1992).

101. R. Naccache, F. Vetrone, J. C. Boyer, J. A. Capobianco, A. Speghini, M. Bettinelli, *To be submitted* (2006).

102. R. Krsmanovic, S. Polizzi, P. Canton, *Mater. Sci. Forum* **494**, 143-148 (2005).

103. R. Balda, J. Fernández, A. Mendioroz, M. Voda, M. Al-Saleh, *Opt. Mater.* **24**, 91-95 (2003).

104. R. Balda, J. Fernández, A. Mendioroz, M. Voda, M. Al-Saleh, *Phys Rev B* **68**, 165101/165101-165101/165107 (2003).

105. R. Balda, M. Voda, M. Al-Saleh, J. Fernández, *J. Lumin.* **97**, 190-197 (2002).

106. K. D. Oskam, A. J. Houtepen, A. Meijerink, *J. Lumin.* **97**, 107-114 (2002).

107. M. Malinowski, Z. Frukacz, M. F. Joubert, B. Jacquier, *J. Lumin.* **75**, 333-339 (1997).

108. M. Malinowski, M. Kowalska, R. Piramidowicz, T. Lukasiewicz, M. Swirkowicz, A. Majchrowski, *J. Alloys Compd.* **323-324**, 214-217 (2001).

109. J. A. Capobianco, J. C. Boyer, F. Vetrone, A. Speghini, M. Bettinelli, *Chem. Mater.* **14**, 2915 (2002).

110. B. R. Judd, *J. Chem. Phys.* **44**, 839-840 (1966).

111. F. Vetrone, J. C. Boyer, J. A. Capobianco, A. Speghini, M. Bettinelli, *J. Phys. Chem. B* **107**, 10747-10752 (2003).

112. R. Balda, J. Fernandez, I. S. d. Oscariz, M. VOda, A. J. Garcia, *Phys. Rev. B* **59**, 9972-9980 (1999).

113. A. Lorenzo, L. E. Bausá, J. G. Solé, *Phys. Rev. B* **51**, 16643 (1995).

114. G. K. Liu, H. Z. Zhuang, X. Y. Chen, *Nano Lett.* **2**, 535-539 (2002).

115. A. Lorenzo, L. E. Bausá, J. G. Solé, *Phys. Rev. B* **51**, 16643-16650 (1995).

116. H. Chen, R. Lian, M. Yin, L. Lou, W. Zhang, S. Xia, J.-C. Krupa, *J. Phys.: Condens. Matter* **13**, 1151 (2001).

117. R. Naccache, F. Vetrone, J. C. Boyer, J. A. Capobianco, A. Speghini, M. Bettinelli, *J. Nanosci. Nanotechno.* **4**, 1025 (2004).

118. E. Nakazawa, *Phosphor Handbook.* W. M. Y. S. Shionoya, Eds. , Ed. (CRC Press, 1999).

119. E. Nakazawa, S. Shionoya, *Phys. Rev. Lett.* **25**, 1710-1712 (1970).

120. R. C. Naik, N. P. Karanjikar, M. A. N. Razvi, *J. Lumin.* **54**, 139 (1992).

121. F. Auzel, paper presented at the Proc, IEEE 1973.

122. M. Inokuti, F. Hirayama, *J. Chem. Phys.* **43**, 1978 (1965).

123. V. Lupei, A. Lupei, G. Boulon, *Spectrochim. Acta, Part A* **55**, 783-794 (1999).

124. A. Lupei, H. Gross, P. Reiche, *J. Phys.: Condens. Matter* **7**, 5701-5712 (1995).

125. E. Antic-Fidancev, M. Lemaitre-Blaise, J. C. Krupa, P. Caro, *Czech J. Phys. B* **38**, 1269 (1988).

126. E. Antic-Fidancev, M. Lemaitre-Blaise, P. Porcher, *J. Alloys Compounds* **207-208**, 90.

127. M. Malinowski, P. Szxzepanski, W. Wolinski, R. Wolski, Z. Frukacz, *J. Phys.: Condens. Matter* **5**, 6469 (1993).

128. F. Maglia, V. Buscaglia, S. Gennari, P. Ghigna, M. Dapiaggi, A. Speghini, M. Bettinelli, *J. Phys. Chem. B* **110**, 6561-6568 (2006).

129. R. Balda, J. Fernandez, A. Mendioroz, M. Voda, M. Al-Saleh, *Phys. Rev. B: Condens. Matter* **68**, 165101/165101-165101/165107 (2003).

130. A. J. Barbosa, F. A. D. Filho, Y. Messaddeq, S. J. L. Ribeiro, R. R. Goncalves, S. R. Luethi, A. S. L. Gomes, *J. Non-Cryst. Solids* **352**, 3636-3641 (2006).

131. S. Berneschi, M. Bettinelli, M. Brenci, R. Calzolai, A. Chiasera, M. Ferrari, C. Nunzi, P. Gualtiero, S. Stefano, A. Speghini, J. Zheng, G. C. Righini, *Proceedings of SPIE-The International Society for Optical Engineering* **5350**, 140-146 (2004).

132. J. C. Boyer, F. Vetrone, J. A. Capobianco, A. Speghini, M. Bettinelli, *Chem. Phys. Lett.* **390**, 403-407 (2004).

133. A. S. S. d. Camargo, E. R. Botero, E. R. M. Andreeta, D. Garcia, J. A. Eiras, L. A. O. Nunes, *Appl. Phys. Lett.* **86**, 241112/241111-241112/241113 (2005).

134. E. Cantelar, F. Cusso, *J. Lumin* **102-103**, 525-531 (2003).

135. A. Chiasera, C. Tosello, E. Moser, M. Montagna, R. Belli, R. R. Goncalves, G. C. Righini, S. Pelli, A. Chiappini, L. Zampedri, M. Ferrari, *J. Non-Cryst. Solids* **322**, 289-294 (2003).

136. L. C. Courrol, L. V. G. Tarelho, L. Gomes, N. D. Vieira, F. C. Cassanjes, Y. Messaddeq, S. J. L. Ribeiro, *J. Non-Cryst. Solids* **284**, 217-222 (2001).

137. H. Desirena, E. D. l. Rosa, L. A. Diaz-Torres, G. A. Kumar, *Opt. Mater.* **28**, 560-568 (2006).

138. D. Hreniak, P. Gluchowski, W. Strek, M. Bettinelli, A. Kozlowska, M. Kozlowski, *Mater. Sci.* **24**, 405-413 (2006).

139. B. Jacquier, A. Remillieux, M. F. Joubert, P. Christensen, H. Poignant, *J. Non-Cryst. Solids* **161**, 241-244 (1993).

140. Y. Kishi, S. Tanabe, S. Tochino, G. Pezzotti, *J. Am. Ceram. Soc.* **88**, 3423-3426 (2005).

141. J. Li, H. Hu, F. Gan, *Chin. Opt. Lett.* **1**, 702-704 (2003).

142. R. Lisiecki, W. Ryba-Romanowski, T. Lukasiewicz, *Appl. Phys. B* **81**, 43-47 (2005).

143. S. A. Lopez-Rivera, J. Martin, A. Florez, V. Balassone, *J. Lumin* **106**, 291-299 (2004).

144. X. Mateos, R. Sole, J. Gavalda, M. Aguilo, F. Diaz, J. Massons, *J. Lumin* **115**, 131-137 (2005).

145. X. Mateos, R. Sole, J. Gavalda, M. Aguilo, J. Massons, F. Diaz, *Opt. Mater.* **28**, 423-431 (2006).

146. A. Meijerink, R. Wegh, P. Vergeer, T. Vlugt, *Opt. Mater.* **28**, 575-581 (2006).

147. J. A. Munoz, E. Cantelar, J. A. Sanz-Garcia, R. Duchowicz, D. Serrano, E. Dieguez, G. Lifante, F. Cusso, *Radiat Eff. Defects Solids* **150**(613-617 (1999).

148. G. Ozen, J. P. Denis, P. Goldner, X. Wu, M. Genotelle, F. Pelle, *Appl. Phys. Lett.* **62**, 928-930 (1993).

149. G. Qin, W. Qin, S. Huang, C. Wu, B. Chen, S. Lu, E. Shulin, *Solid State Commun.* **120**, 211-214 (2001).

150. G. Qin, W. Qin, C. Wu, D. Zhao, J. Zhang, L. Jisen, H. Shaozhe, S. Huang, W. Xu, *J. Non-Cryst. Solids* **347**, 52-55 (2004).

151. J. Qiu, M. Shojiya, R. Kanno, Y. Kawamoto, *Opt. Mater.* **13**, 319-325 (1999).

152. G. C. Righini, S. Pelli, M. Brenci, M. Ferrari, C. Duverger, M. Montagna, R. Dall'Igna, *J. Non-Cryst. Solids* **284** 223-229 (2001).

153. D. F. di Sousa, F. Batalioto, M. J. V. Bell, S. L. Oliveira, L. A. O. Nunes, *J. Appl. Phys.* **90**, 3308-3313 (2001).

154. C. Strohhofer, A. Polman, *J. Appl. Phys.* **90**, 4314-4320 (2001).

155. F. Su, Z. Deng, *J Fluoresc* **16**, 69-75 (2006).

156. X. J. Wang, M. K. Lei, T. Yang, B. S. Cao, *Opt. Mater.* **26**, 253-259 (2004).

157. M. J. Weber, *Phys. Rev. B: Sol. Stat.* **[3]4**, 3153-3159 (1971).

158. W. You, Y. Lin, Y. Chen, Z. Luo, Y. Huang, *J. Cryst. Growth* **270**, 481-485 (2004).

159. H. Yu, L. Zhao, J. Meng, Q. Liang, X. Yu, B. Tang, J. Xu, *Chin. Opt. Lett.* **3**, 469-471 (2005).

160. J. Zhang, S. Dai, S. Xu, G. Wang, L. Zhang, L. Hu, *Chin. Opt. Lett.* **2**, 600-603 (2004).

161. J. Zhou, F. Moshary, B. M. Gross, M. F. Arend, S. A. Ahmed, *J. Appl. Phys.* **96**, 237-241 (2004).

Appendix

A1.1 Synthesis of the Praseodymium-Doped Gadolinium Gallium Garnet Bulk Sample (Single Crystal)

The single crystal of gadolinium gallium garnet ($Gd_3Ga_2Ga_3$) doped with 1 mol% Pr^{3+} was grown using the Czochralski technique. This technique involves the use of a crystalline seed which is immersed in the melt contained in a crucible. The seed is drawn from the melt resulting in crystal growth. Growth occurs at the solid-liquid interface. The rate of withdrawal of the seed from the melt directly affects the diameter of the crystal. Long and thin crystals may be obtained using a fast pull rate while a slow pull rate would result in a single crystal of a larger diameter [100].

A1.2 Synthesis of the Praseodymium-Doped Gadolinium Gallium Garnet Nanocrystals

Cubic $Gd_3Ga_5O_{12}$ nanocrystals doped with 0.1, 1, 5 and 10 mol% Pr^{3+} were prepared using a solution combustion (propellant) synthesis procedure [101]. This synthesis approach involves an exothermic reaction between an oxidizer and an organic fuel, such as metal nitrates and carbohydrazide, respectively. An aqueous solution containing appropriate quantities of carbohydrazide $(NH_2NH)_2CO$ (Aldrich, 98%), $Gd(NO_3)_3{\cdot}6H_2O$ (Aldrich, 99.99%), $Ga(NO_3)_3{\cdot}H_2O$ (Aldrich, 99.999%) and $Pr(NO_3)_3{\cdot}6H_2O$ (Aldrich, 99.9%) was prepared. The carbohydrazide was added to the metal nitrate in a molar ratio of 2.5:1 after which the precursor solution was heated using a Bunsen flame. The auto combustion process took place, after the solvent was allowed to evaporate, with the evolution of a brown fume and the highly porous mass of nanocrystalline powder was formed. After combustion, the low-density powders were

fired for 1 hour at 500 °C in order to decompose the residual oxidizer and fuel. The large amounts of gaseous products generated are essential in the synthesis procedure as they increase the surface area of the powders. As more gases are liberated, the agglomerates disintegrate causing heat release from the system thereby hindering particle aggregation.

Co-doped samples were prepared using the same synthesis technique; however, the appropriate quantities of tripositive ytterbium (Yb^{3+}) from $Yb(NO_3)_3 \cdot 6H_2O$ were added instead of $Pr(NO_3)_3 \cdot 6H_2O$.